Title
New Rotary Engine Designs by Deviation Function Method

Permalink
https://escholarship.org/uc/item/2w12f40z

Author
Warren, Sarah

Publication Date
2012

Peer reviewed|Thesis/dissertation

UNIVERSITY OF CALIFORNIA
Los Angeles

New Rotary Engine Designs by Deviation Function Method

A dissertation submitted in partial satisfaction of the

requirements for the degree of Doctor of Philosophy

in Mechanical Engineering

by

Sarah Elizabeth Warren

2012

ABSTRACT OF THE DISSERTATION

New Rotary Engine Designs by Deviation Function Method

by

Sarah Elizabeth Warren

Doctor of Philosophy in Mechanical Engineering

University of California, Los Angeles, 2012

Professor Daniel C. H. Yang, Chair

Conventional rotary engine designs are based on an epitrochoidal housing bore that is found by the path of the point at the rotor profile's apex. To seal the engine, the rotor apexes are replaced by spring-loaded apex seals that slide along the housing bore during rotation. The conventional designs are limited to the point-based epitrochoid housing profiles and cannot incorporate the profile of the apex seal. This dissertation presents the complete theory and algorithm of the deviation function (DF) method of rotary engine design. This method is based on conjugate pair design and generates new engine profiles from generating curves. The DF method of rotary engine design by apex seal profile is introduced and developed for generating new profile designs in which the housing profile conforms to the apex seal profile, for better sealing. The DF method of design by geometric parameters is developed to select profiles using the standard rotary engine geometry. Maximum theoretical compression ratio and swept area are two criteria that have a range of possible DF-designed profile solutions. For the apex seal design and selection process, a sealing index is defined and a multi-apex-sealing grid is developed to further improve apex sealing. The DF method of rotary engine design is extended to noncircular pitch curves, for generating more new

profiles that incorporate a variable speed ratio between the rotor and main shaft.

By using the DF method, a larger variety of engine profiles is available to meet multiple design criteria and allow more flexibility in the design process. Some example deviation functions are provided for process illustration and design development. Engine profile designs and methods using circular pitch curves are developed using both arc-based and nonarc-based apex seal profiles. Engine profile designs with noncircular pitch curves are developed using the arc-based seal profile.

The dissertation of Sarah Elizabeth Warren is approved.

Rajit Gadh

Michael K. Stenstrom

Tsu-Chin Tsao

Daniel C. H. Yang, Committee Chair

University of California, Los Angeles

2012

Dedicated to

Etta Warren and Dorothy Kohashi

Contents

List of Tables

List of Figures

ACKNOWLEDGEMENTS

More people than I can recognize here have helped me with this project. They include mechanics, machinists, colleagues, professors, friends, and family.

I must certainly thank Professor Yang for his support, guidance, and most of all, patience. There could not have been a better advisor for me. My lab mates Seung Ryong Han and Chih-Yung Huang and their wives provided both empathy and perspective. My brother, Daniel, has never doubted me, and my friend, Louis Sloup, got me through it.

Most of all, my various motorcycles. There wouldn't be anything if I hadn't had them to keep me happy. My parents wanted me to achieve this goal more than anyone, and motorcycling made me want it too.

2003	B.S. in Engineering & Applied Science
	Caltech, Pasadena, CA
2005	M.S. in Ocean Engineering
	University of Rhode Island, Kingston, RI
2005 - 2008	GAANN Award
	University of California, Los Angeles, CA
2008 - 2011	Teaching Assistant
	University of California, Los Angeles, CA

Chapter 1

Introduction

At the 2011 Los Angeles Auto show, the CEO of Mazda Motor Corporation, Takashi Yamanouchi, announced the discontinuation of the RX-8, the solitary rotary engine powered car in production [10, 4]. The first rotary engine car was made by German auto manufacturer NSU [9]. It was an engineer at NSU, Felix Wankel, who first developed the design method and the rotary engine as it is now. By 1972 most engine manufacturers in the world had obtained a license for the Wankel engine and were planning to build their own because of its specific power; it is roughly half the size, weight, and manufacturing cost for the same horsepower of a reciprocating piston engine [9]. It is also naturally smoother running, quieter, with less vibration while operating at higher speeds [36]. Compared to a piston engine, it has a more compact shape, fewer than half the moving parts, and is more fuel-versatile [24].

The oil embargo of 1973 caused a decline in rotary engine production and applications because compared to piston engines, the rotary is not as fuel-efficient nor emissions-compliant. Since then Mazda has become the only company producing a car with the rotary engine; and steadily relegated it to fewer vehicle models. By 2003, the RX-8 was the only rotary-powered car on the market. In 2011 the RX-8 had a 1.3 liter, 2-rotor Renesis rotary engine that produces 232 horsepower at 8500 RPM with city-gas-mileage of 16 miles per gallon.

This vehicle did not meet the European emissions requirements [23].

The rotary engine has been used in most applications of internal combustion engines: cars, motorcycles, watercraft, aircraft, snowmobiles, and auxiliary power units. Car companies and aircraft manufacturers have used a rotary engine in concept hybrid vehicles, race vehicles, and special applications, because of the small size and shape coupled with its quiet, low-vibration running. The Wankel-designed profiles of the rotary engine have also been implemented as compressors, generators, and superchargers [5]. Recent research achievements include the fabrication of small-scale Wankel rotary engines, on the order of 10^1 mm in diameter [15, 17], and microelectricalmechanical system (MEMS) rotary engines on the order of 10^{-1} mm in diameter [14], both for portable power systems.
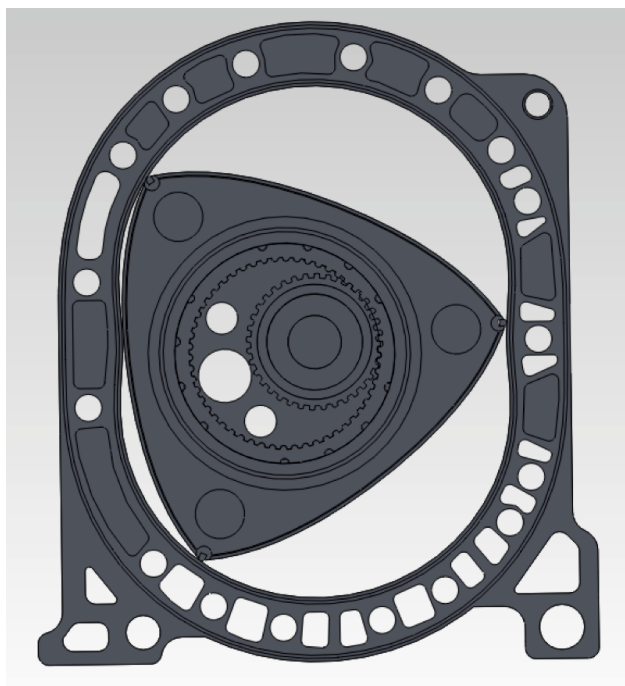
Figure 1.1: CAD model of rotary engine rotor and trochoidal housing.

The basic structure of a rotary engine consists of a triangular rotor eccentrically mounted onto the engine's main shaft, the epitrochoidal housing that encloses the rotor's movement, and two plates that sandwich the rotor and housing to enclose the chambers. Figure 1.1 is the rotor and housing of a CAD-modeled rotary engine without the front and back plates. This
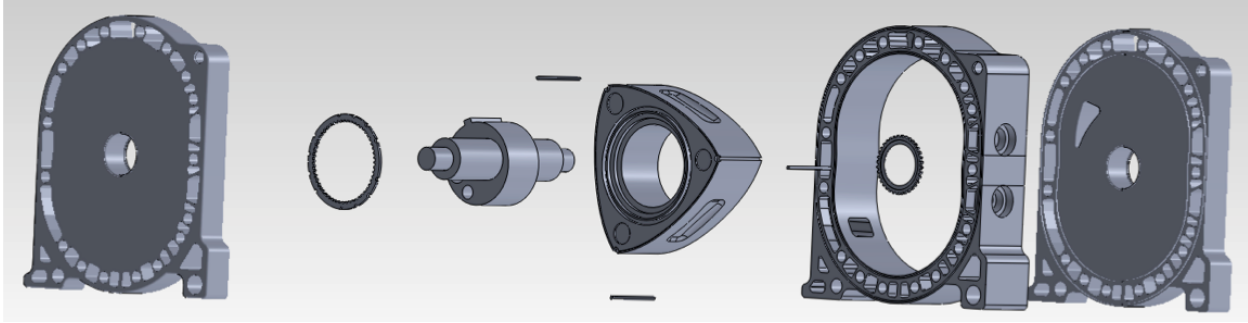
Figure 1.2: Exploded view of a rotary engine CAD model.

shows the trochoidal shape of the housing bore, the rotor, and the three chambers enclosed between the rotor flanks and housing. The three apexes of the rotor remain in contact with the housing bore at all times, so the chamber volumes are isolated from each other while constantly changing. Figure 1.2 shows the exploded view of the engine model, including the front and rear plates, the main shaft, and the rotor's apex seals. The rotor is positioned eccentrically inside the housing and its orientation is determined by a gear pair: an internal ring gear mounted on the rotor has a 3:2 gear ratio with a stationary gear mounted in the housing. The gears position the rotor inside the housing and do not transmit torque. The engine's main shaft rotates three times for a single rotation of the rotor, so there is a power stroke for every main shaft revolution. Power is transmitted when the combustion process expands its volume against the rotor face, creating a force on the main shaft. Because of the eccentric, this force has the leverage on the main shaft to create a torque and generate motion. The power stroke occurring on every revolution of the main shaft is the reason the Wankel produces double the horsepower of a same-sized piston engine, in which a single cylinder delivers a power stroke for every two revolutions of the crank shaft.

Figure 1.3 illustrates the operation of a rotary engine by following the complete revolution of one rotor flank, labeled 1, as it experiences the four strokes of the Otto cycle. The charge is represented by the five small circles. Figure 1.3a shows the intake stroke, although the intake port is sometimes cut into the sidewall of the engine to avoid overlap. Figures 1.3e to 1.3g show the compression stroke and Figure 1.3h indicates the spark ignition. Figure 1.3i

4

(a) Intake   (b)   (c)   (d)

(e) Compression   (f)   (g)   (h) Ignition

(i) Power   (j)   (k)   (l)

(m) Exhaust   (n)   (o)   (p)
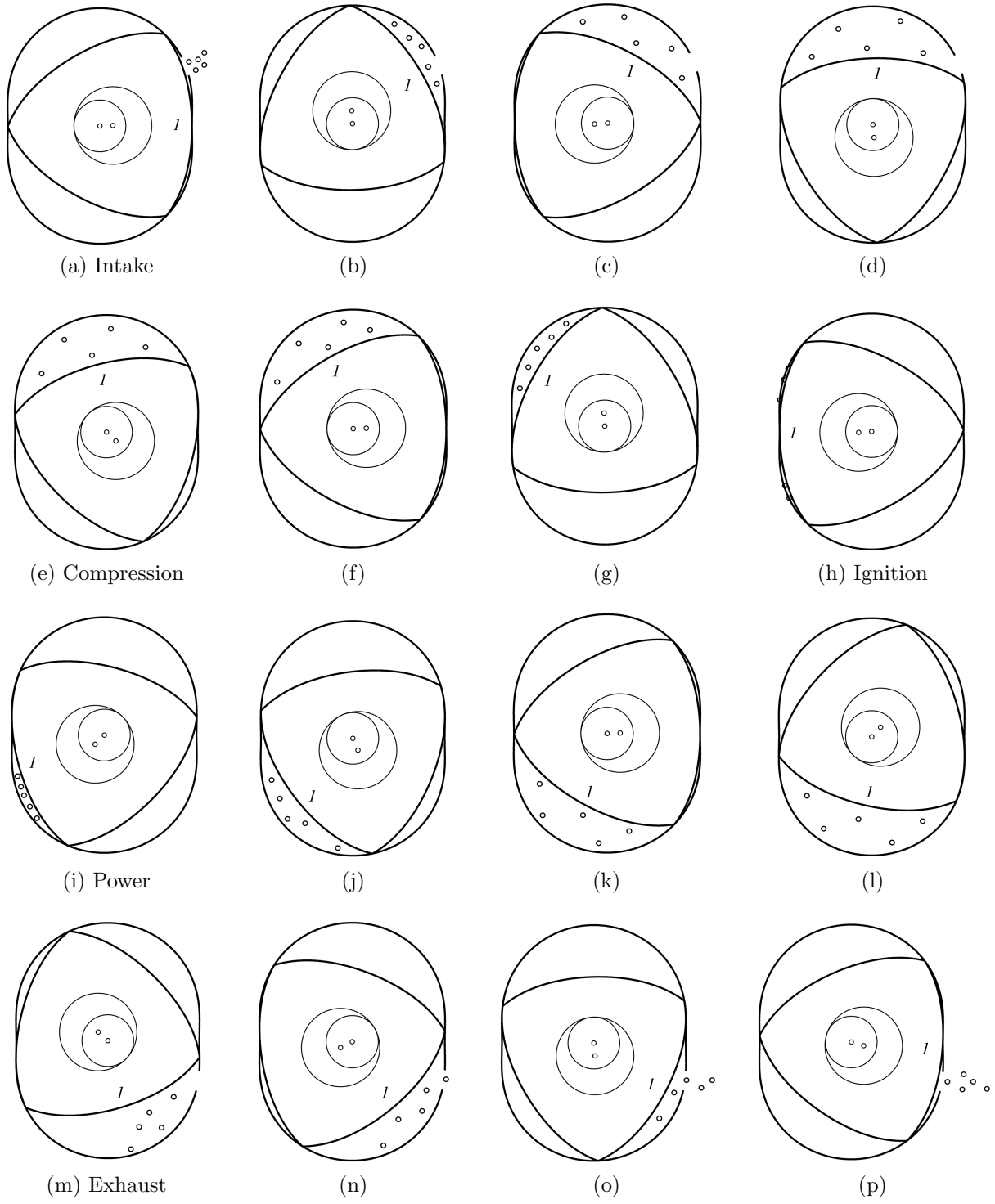
Figure 1.3: Otto cycle stages for the rotary engine.

shows the expansion of the combustion gasses against rotor flank 1, and finally Figure 1.3m shows the exhaust port opened and the exhaust gas being expelled. By Figure 1.3p, flank 1 has almost returned to its original position and the cycle will begin again. The unique design of the rotary engine allows this process of internal combustion to occur simultaneously on all sides of the rotor; in other words, three thermodynamic cycles occur at the same time, each one 120° out of phase from the other two.

The first rotary engine patent of Felix Wankel is from 1929, and he continued development through 1960 [24]. Ansdale in 1968 [1] and Yamamoto in 1981 [37] derived the equations for the housing bore and rotor profiles, and the parameters and performance criteria that are used to design a rotary engine. Colbourne classified eight types of trochoidal shapes and their conjugate envelopes, including the type used for rotary engines [8]. Shung and Pennock derived the closed-form equations for the trochoids and envelopes [30]. From 1990 to 2000, researchers Beard and Pennock made several studies of rotary engine characteristics and performance [6, 7, 25]. Since the rotary engine design method was established by Wankel, the principles have remained unchanged.

The disadvantages of the rotary can be attributed to two issues that have dogged the engine's development since inception. One is the unique design challenge of apex sealing and the other is the limitation of the trochoidal profiles. The lower fuel efficiency and difficulty meeting emissions regulations are caused in part by the inability to seal the engine chambers at the rotor apexes. This hinders other engine efficiencies, including the combustion efficiency, compared to those of a piston engine. The combustion chamber of a rotary engine might be improved by changing its shape, but rotary engine designs have a limited range for profile adjustment. The variety of profiles for the housing bore and rotor are governed by a ratio of two geometric parameters, called the K factor or trochoid constant. Due to the importance and difficulty of effective apex sealing, the K factor is optimized primarily for sealing. The upshot is that the housing and rotor profiles used in practice are geometrically similar, regardless of the application.

Regarding the RX-8, Mazda's director of research and development cited the company's decision to reduce the fuel consumption and emissions of all their vehicles by 30% of the 2008 levels. Until that goal was achieved, the rotary engine would not appear in Mazda's production lineup. However, CEO Yamanouchi stated that as long as he is involved with Mazda, rotary engine development will continue [10, 26].

A new design method called the deviation function (DF) method is developed and applied here to rotary engine design. This method is first introduced to design general rotary profiles that can be for numerous applications. Then the DF method is used to design rotary engines based on the apex seal profile for more engine profile variety and improved sealing. High-conforming housing profiles and different apex seal configurations are introduced for a wider variety of optimal sealing possibilities. Finally, noncircular pitch curves are introduced as another DF method of rotary engine profile design. The contents of this dissertation are organized as follows:

In Chapter 2, the general deviation function method of rotary engine design is introduced and the theory and algorithm are developed in detail. This method provides many more possibilities than the conventional rotary engine design method by using curves in addition to points to generate the conjugate profiles. Three example deviation functions are provided and some example rotary engine profiles are developed for process illustration.

In Chapter 3, the deviation function method of rotary engine design by apex seal profile is introduced and developed in detail. This method designs the profile of the apex seal by selecting the deviation function, then generating the conjugate housing profile. This results in a housing bore that conforms to the apex seal. Two types of apex seal profiles are designed, arc-based and nonarc-based, and both are used to generate example engine profiles.

In Chapter 4, the deviation function method of rotary engine design by geometric parameters is introduced as a new method of profile design that is independent of apex sealing capability. This method selection is for the two profile characteristics specific swept area and maximum theoretical compression ratio. These criteria are related to the overall en-

7

gine performance and can be determined by the geometry of the profiles. As examples, the previously used arc-based and nonarc-based deviation functions are rewritten in terms of the standard geometric parameters: rotor radius and eccentricity. Plots relating the swept area and compression ratio with the DF parameters are provided, along with tables to aid in design selection.

In Chapter 5, an analysis of apex sealing is presented by first examining apex seal interference in conventional rotary engines. Then a sealing index is defined and developed in order to quantify and compare DF-designed engine profiles and the corresponding apex seal profiles. Mazda's rotary engine is used to represent the conventional apex sealing and its technical specifications are used for comparison with similarly-sized DF-designed rotary engines and apex seals.

In Chapter 6, a multi-apex-sealing grid is proposed as a possible alternative to the single apex seal configuration. The multi-apex-sealing grid offers some advantages such as multiple barriers against leakage, and preventing apex seals from experiencing a reversal of resultant force direction, which can cause the seal to separate from the housing bore. Some multi-apex-sealing configurations are provided and the interference is compared to that of a conventional rotary engine.

In Chapter 7, noncircular pitch curves are applied to rotary engine design by using the deviation function method by apex seal profile. This generates more engine profiles with different characteristics, such as a variable speed ratio. These designs require unconventional gearing, but afford manipulation of apex velocities and thermodynamic phase timing. Example engine profiles are developed using an arc-based seal profile.

In Chapter 8, concluding remarks and significant contributions are summarized, and future work on this topic is proposed.

Chapter 2

Deviation Function Method of Rotary Engine Design

The conventional design method of rotary engines is limited to an epitrochoidal housing bore profile and the corresponding inside envelope for the rotor profile. An epitrochoid is found by the path of a single point, and all conventional profiles are derived from this design. To generate new rotary engine profiles, the general deviation function method for rotary engine design is presented here in detail. This is a method of conjugate pair design and can use generating curves to create rotary engine profiles. The deviation function measures the distance between the pitch circle and the profile, modifying the pitch circles of the rotor and housing in order to generate their conjugate profiles. By using curves instead of a single point to generate the profiles, this unconventional method allows for many more profile solutions than what is available to the conventional rotary engine design method. Three example deviation functions are introduced to provide new rotary engine profiles and demonstrate the design process.

2.1 Introduction

The deviation function (DF) method is a relatively new method for conjugate pair design, developed by Yang et al. [42]. The theory is based on reshaping an original pitch curve using a function to measure the amount of deviation. This method has some advantages over conventional methods when applied to involute curves and rotary mechanisms, such as generating many more possible designs, a more intuitive design process, and the incorporation of mechanical properties and analysis during the design process [33]. In addition, the DF method can utilize noncircular pitch curves without higher order nonlinear equations [33]. Tong et al. applied the DF method to lobe pumps and their identical, external pitch curves [33, 41, 35]. Liu et al. used the DF method of lobe pump design to generate trapping-free, high sealing rotors [20]. Yan et al. applied the DF method to circular pitch gerotor design for switch angle assignability [38, 39]. Then Yan et al. developed a methodology for generating noncircular internal pitch curves [38, 40] and then applied the DF method to gerotor pumps [38]. Finally, Tong et al. fully developed the general deviation function algorithm specifically for internal noncircular pitch curves and demonstrated how it applies to gerotor design [34]. Here the deviation function is developed for rotary engine design.

2.2 Deviation Function (DF) Method

A conventional rotary engine is also called the Wankel engine, and it is designed by first generating an epitrochoid for the engine housing. An epitrochoid is generated by a single point attached to a circle that rolls, without slipping, on a stationary circle. These circles are known as generating circles, and the point is called the generating point. The epitrochoid is the locus of the point; in other words, the path of the point traces the epitrochoid. This concept is illustrated in Figure 2.1a. To find the profile of the rotor, the housing profile is rotated using the same pitch circles as the engine gears. The inside envelope of this motion is the conjugate profile of the rotor.

(a) Epitrochoid generated by a point.   (b) Engine housing generated by a curve.
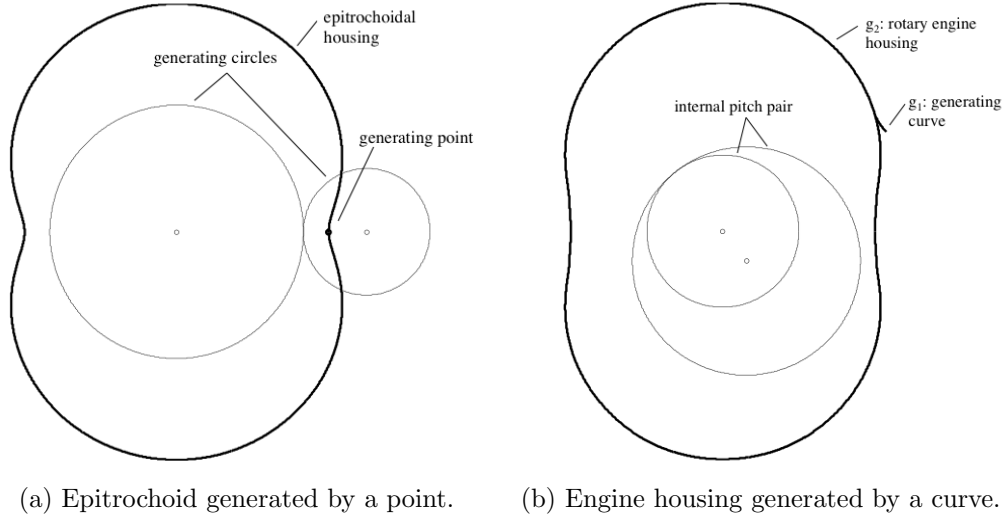
Figure 2.1: Conventional & DF methods for rotary housing generation.

The DF method for rotary engines uses a curve, instead of a point, to generate the 2-lobed engine housing. The internal pitch circles that correspond to the engine's housing and rotor are utilized for the profile generations as shown in Figure 2.1b. Generating curve, g_1, is attached to the larger pitch circle, which has rolling contact with the stationary smaller pitch circle. The envelope of the g_1 curve motion creates a possible housing profile, designated the generated curve g_2.

The DF method is begun by choosing a deviation function, $e_1(\theta_1)$, that defines the radii of deviation circles, shown in Figure 2.2. The centers of the deviation circles lie on pitch circle p_1, and the function e_1 describes the amount of deviation from the original pitch circle as a function of position angle θ_1. All the deviation circles defined by $e_1(\theta_1)$ form a family of curves whose envelopes are shown in heavy and dashed lines, $g_1(\theta_1)$ and $q_1(\theta_1)$. The envelope curve normal is labeled ψ_1 and is also a function of θ_1.

The generating curve is either g_1 or q_1, and once it's determined, it is referred to as g_1. g_1 exists over a certain range, determined by the switch angle, θ_{1s}, illustrated in Figure 2.3. The switch angle determines the conjugating range of the g_1 curve, and so affects the g_2

11
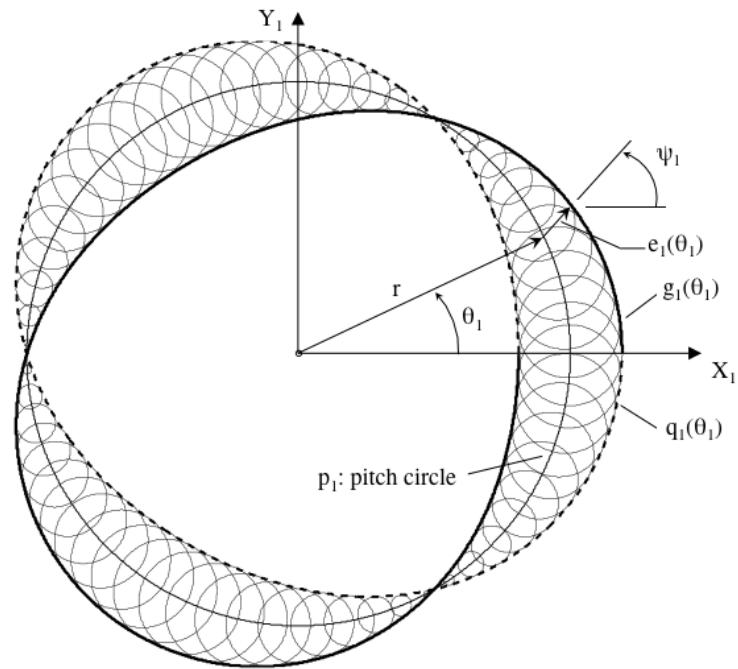
Figure 2.2: Deviation function method.
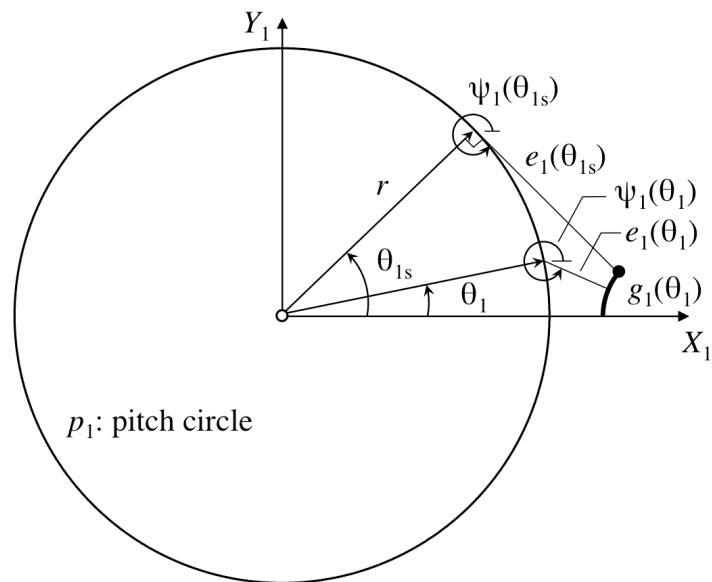
Figure 2.3: Generating curve g_1.

profile. The equation for $g_1(\theta_1)$ is derived from envelope theory:

$$g_{1x} = r_1 \cos\theta_1 + e_1(\theta_1)\cos\psi_1 \qquad (2.1)$$

$$g_{1y} = r_1 \sin\theta_1 + e_1(\theta_1)\sin\psi_1$$

where ψ_1 is the angle of the curve normal in frame $X_1 Y_1$ and is found by:

$$\sin(\psi_1 - \theta_1) = -\frac{e_1(\theta_1)'}{r_1} \qquad (2.2)$$

The two solutions for ψ_1 are:

$$\psi_1 = \theta_1 - \sin^{-1}\frac{e_1'}{r_1} \qquad (2.3a)$$

$$= \theta_1 + \sin^{-1}\frac{e_1'}{r_1} + \pi \qquad (2.3b)$$

where

$$e' = \frac{de}{d\theta_1}$$

The g_1 and q_1 envelopes correspond to equations (2.3a) and (2.3b) respectively.

To apply the DF method, the deviation function $e(\theta_1)$ must be defined over a sufficiently large segment of the pitch curve, it should be a C^1 continuous, monotonically increasing function, and satisfy some kinematic constraints. To ensure the existence of the generating envelopes, the derivative of the deviation function must satisfy:

$$e'^2 \le r_1^2 + r_1'^2$$

Otherwise the normal angle ψ_1 becomes imaginary due to the square root of a negative number. To obtain a smooth profile on the generated housing, e must have C^1 continuity.

So at the switch angle, $\theta_1 = \theta_{1s}$, the deviation function must be zero:

$$e(\theta_{1s}) = 0$$

To obtain a smooth g_2 profile and prevent discontinuities, the generated profile $g_1(\theta_1)$ should be monotonically increasing [33]:

$$e' \leq r_1' \quad \text{and} \quad \psi_1' \leq \frac{\sqrt{r_1^2 + r_1'^2 - e'^2}}{e}$$

$$\text{or} \qquad e' \geq -r_1' \quad \text{and} \quad \psi_1' \geq -\frac{\sqrt{r_1^2 + r_1'^2 - e'^2}}{e}$$

A summary of the boundary conditions for the deviation function is provided in Table 2.1.

Before using g_1 to generate g_2, the location of $g_1(\theta_1 = 0)$ should be checked to prevent loops occurring in the g_2 profile, as shown in Figure 2.5b. These are caused by the generating curve falling inside the p_1 pitch curve by a distance greater than l. In other words, $g_1(\theta_1 = 0)$ lies inside p_2 when p_2 and p_1 are centered at the same origin.

Figure 2.4 illustrates the generation of housing profile g_2. The housing-associated pitch curve p_2 has stationary reference frame $X_2 Y_2$ and the rotor-associated pitch curve p_1 has reference frame $X_1 Y_1$, the g_1 generating curve, and pure rolling contact with p_2. As p_1 rolls on p_2, a family of g_1 curves emerges, whose envelope is the g_2 profile. This envelope can be found by the contact point between g_1 and g_2, denoted point C in Figure 2.4. The normal line n-n at C is normal to both g_1 and g_2 at that point, and contains the instantaneous center I, according to the kinematics of direct contact. It also contains a future instant center, J, implying that the contact point C moves along g_1 in a periodic motion. Thus, a half lobe of the housing profile, from point A_2 to B_2, is described by the contact point moving from one end of the g_1 curve to the other, then back to the beginning again. These two trips are
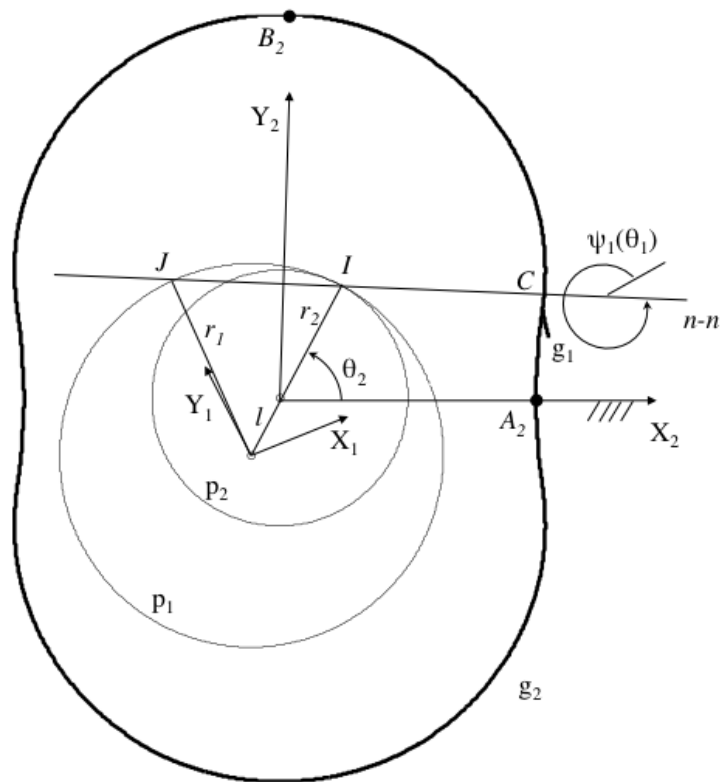
Figure 2.4: Housing profile g_2, generated by g_1.

referred to as forward contact and reverse contact. Forward contact:

$$x_2 = r_2 \cos \theta_2 + e_2 \cos \psi_2 \qquad (2.4)$$

$$y_2 = r_2 \sin \theta_2 + e_2 \sin \psi_2$$

where

$$r_2 = r_1 - l$$

$$e_2 = e_1(\theta_1)$$

$$\theta_2 = \frac{n}{n-1}\theta_1, \qquad 0 \le \theta_1 \le \theta_{ls}$$

$$\psi_2 = \frac{\theta_2}{n} + \psi_1(\theta_1)$$

Reverse contact:

$$x_2^* = r_2 \cos \theta_2^* + e_2^* \cos \psi_2^* \qquad (2.5)$$

$$y_2^* = r_2 \sin \theta_2^* + e_2^* \sin \psi_2^*$$

where

$$\theta_2^* = \frac{n}{n-1}(2\psi_1 - \theta_1 - \pi)$$

$$\psi_2^* = \frac{\theta_2^*}{n} + \psi_1(\theta_1)$$

$$e_2^* = e_1(\theta_1) + IJ, \quad 0 \le \theta_1 \le \theta_{ls}$$

$$IJ = 2r_1 \cos(\psi_1 - \theta_1)$$

For a smooth gerotor profile the forward and reverse contact of g_2 generation must be continuous at the switch point, angle θ_{1s}. The curve will be smooth if the curve normal angle, $\psi_2(\phi_2)$, is continuously differentiable, a constraint for $\psi_1(\theta_1)$, from the above equations. The function $\psi_1(\theta_1)$ decreases as θ_1 increases, reaching its minimum at the switch point,

16

$\theta_1 = \theta_{1s}$. So at the switch angle, when ψ_1 reaches its minimum value and reverses direction, the following constraint must be true:

$$\psi_1'(\theta_{1s}) = \frac{d\psi_1}{d\theta_1}(\theta_{1s}) = 0$$

Differentiating both sides of equation (2.2) with respect to θ_1 and solving for $\psi_1'(\theta_1)$:

$$\frac{d\psi_1}{d\theta_1} = 1 - \frac{e_1''}{r_1 \cos(\psi_1 - \theta_1)} \tag{2.6}$$

Evaluating equation (2.6) at θ_{1s}:

$$\frac{e_1''(\theta_{1s})}{r_1 cos(\psi_1(\theta_{1s}) - \theta_{1s})} = 1 \tag{2.7}$$

where $\psi_1(\theta_{1s}) - \theta_{1s} = 3\pi/2$, so the following constraint must be true:

$$e_1''(\theta_{1s}) = 0 \tag{2.8}$$

Applying L'Hopital's Rule to evaluate equation (2.7),

$$\lim_{\theta_1 \to \theta_{1s}} \frac{e_1''}{r_1 \cos(\psi_1 - \theta_1)} = \lim_{\theta_1 \to \theta_{1s}} \frac{e_1'''}{-r_1 \sin(\psi_1 - \theta_1)(\psi_1' - \theta_1)} = 1$$

Yields a final kinematic constraint on deviation function e_1:

$$e_1'''(\theta_{1s}) = -r_1 \tag{2.9}$$

This ensures that the whole g_2 rotor will have C^1 continuity. Although a C^1 continuous function is described as smooth, it can still have areas where the radius of curvature approaches zero. These places are called cusps and an example is shown in Figure 2.5a. The following formula can be used to check the g_2 radius of curvature, ρ_{g_2}, for any angle using

(a) g_2 containing cusps (b) g_2 crossing over itself
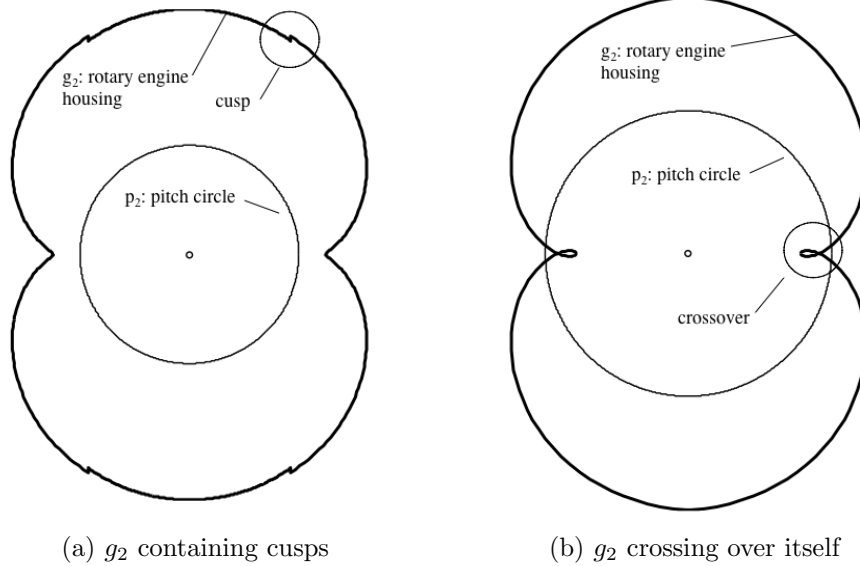
Figure 2.5: A housing profile cannot contain cusps or cross over itself.

the deviation function:

$$\rho_{g_2} = \cfrac{1}{\cfrac{\left(\frac{1}{r_1-l} - \frac{1}{r_1}\right)}{\cos(\psi_1 - \theta_1)} - \cfrac{1}{e_1 + d_{IJ} + \rho_{g_1}}} + e_1 + d_{IJ} \qquad (2.10)$$

where $\rho_{g_1} = r_1 \cos(\psi_1 - \theta_1)/\psi_1' - e_1$, $d_{IJ} = 0$ for the forward contact portion of g_2, and $d_{IJ} = IJ$ for the reverse contact portion of g_2.

The rotor profile is found from generating curve g_3, a half lobe of the rotor. g_3 is part of the inside envelope of the housing g_2 as it is rolled by its pitch curve p_2, as shown in Figure 2.6. Now the stationary frame is X_1Y_1 and X_2Y_2 is moving. The contact point C_3 is a point on g_2 and g_3 and the normal line n-n has angle ψ_2 and the two instant centers, I and I_3, fall on the line.

$$x_3 = r_1 \cos \phi_1 + e_3 \cos \psi_3 \qquad (2.11)$$

$$y_3 = r_1 \sin \phi_1 + e_3 \sin \psi_3$$

18

where

$$\phi_1 = \frac{n-1}{n}\theta_2^*$$

$$\psi_3 = \psi_2^* - \frac{\phi_1}{n-1}$$

$$e_3 = e_2 + II_3$$

$$II_3 = -2r_2\sin(\theta_2^* - \theta_2)$$

Figure 2.6: Rotor profile g_3, generated by g_2.

Once the inside envelope, g_3, has been determined, it must be verified as a hypothetical rotor. The geometric criterion for a rotary engine profile requires the rotor maintain contact with the housing at all three apexes. This is crucial for two reasons: there must be three enclosed chambers at all times between the rotor and the housing; and the motion of a

(a) g_3 apex breaches housing profile   (b) g_3 apex not in contact with housing
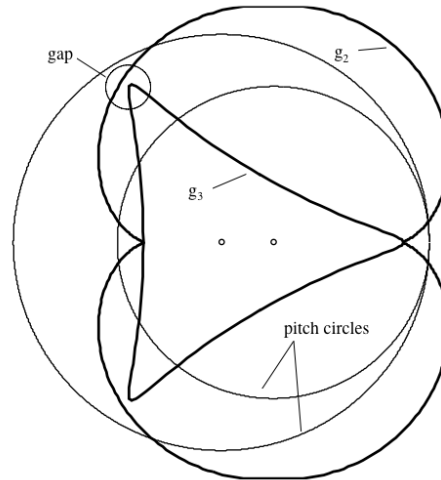
Figure 2.7: The rotor apexes must maintain contact with the housing profile.

hypothetical rotor must be confined to within the housing profile. Figure 2.7 shows profile results that cannot be used as rotary engines. In Figure 2.7a, the rotor profile does not lie within the housing profile and Figure 2.7b shows a rotor with 2 apexes not in contact with the housing profile.

Table 2.1: Deviation function algorithm for rotary engine design

Step 1: select number of lobes	$n = 3$ for rotary engine
Step 2: select e_1 satisfying	$e_1'(0) = 0$
	$e_1'(\theta_{1s}) = r_1$
	$e_1''(\theta_{1s}) = 0$
	$e_1'''(\theta_{1s}) = -r_1$
Step 3: obtain g_1	Generating curve: g_1 or q_1
Step 4: check for crossovers	g_1 lies outside p_2
Step 5: obtain g_2	Generated housing: g_2
Step 6: check for cusps on g_2	$\rho_{g_2} \neq 0$
Step 7: obtain g_3	Inside envelope of g_2
Step 8: check g_3 apex contact	

2.3 Examples of rotary engine design

2.3.1 A 4th order polynomial deviation function

In this example, the deviation function is selected to be a 4th order polynomial. A possible generating curve resulting from this deviation function is shown in Figure 2.8.

$$e_1(\theta_1) = r_1(a_4\theta_1^4 + a_3\theta_1^3 + a_2\theta_1^2 + a_1\theta_1 + a_0), \qquad 0 \leq \theta_1 \leq \theta_{1s} \qquad (2.12)$$

The coefficients are found by applying the boundary conditions summarized in Table 2.1.

$$a_4 = \frac{1}{8\theta_{1s}}\left(1 - \frac{2}{\theta_{1s}}\right)$$

$$a_3 = -\frac{1}{3} + \frac{1}{\theta_{1s}}$$

$$a_2 = 0.25\theta_{1s} - \frac{1.5}{\theta_{1s}}$$

$$a_1 = 0$$

The parameters θ_{1s} and a_0 are free parameters and are used to generate different rotary engine profiles.
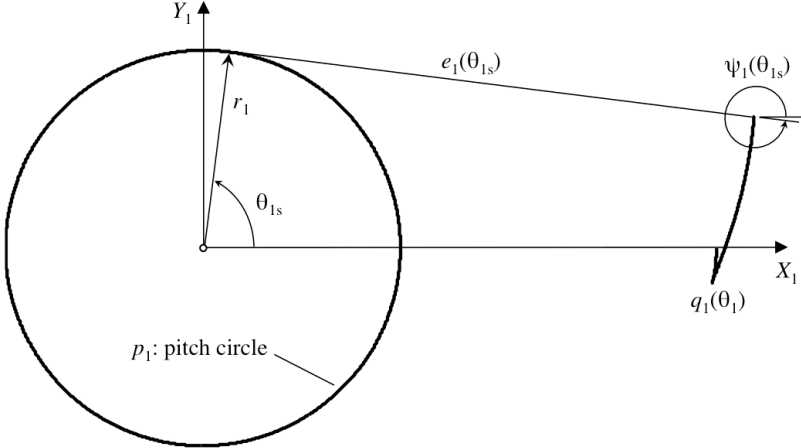
Figure 2.8: Polynomial deviation function e_1 and a nonarc generating curve.

Some example engine profiles are shown in Figure 2.9 along with the corresponding parameters in Table 2.2.

(a)   (b)   (c)
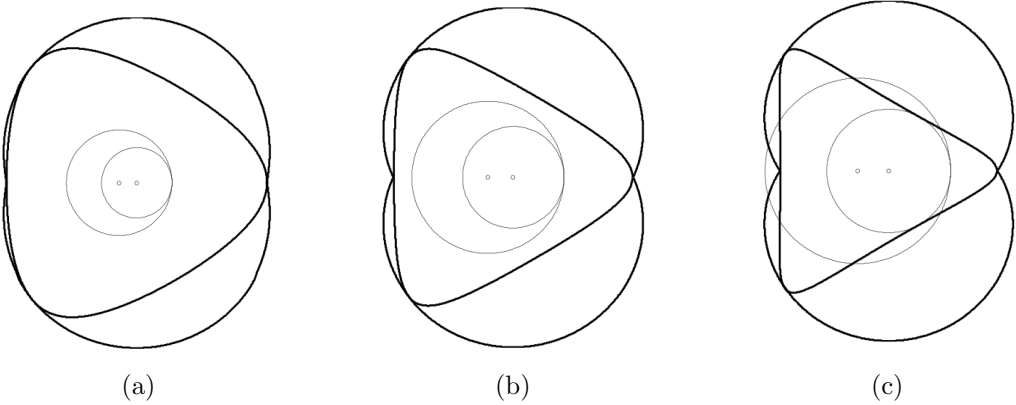
Figure 2.9: Rotary engine profiles from a 4th order polynomial DF.

Table 2.2: Deviation function parameters for Figure 2.9

Figure No.	n	l	θ_{1s}	a_0
Fig. 2.9a	3	1	$\pi/3$	-1.8
Fig. 2.9b	3	1	$\pi/3.5$	-0.9
Fig. 2.9c	3	1	$\pi/4$	-0.5

Table 2.3: Deviation function parameters for Figure 2.11

Figure No.	n	l	θ_{1s}	a_0
Fig. 2.11a	3	1	$\pi/4.8$	-2.2
Fig. 2.11b	3	1	$\pi/5.5$	-3
Fig. 2.11c	3	1	$\pi/4$	-1

2.3.2 A nonarc-based sinusoidal deviation function

For this example, a sinusoidal deviation function is used that results in an oval generating curve. A possible generating curve from this deviation function is shown in Figure 2.10.

$$e_1(\theta_1) = r_1(a_3 \cos^3 \theta_1 + a_2 \cos^2 \theta_1 + a_1 \cos \theta_1 + a_0), \qquad 0 \leq \theta_1 \leq \theta_{1s} \qquad (2.13)$$

After applying the boundary conditions summarized in Table 2.1, the coefficients in this deviation function are:

$$a_3 = \frac{\cos^2 \theta_{1s}}{2 \sin^5 \theta_{1s}}$$

$$a_2 = \frac{\cos \theta_{1s}}{2 \sin^3 \theta_{1s}} - 3a_3 \cos \theta_{1s}$$

$$a_1 = \frac{1}{\sin \theta_{1s}} - 3a_3 \cos^2 \theta_{1s} - 2a_2 \cos \theta_{1s}$$

Some engine profile results are shown in Figure 2.11 and the corresponding deviation function parameters are given in Table 2.3.
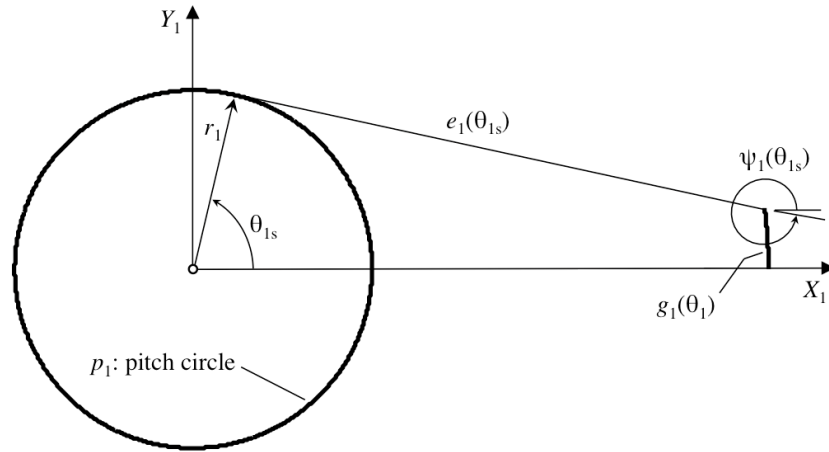
Figure 2.10: Sinusoidal deviation function e_1 and a nonarc generating curve.

(a)   (b)   (c)
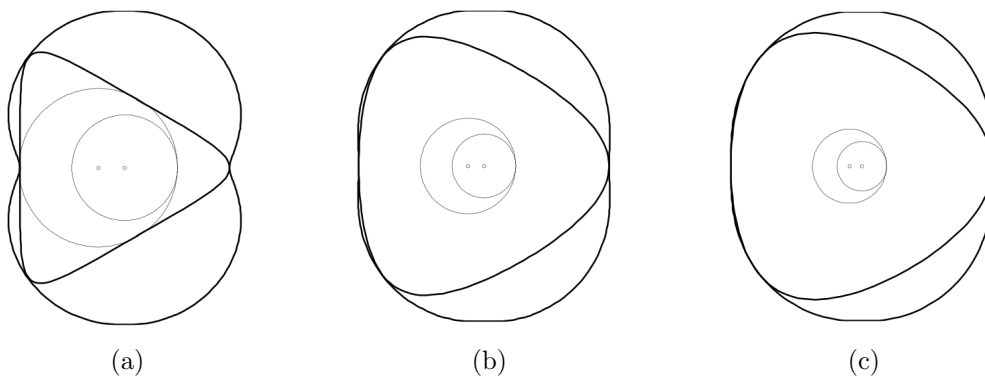
Figure 2.11: Rotary engine profiles from a nonarc-based sinusoidal DF.

2.3.3 An arc-based deviation function

For this example, an arc-based deviation function is found for defining a circular arc generating curve. As shown in Figure 2.12, a free parameter ρ represents the radius of the generating arc g_1, and free parameter a is the distance between the pitch circle center and the arc center.
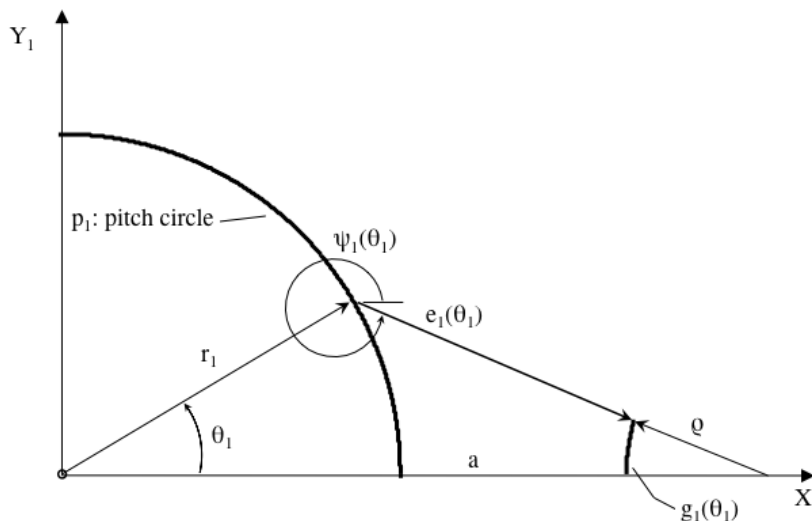
Figure 2.12: Deviation function e_1 for a circular arc generating curve.

$$e_1(\theta_1) = \sqrt{a^2 + r_1^2 - 2ar_1\cos(\theta_1)} - \rho \qquad 0 \leq \theta_1 \leq \theta_{1s} \qquad (2.14)$$

The sign of ρ determines whether the generating curve is convex or concave. For the convex configuration, shown in Figure 2.12, a positive ρ value is subtracted in the equation (2.14). For the concave configuration, not shown, a positive ρ would be added in equation (2.14). The switch angle is directly calculated by $\theta_{1s} = \cos^{-1}(\frac{r_1}{a})$, and thus θ_{1s} can be manipulated. Figure 2.13 shows some example engine profiles and Table 2.4 provides the corresponding DF equation values.

<div style="text-align:center">(a)   (b)   (c)</div>
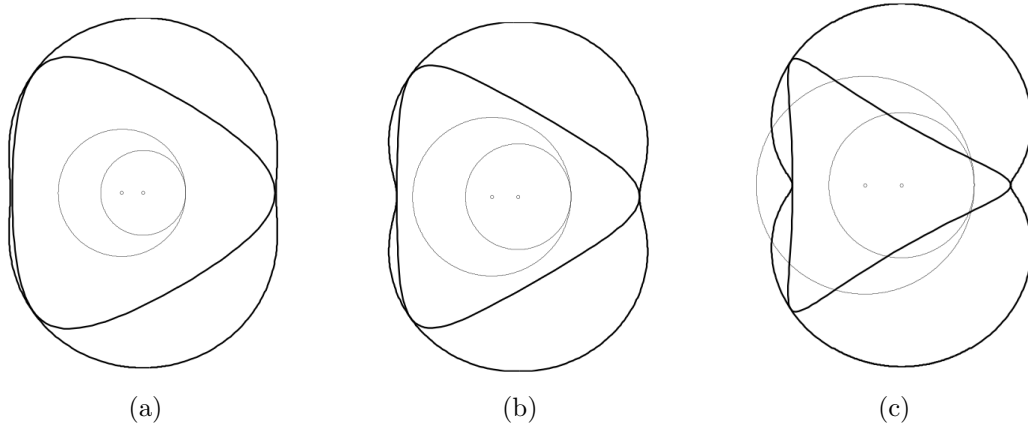
Figure 2.13: Rotary engine profiles from an arc-based DF.

Table 2.4: Deviation function parameters for Figure 2.13

Figure No.	n	l	a	ρ
Fig. 2.13a	3	2	15	0.5
Fig. 2.13b	3	.5	10	7.2
Fig. 2.13c	3	1.2	5	0.2

2.4 Conclusions

Conventional rotary engine design is limited to epitrochoids for the housing bore profiles, which are generated by a single point. The conjugate rotor profile is found by the inside envelope of the epitrochoid. The variety of profiles by this method is further limited by the practicality of implementation, resulting in profile similarity among rotary engines. The inflexibility of these designs prevents specialization or optimization of performance characteristics. The DF method of rotary engine design generates new rotary engine profiles. The fundamental difference between the DF method and the conventional method is the DF method can generate profiles from curves and points, and there are many possibilities for the generating curve. The deviation function method is derived and applied here to rotary engine design and the entire algorithm is summarized in eight steps. To illustrate the design process, three example deviation functions are introduced and used to generate possible en-

<div style="text-align:center">26</div>

gine profiles. Many more designs can be found by changing the DF parameters and by using other deviation functions. The number and variety of profiles available by this method are much greater than by the conventional design method. Also by using the DF method, the free parameters of the function can be used to make methodical adjustments and affect the profile geometry. This will also affect the mechanical properties and performance characteristics. With this new design method and the increased variety for rotary engine profiles the rotary engine can be modified and optimized beyond the conventional design.

Chapter 3

DF Engine Design by Apex Seal Profile

Conventional rotary engines are based on a trochoidal-type housing bore profile and its inside envelope is the basis of the rotor profile. To seal the chambers, spring-loaded apex seals are used in place of the designed rotor apexes. The conventional design method is limited to an epitrochoidal-based housing and does not consider the apex seal profile. For the first time, complete theory and algorithm are developed for the design of rotary engines based on the apex seal profile. This method, based on the deviation function (DF) method of conjugate pair design, generates the engine housing that is conjugate to the apex seal. A larger variety of engine profiles can be found by using the DF method of rotary engine design, and designing by apex seal results in the housing profile conforming to the seal profile. Some example results from arc-based and nonarc-based apex seal profiles are provided for design and process illustration.

3.1 Introduction

The conventional rotary engine profiles are based on a two-lobed epitrochoid and its inside envelope, which become the housing bore and rotor profiles, respectively. This rotor design

has three apexes that maintain contact with the housing throughout the planetary rotation [8]. For practical applications, instead of the true trochoid and its envelope, a parallel trochoid is used, along with a parallel envelope [37]. This allows some clearance between the engine housing and rotor; then to seal the three chambers, sliding apex seals are inserted into the rotor apexes. The seals are spring-loaded so they will maintain contact with the housing as much as possible during rotation [37, 1, 24].

The conventional method of rotary engine design cannot consider the profile of an apex seal and is strictly limited to epitrochoidal-type housing profiles, defined by two independent lengths [8]. In order to incorporate the profile of the apex seal into the design process, this paper introduces a new method for rotary engine design. This design process first applies the deviation function (DF) method of conjugate curve design to the geometry of the apex seal profile, then generates the conjugate housing, and lastly the conjugate rotor flanks. Because the engine housing design is based on the apex profile, better housing-to-rotor conformity can be achieved, and therefore sealing capability can be improved. This improved apex sealing will improve engine efficiency and reduce the forces on the apex seals. This will reduce wear on the seals and inside the housing, and improve the longevity of the engine. The incorporation of apex seal profiles into the rotary engine design process also makes a larger variety of new rotary engine profiles possible.

The deviation function (DF) method is a relatively new method for conjugate pair design, originally developed by Yang et al. [42]. The theory is based on reshaping an original pitch curve using a function to measure the amount of deviation. This method has some advantages over conventional methods when applied to involute curves and rotary mechanisms, such as an increase in the possible designs, a more intuitive design process, incorporation of mechanical properties and analysis during the design process, and the ability to utilize noncircular pitch curves without high order nonlinear equations [33]. Tong applied the DF method to lobe pumps and their identical, external pitch curves [33]. Yan et al. developed a methodology for generating noncircular internal pitch curves in [40] and then applied the

29

DF method to gerotor pumps [38]. Finally, Tong et al. fully developed the general deviation function algorithm specifically for internal noncircular pitch curves and demonstrated how it applies to gerotor design [34]. Here the deviation function is developed for rotary engine design by apex seals.

3.2   Rotary Engine Design by Apex Seal Profile

The deviation function method of rotary engine design described previously has many possibilities for the deviation function, the generating curve, and the resulting designs. This chapter introduces a useful variation in the method and how to apply it for a specific design purpose. So far, the steps of the deviation function method have followed the design steps of the conventional rotary engine; first the housing profile, then the rotor profile, are generated from the internal envelope. This section describes how to apply the deviation function method to design the apexes of the rotor, which are always in contact with the engine housing. In an actual engine, these apexes are replaced by seals to prevent gas leaks between adjacent chambers. Analogous to piston rings in a reciprocating engine, the apex seals are crucial to the engine's operation, efficiency, and longevity [1, 37]. Here, the deviation function method is used to design the apexes of the rotor first, then the housing, as a conjugate curve.

3.2.1   Design the generating curve g_1, the apex seal

The apex seals of a rotary engine are cylindrical steel inserts, shown in Figure 3.1, that are in contact with the engine housing as the rotor moves. There are three rotor apexes and each one has a single apex seal. If the rotor profile is positioned as in Figure 3.2, then the seal is a small curve symmetrical about the X_1 axis. To design the rotary engine based on the apex seal, the generating curve g_1 is designed as the profile of the lower half of the apex seal. To be the profile of an apex seal, g_1 must be relatively small, below the X_1 axis,
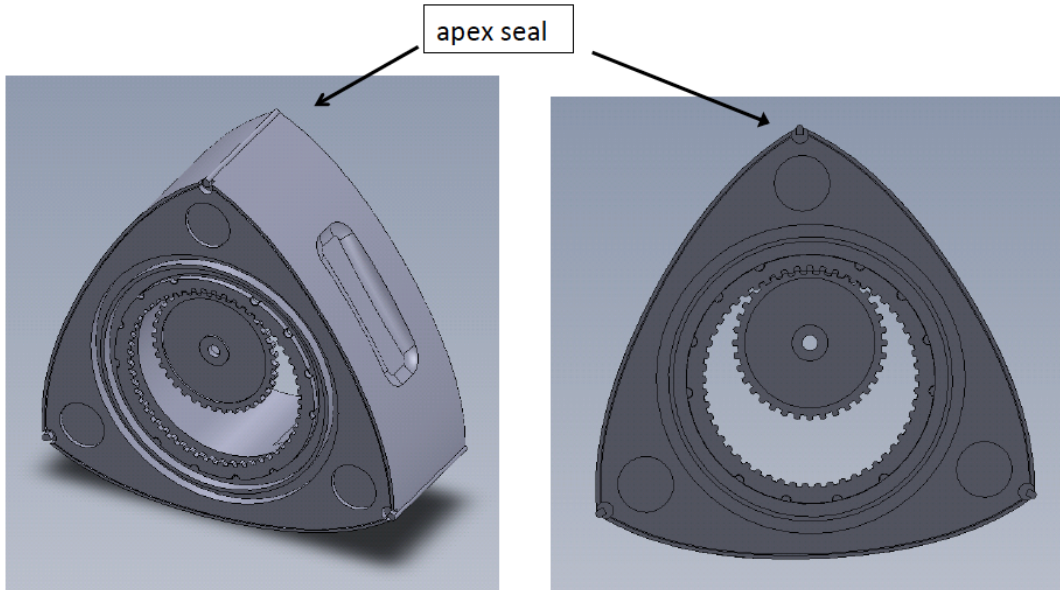
Figure 3.1: CAD model of a conventional rotor with the apex seal.

and concave. It must also be positioned appropriately; its location will determine the rotor radius. Figure 3.3 shows the design of the g_1 curve from an arc-based deviation function $e_1(\theta_1)$.
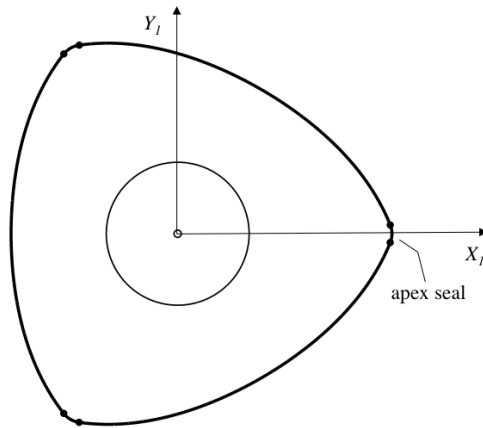
Figure 3.2: Apex seal locations on a rotor.

For the apex seal design, the generating curve g_1 is an inside envelope. The equation for
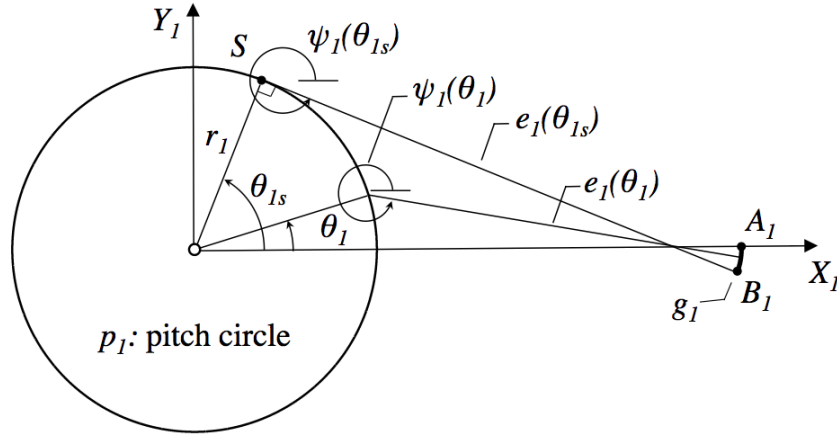
Figure 3.3: Generating curve g_1 is designed as half of an apex seal.

$g_1(\theta_1)$ is derived from envelope theory:

$$g_{1x} = r_1 \cos\theta_1 + e_1(\theta_1)\cos\psi_1 \tag{3.1}$$

$$g_{1y} = r_1 \sin\theta_1 + e_1(\theta_1)\sin\psi_1$$

where ψ_1 is the angle of the curve normal in frame X_1Y_1 and is found by:

$$\sin(\psi_1 - \theta_1) = -\frac{e_1(\theta_1)'}{r_1} \tag{3.2}$$

The solution for ψ_1 is found by solving the following equation:

$$\psi_1 = \theta_1 - \sin^{-1}\frac{e_1'}{r_1}$$

where

$$e' = \frac{de}{d\theta_1}$$

In order to apply the DF method, the deviation function $e(\theta_1)$ must be defined over a sufficiently large segment of the pitch curve, and be a C^1 continuous, monotonically increasing function. Also, to ensure the existence of the generating envelopes, the derivative of the

32

deviation function must satisfy:

$$e'^2 \leq r_1^2 + r_1'^2$$

Otherwise the normal angle ψ_1 becomes imaginary due to the square root of a negative number. To obtain a smooth profile on the generated housing, $e_1(\theta_1)$ must have C^1 continuity. Therefore, at the switch angle, $\theta_1 = \theta_{1s}$, the deviation function must be zero:

$$e(\theta_{1s}) = 0$$

To obtain a smooth g_2 profile and avoid discontinuities, the generated profile $g_1(\theta_1)$ should be monotonically increasing [33]:

$$e' \leq r_1' \quad \text{and} \quad \psi_1' \leq \frac{\sqrt{r_1^2 + r_1'^2 - e'^2}}{e}$$

$$\text{or} \qquad e' \geq -r_1' \quad \text{and} \quad \psi_1' \geq -\frac{\sqrt{r_1^2 + r_1'^2 - e'^2}}{e}$$

A summary of the kinematic constraints and boundary conditions for the deviation function method is provided in Table 3.1.
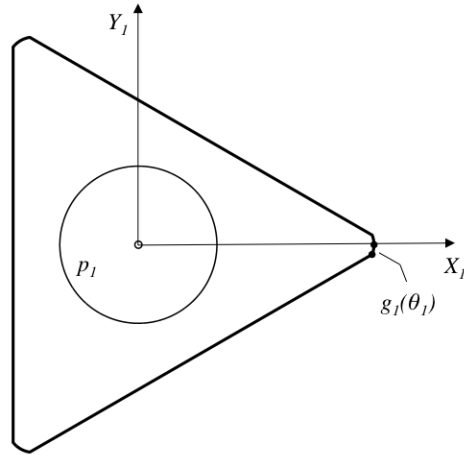
Figure 3.4: Three apex seals joined by straight lines to form a basic rotor.

Once the generating curve g_1 has been determined, a hypothetical rotor can be drawn using only the apex seals. By connecting the three apex seals with straight lines, as drawn in

33

Figure 3.4, a simple rotor is created. This rotor is possible because the only part of a rotor that has contact with the housing is the apex seals. The flanks of the rotor can be straight lines, under-cuts (meaning concave), or over-cuts (meaning convex). In conventional rotary engine design, the rotor is the inside envelope of the housing, which is an over-cut, making the rotor as large as possible.

3.2.2 Design the generated curve g_2, the engine housing
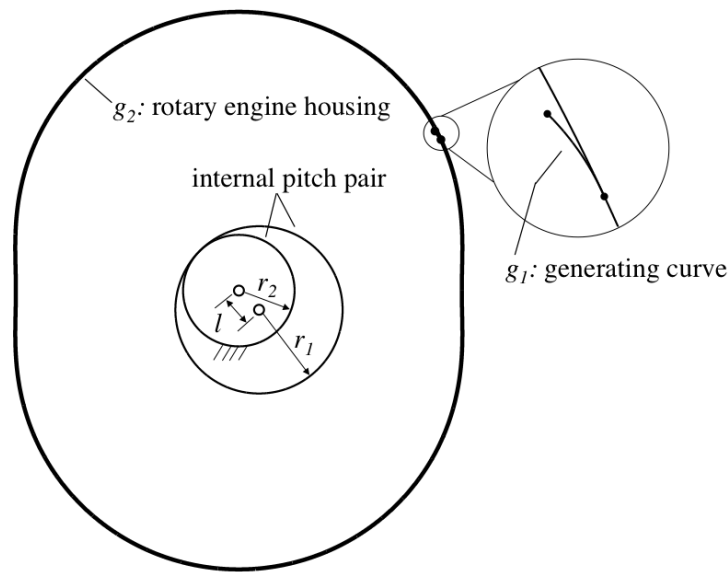
Figure 3.5: Generating g_2 from the apex seal, g_1.

Figure 3.5 shows the conjugate curve g_2 is generated by g_1. The pitch curve of g_1 is rolled around the pitch curve of g_2 in the same sense the rotor rotates inside an engine. The housing bore profile g_2 is the envelope of the apex seal profile, g_1. Figure 3.5 depicts the generation of housing profile g_2. The housing pitch curve p_2 has a stationary reference frame X_2Y_2 and the rotor pitch curve p_1 has moving reference frame X_1Y_1. The pitch pair have pure rolling contact. As p_1 rolls on p_2, a family of g_1 curves emerges, whose envelope is the g_2 profile. This envelope can be found by the contact point between g_1 and g_2, denoted point C in Figure 3.6. The normal line n-n at C is normal to both g_1 and g_2, and identifies two instantaneous centers, I and J, according to the kinematics of direct contact. In Figure 3.6, the current

instant center is J and the previous instant center is I. This means that Figure 3.6 is showing a position of reverse contact. In other words, the point C has travelled to the farthest point on the apex seal and is now returning to the beginning. These two trips are referred to as forward contact and reverse contact.

Forward contact:

$$x_2 = r_2 \cos \theta_2 + e_2 \cos \psi_2 \tag{3.3}$$

$$y_2 = r_2 \sin \theta_2 + e_2 \sin \psi_2$$

where

$$r_2 = r_1 - l$$

$$e_2 = e_1(\theta_1)$$

$$\theta_2 = \frac{n}{n-1}\theta_1, \qquad 0 \le \theta_1 \le \theta_{ls}$$

$$\psi_2 = \frac{\theta_2}{n} + \psi_1(\theta_1)$$

Reverse contact:

$$x_2^* = r_2 \cos \theta_2^* + e_2^* \cos \psi_2^* \tag{3.4}$$

$$y_2^* = r_2 \sin \theta_2^* + e_2^* \sin \psi_2^*$$

where

$$\theta_2^* = \frac{n}{n-1}(2\psi_1 - \theta_1 - \pi)$$

$$\psi_2^* = \frac{\theta_2^*}{n} + \psi_1(\theta_1)$$

$$e_2^* = e_1(\theta_1) + IJ, \qquad 0 \le \theta_1 \le \theta_{ls}$$

$$IJ = 2r_1 \cos(\psi_1 - \theta_1)$$

35

Figure 3.6: Generation of the housing bore profile g_2.

For a smooth engine housing profile, the forward and reverse contact of apex seal g_1 must be continuous at the switch point, angle θ_{1s}. The g_2 curve will be smooth if the curve normal angle, $\psi_2(\phi_2)$, is continuously differentiable. From the g_2 equations, this is a constraint for $\psi_1(\theta_1)$. The function $\psi_1(\theta_1)$ decreases as θ_1 increases, reaching its minimum at the switch point, $\theta_1 = \theta_{1s}$. Therefore at the switch angle, when ψ_1 reaches its minimum value and reverses direction, the following constraint must be true:

$$\psi_1'(\theta_{1s}) = \frac{d\psi_1}{d\theta_1}(\theta_{1s}) = 0$$

Differentiating both sides of equation (3.2) with respect to θ_1 and solving for $\psi_1'(\theta_1)$:

$$\frac{d\psi_1}{d\theta_1} = 1 - \frac{e_1''}{r_1 \cos(\psi_1 - \theta_1)} \tag{3.5}$$

36

Evaluating equation (3.5) at θ_{1s}:

$$\frac{e_1''(\theta_{1s})}{r_1 cos(\psi_1(\theta_{1s}) - \theta_{1s})} = 1 \tag{3.6}$$

where $\psi_1(\theta_{1s}) - \theta_{1s} = 3\pi/2$, so the following constraint must be true:

$$e_1''(\theta_{1s}) = 0 \tag{3.7}$$

Applying L'Hopital's Rule to evaluate equation (3.6),

$$\lim_{\theta_1 \to \theta_{1s}} \frac{e_1''}{r_1 \cos(\psi_1 - \theta_1)} = \lim_{\theta_1 \to \theta_{1s}} \frac{e_1'''}{-r_1 \sin(\psi_1 - \theta_1)(\psi_1' - \theta_1)} = 1$$

Yields the final kinematic constraint on deviation function e_1:

$$e_1'''(\theta_{1s}) = -r_1 \tag{3.8}$$

3.2.3 Design the generated curve g_3, the rotor flank

The rotor profile is found by generating curve g_3, a half lobe of the rotor. g_3 is from the inside envelope of the housing g_2 as its pitch curve, p_2, is rolled on p_1. The inside envelope is determined only by the forward contact portion of the g_2 curve, denoted $g_{2forward}$, now the generating curve. In Figure 3.7, there is pure rolling contact between p_1 and p_2, and the X_1Y_1 frame is stationary while X_2Y_2 is moving. The contact point C_3 is a point on $g_{2forward}$ and g_3, and the normal line n-n has angle ψ_3^*, as indicated. There are two instant centers, I and I_3, that fall on the line. The position shown in Figure 3.7 has instant center I_3, and instant center I is a previous one. Analogous to the generation of the g_2 housing curve, the contact on $g_{2forward}$ is also periodical. The forward contact points retrace the original g_1 apex seal, as expected, since this is the reverse of the process that generated $g_{2forward}$ from g_1. The reverse contact points generate the rotor flank, g_3.

37
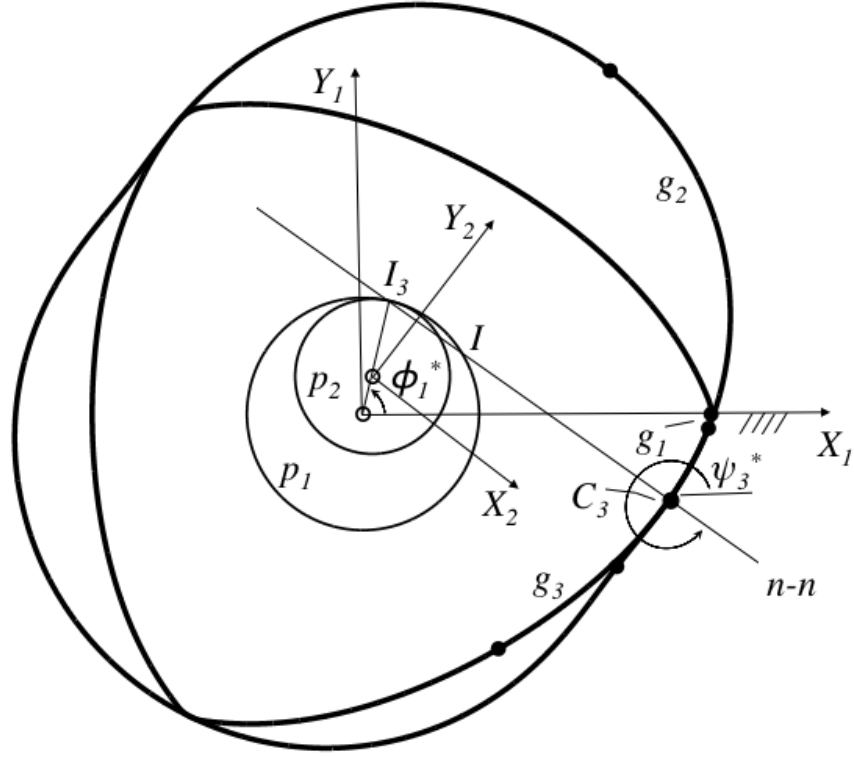
Figure 3.7: Generating rotor flanks, conjugate curve g_3.

Forward Contact:

$$x_3 = r_1 \cos \phi_1 + e_3 \cos \psi_3 \qquad (3.9)$$

$$y_3 = r_1 \sin \phi_1 + e_3 \sin \psi_3$$

where

$$\phi_1 = \frac{n-1}{n} \theta_2$$

$$\psi_3 = \psi_2 - \frac{\phi_1}{n-1}$$

$$e_3 = e_2$$

38

Reverse Contact:

$$x_3^* = r_1 \cos \phi_1^* + e_3^* \cos \psi_3^* \tag{3.10}$$

$$y_3^* = r_1 \sin \phi_1^* + e_3^* \sin \psi_3^*$$

where

$$\phi_1^* = \frac{n-1}{n} \theta_2$$

$$\psi_3^* = \psi_2 - \frac{\phi_1^*}{n-1}$$

$$e_3^* = e_2 + I_3 I$$

$$I_3 I = 2 r_2 \sin(\psi_2 - \theta_2)$$
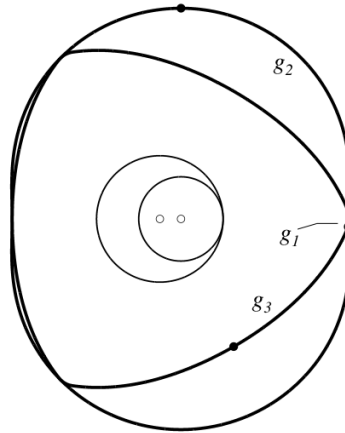
Figure 3.8: DF-designed rotary engine profile.

Figure 3.8 shows a complete rotary engine profile, designed and generated by the apex seal. The curves g_1, g_2, and g_3 are all identified as half-lobes of the apex seal, housing, and rotor flank, respectively.

Table 3.1: DF algorithm for rotary engine design by apex seal

Step 1: Select number of lobes	$n = 3$ for rotary engine
Step 2: Select e_1 satisfying	$e_1'(0) = 0$
	$e_1'(\theta_{1s}) = r_1$
	$e_1''(\theta_{1s}) = 0$
	$e_1'''(\theta_{1s}) = -r_1$
Step 3: Obtain g_1 satisfying	Positioned below the X_1 axis
	Concave
	Apex seal length
	Rotor radius distance from origin
Step 4: Obtain g_2	Outside envelope of g_1
Step 5: Obtain g_3	Inside envelope of $g_{2forward}$

3.3 Examples of rotary engine design

3.3.1 An arc-based deviation function

An arc-based apex seal profile will result from an arc-based deviation function. Equation (3.11) was derived for a circular arc generating curve. As shown in Figure 3.9, a free parameter ρ represents the radius of the generating arc g_1, and therefore also the radius of the apex seal profile. The free parameter a is the distance between the pitch circle center and the arc center. The rotor radius is $a - \rho$ (scaled to an eccentricity of 1), where ρ is negative for a concave generating curve.

$$e_1(\theta_1) = \sqrt{a^2 + r_1^2 - 2ar_1 \cos(\theta_1)} - \rho \qquad 0 \leq \theta_1 \leq \theta_{1s} \qquad (3.11)$$

The switch angle is the crankshaft position (rotor's center position) at which the contact point on the apex seal reverses direction, and it governs the conjugating range between the housing and the rotor. This is calculated by $\theta_{1s} = \cos^{-1}(\frac{r_1}{a})$, and can thus be manipulated. Figure 3.10 shows the resulting engine profiles for three different apex seal profiles. Table 3.2

Table 3.2: Deviation function parameters for Figure 3.10

Figure No.	n	l	a	ρ	θ_{1s}
Fig. 3.10a	3	1	8	-1	68°
Fig. 3.10b	3	1	9	-0.1	71°
Fig. 3.10c	3	1	6	-2	60°

provides the DF equation parameters corresponding to Figure 3.10. For conventional rotary engines, the number of lobes is $n = 3$ and the pitch radii ratio is 2:3, so here $l = 1$ for all the examples. The eccentricity and number of lobes can be changed for other rotary mechanisms or modified rotary engines because l and n are free parameters that can be chosen.
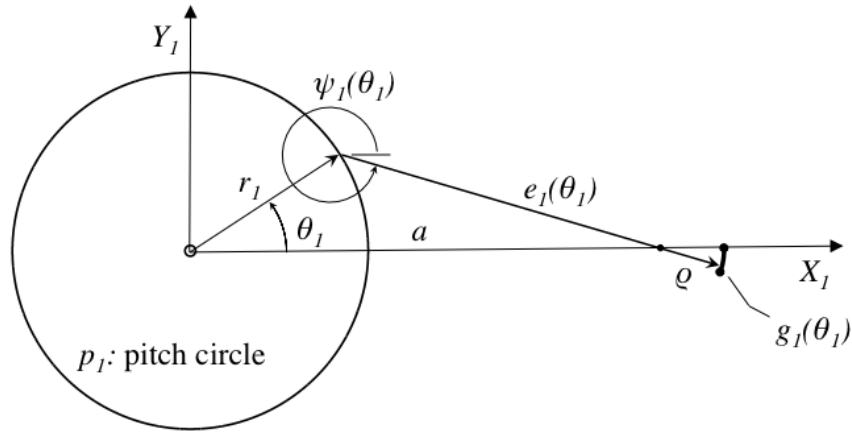
Figure 3.9: Arc-based apex seal profile.

3.3.2 A nonarc-based sinusoidal deviation function

For a nonarc-based apex seal, a nonarc-based deviation function is provided here as an example. Equation (3.12) is a sinusoidal deviation function that has an oval-shaped envelope and therefore results in an oval generating curve. The generating curves of this deviation function come from the inside envelope of the deviation circles, $q_1(\theta_1)$. A possible generating
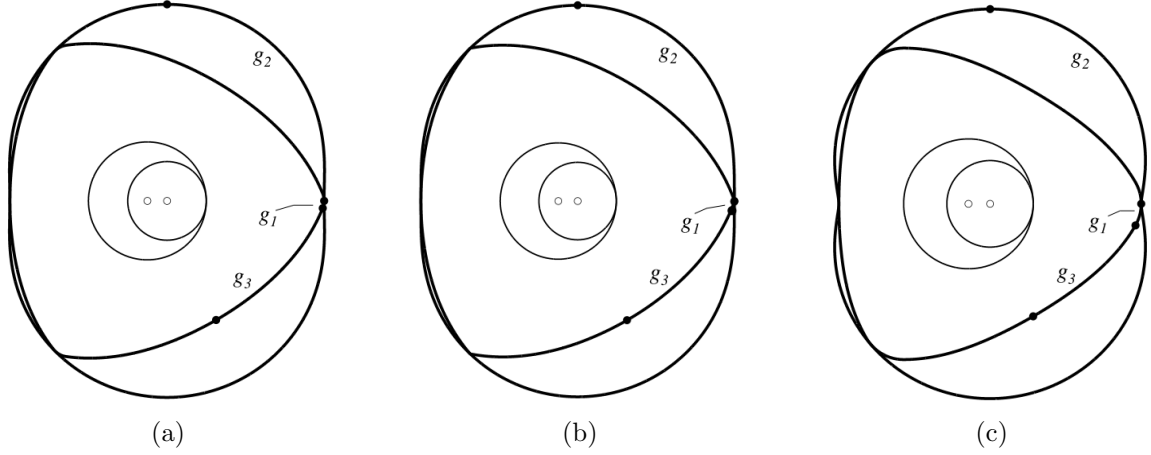
Figure 3.10: Rotary engine profiles designed by apex seal.

curve is shown in Figure 3.11.

$$e_1(\theta_1) = r_1(a_3 \cos^3 \theta_1 + a_2 \cos^2 \theta_1 + a_1 \cos \theta_1 + a_0), \quad 0 \leq \theta_1 \leq \theta_{1s} \tag{3.12}$$

After applying the boundary conditions summarized in Table 3.1, the coefficients in this deviation function are:

$$a_3 = \frac{\cos^2 \theta_{1s}}{2 \sin^5 \theta_{1s}}$$

$$a_2 = \frac{\cos \theta_{1s}}{2 \sin^3 \theta_{1s}} - 3a_3 \cos \theta_{1s}$$

$$a_1 = \frac{1}{\sin \theta_{1s}} - 3a_3 \cos^2 \theta_{1s} - 2a_2 \cos \theta_{1s}$$

The free parameters for this deviation function are n, l, θ_{1s}, and a_0. For conventional rotary engines, $n = 3$, and to maintain the same 2:3 gear ratio as in a conventional rotary engine is used, then $l = 1$ for $r_1 = nl$ and $r_2 = r_1 - l$. Figure 3.12 shows some example engine profiles for various apex seal profiles and Table 3.3 provides the corresponding DF equation parameters.
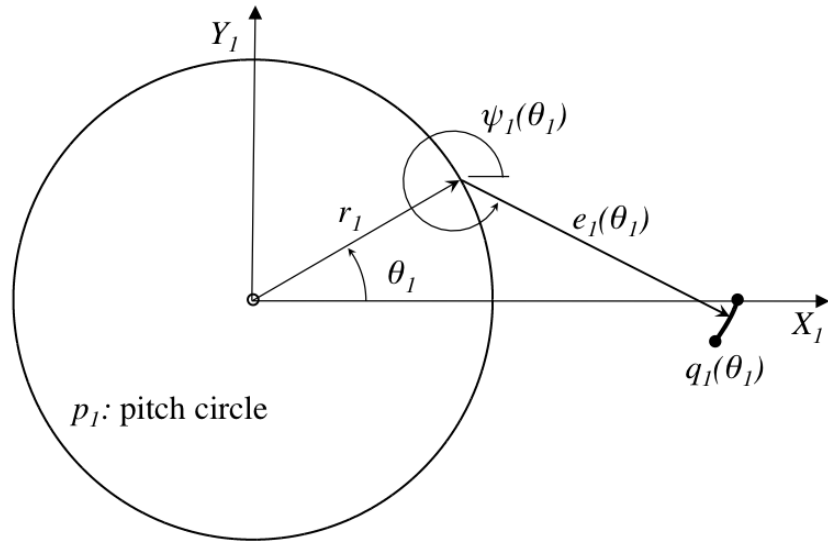
Figure 3.11: Nonarc-based apex seal profile.
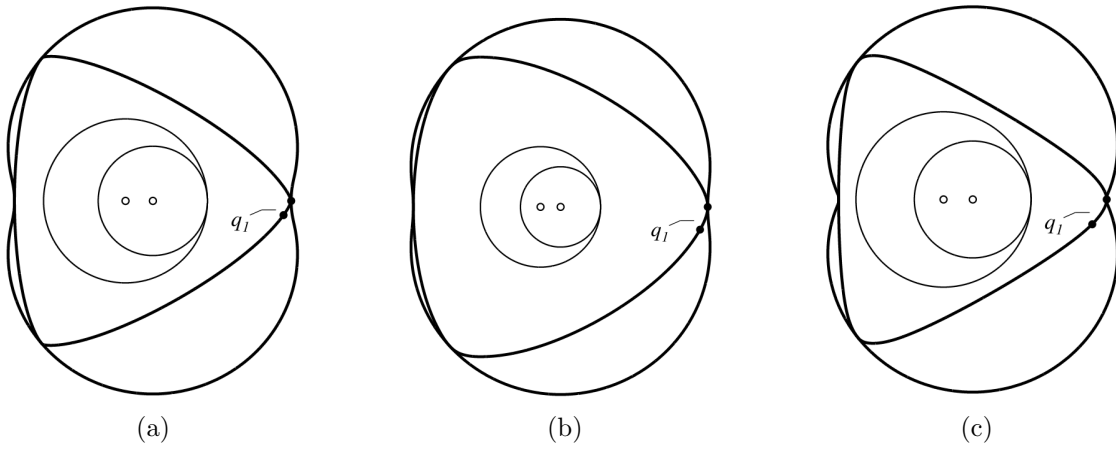
Figure 3.12: Rotary engine profiles designed by apex seal.

Table 3.3: Deviation function parameters for Figure 3.12

Figure No.	n	l	θ_{1s}	a_0
Fig. 3.12a	3	1	$\pi/3.35$	-2.3
Fig. 3.12b	3	1	$\pi/3$	-3
Fig. 3.12c	3	1	$\pi/4$	-2.4

3.4 Conclusions

The theory and deviation function algorithm described here is a new method for rotary engine design by the apex seal profile. This method incorporates the geometry of the apex seal into the design process and generates a larger variety of profiles than the conventional method of rotary engine design. The housing profiles generated by using the DF method have an advantage over the conventional profiles because they are conjugate to the apex seal profile, and therefore conform to the seals that they are based on. The conformity between the seal and the housing can be used to improve the sealing capability and effectiveness and thus minimize leaks. Another advantage is that the forces on the apex seals can be reduced, thus reducing the wear on the seals and the housing. The reduced wear can increase the longevity of the seals and the engine.

The example seal profiles included arc-based and nonarc-based apex seals, which encompasses the changing profile of apex seals normally used in rotary engine applications. Special apex seal profiles and the conforming housing bore can be investigated by using this method of design. For other applications, the number of lobes and the eccentricity of the engine can be modified from the conventional values in order to find a wider range of design possibilities. In practice, this would require changes to the conventional rotary engine gear ratio. By modifying these parameters, this design method can also be applied to other rotary mechanisms that use apex seals.

Chapter 4

DF Engine Design by Geometric Parameters

For a specific engine application, power output and volumetric displacement are typically considered at the outset of the design process. In rotary engine design, these two can be largely determined by the rotor and housing profiles because the theoretical maximum compression ratio and swept area can be calculated. The conventional design process utilizes a geometric ratio called the K factor: the rotor-radius-to-eccentricity ratio. It associates various design and performance characteristics, including apex sealing capability and maximum compression ratio, to each engine profile. Once the desired volumetric displacement has been determined, the K factor can be adjusted to reconcile apex sealing with compression ratio requirements.

This section introduces the DF method of rotary engine design by geometric parameters, a process independent of apex sealing. The same geometric parameters, rotor radius R, and eccentricity l, are incorporated into the arc-based and nonarc-based deviation functions. Then a specific swept area, A_{sp}, and theoretical maximum compression ratio, ϵ_{th}, are defined and related to the DF design parameters. DF-designed engines offer a range of profiles for each R/l ratio, not limited by apex sealing capability.

4.1 Introduction

The two geometric parameters used to characterize all conventional rotary engine profiles are rotor radius and eccentricity. In Figure 4.1 these are labelled as r_{tip} and l, respectively. The other geometric parameters are the rotor root radius, r_{root}, the rotor pitch radius, r_1, and the housing pitch radius, r_2. The root radius is the distance from the rotor center to the middle of the flank, which is the shortest radius measured on the rotor profile. This radius is the last point on the g_3 curve, found by the inside envelope of the housing profile. The deviation function equations for g_3 confirm:

$$r_{root} = r_{tip} - 2l$$

The rotor tip radius is the distance between the rotor center and the apex, and the furthest radius measured on the rotor profile. The rotor tip radius is the first point of the g_1 curve, and the true apex of the apex seal. Figure 4.2 illustrates how the location of this point is determined by the first deviation circle, or the deviation function evaluated at $\theta_1 = 0$. From this figure, the rotor radius, R, can be written as

$$R = r_1 \pm e_1(0) \tag{4.1}$$

Where $+$ corresponds to the g_1 generating curve and $-$ corresponds to the q_1 generating curve. Equation (4.1) can be rearranged as an initial condition for the deviation function:

$$e_1(0) = \pm(R - r_1) \tag{4.2}$$

For the typical rotary engine gear configuration, the pitch circle radii have the following relationships with the eccentricity:

$$r_1 = 3l$$

$$r_2 = r_1 - l$$

Then in terms of l and R the equation (4.2) becomes

$$e_1(0) = \pm(R - 3l) \tag{4.3}$$

In the profile comparisons presented here, all the DF-designed rotary engines have the eccentricity $l = 1$. These can be scaled to size and used with the conventional $2 : 3$ gear ratio, because the pitch circle radii are $r_1 = 3$ and $r_2 = 2$, corresponding to $l = 1$.
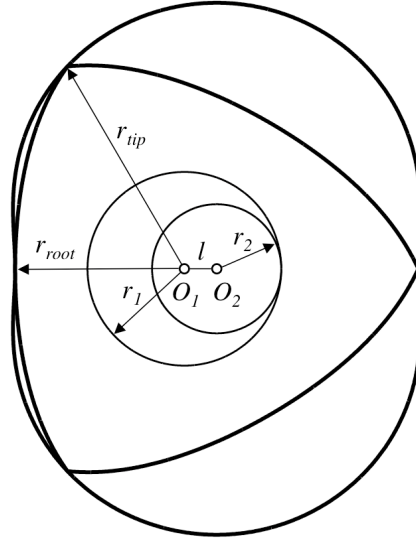
Figure 4.1: The geometric parameters of a rotor profile.

The geometric parameter used to characterize conventional rotary engine profiles is the rotor-radius-to-eccentricity ratio, called the K factor, or trochoid constant. Each profile is uniquely identified by its K factor and since it has a direct relationship with leaning angle, it is used as an indicator of apex sealing capability. The K factor also associates the theoretical maximum compression ratio and swept surface area with the corresponding profile. By conventional design methodology, once the desired volumetric displacement has been determined, the K factor is adjusted to reconcile apex sealing capability with compression ratio requirements.
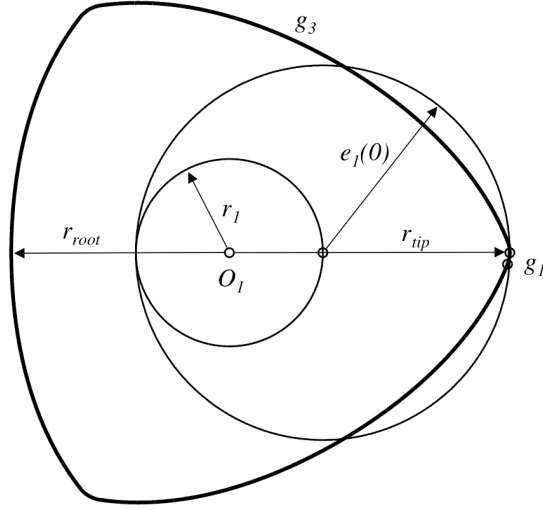
Figure 4.2: The rotor tip radius can be determined by $r_1 + e_1(0)$.

The geometric parameter K can be defined in the same way for DF-designed rotary engines as R/l, but this ratio does not represent a limitation on apex sealing capability nor maximum compression ratio. The R/l ratio is different from the conventional K factor because it is not associated with a single profile. However, it can be used in a similar way: to characterize all the profiles for a particular deviation function. To demonstrate the R/l ratio as part of a selection method, the arc-based and nonarc-based deviation functions are provided. In these examples, the pitch circles have radii $r_1 = 3l$ and $r_2 = 2l$, so these DF-designed profiles can be used with the conventional rotary engine phase gearing. For simplicity, the eccentricity is kept constant at $l = 1$, so the R/l ratio determines the size of the engine and the adjustable DF parameters determine the apex seal profile.

To illustrate the variety of apex seal widths and shapes, independent of R/l ratio, nine different apex seal profiles are shown in Figure 4.3. The R/l ratio is labeled for each corresponding apex seal, and is changing the size of the engine by moving the rotor tip further from the rotor center. These generating curves are from either the arc-based or non-arc based deviation function; adjusting the free parameters within the functions yields differently shaped profiles, different sizes, and ultimately different sealing characteristics. Two seals have the same ratio, $R/l = 7$, which is roughly the K factor of Mazda's rotary engine.

Note that these two seal profiles begin in the same location but have different lengths and curvature. The conventional design method only has one engine profile associated with that K factor. Thus the DF method of engine design by geometric parameters is independent of apex sealing capability.
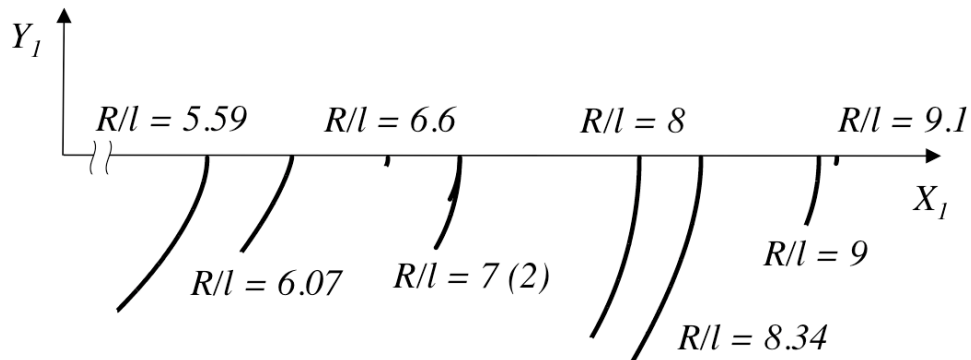
Figure 4.3: Apex seal profiles from the same pitch circle, r_1, and $l = 1$.

4.2 Compression Ratio and Volumetric Displacement

The theoretical maximum compression ratio is calculated by the ratio of the maximum chamber volume to the minimum chamber volume. For rotary engines, this ratio can also be determined from the profiles by using the area of the largest pocket, shown in Figure 4.4a, and the area of the smallest pocket, Figure 4.4b.

$$\epsilon_{th} = \frac{V_{max}}{V_{min}} = \frac{A_{max}B_c}{A_{min}B_c} = \frac{A_{max}}{A_{min}} \tag{4.4}$$

where B_c is the axial width of the chambers.

The volumetric displacement of a rotary engine can be defined in different ways, and one way is to calculate the swept volume. This can be done by subtracting the volume of the rotor from the volume enclosed by the housing.

$$D = V_{swept} = V_{housing} - V_{rotor}$$

(a) Maximum pocket area.　　　　(b) Minimum pocket area.
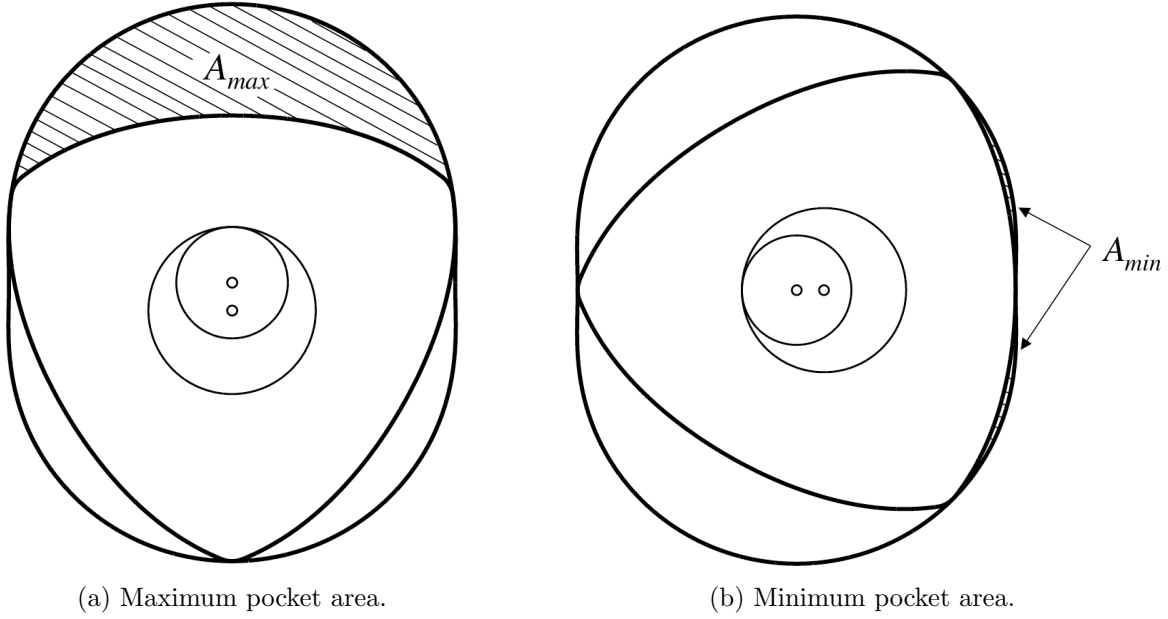
Figure 4.4: Rotor positions of extreme pocket areas.

If the axial width of the rotor and housing is B_c, then the swept volume can be written in terms of the area of the rotor profile and the area enclosed by the housing profile.

$$V_{swept} = (A_{housing} - A_{rotor})B_c = A_{swept}B_c$$

A specific swept area can be defined by normalizing A_{swept} to an eccentricity of $l = 1$. The parameter A_{sp} is now relative to the eccentricity and can be used to compare differently sized profiles.

$$A_{sp} = \frac{A_{swept}}{l} = \frac{A_{housing} - A_{rotor}}{l}$$

4.3 Deviation Functions in terms of Rotor Radius

4.3.1 Arc-based deviation function

An arc-based deviation function was introduced previously for developing rotary engine profiles using an apex seal with a circular arc profile:

$$e_1(\theta_1) = \sqrt{a^2 + r_1^2 - 2ar_1\cos(\theta_1)} - \rho \qquad 0 \le \theta_1 \le \theta_{1s} \qquad (4.5)$$

where ρ is the radius of the arc, r_1 is the rotor's pitch circle radius, and a is the distance between the center of the pitch circle and the center of the arc. To write equation (4.5) in terms of the rotor radius, $R = a + \rho$:

$$e_1(\theta_1) = \sqrt{(R-\rho)^2 + r_1^2 - 2(R-\rho)r_1\cos(\theta_1)} - \rho \qquad 0 \le \theta_1 \le \theta_{1s} \qquad (4.6)$$

In this deviation function equation, the adjustable parameters are the rotor radius, R, and the seal radius of curvature, ρ. In order to compare DF engine profiles with the same R/l ratio, a dimensionless parameter ρ/l is used. To investigate DF engine profiles that will work with conventional rotary engine gear ratios, $l = 1$, $r_1 = 3$, and $r_2 = 2$. Figure 4.5 shows the relationship between four R/l values and the maximum theoretical compression ratio. This compression ratio is a theoretical maximum because it does not include rotor flank depressions or spark plug holes. The compression ratios of four Wankel engine profiles are also indicated; for each R/l there is an equivalent K factor, that corresponds to a single conventional profile. For the arc-based DF-designed rotary engines, the theoretical maximum compression ratio decreases from the conventional profile's value as the seal radius of curvature increases. The reason for this is that the DF-designed engine incorporates the apex seal into the rotor, so the apex region is a circular arc instead of a single point. The more rounded the apex of the rotor, the higher the A_{rotor}, which decreases the compression ratio. If the desired compression ratio is known, then there is a range of possibilities for

51

DF-designed engine profiles and the corresponding circular arc apex seals.
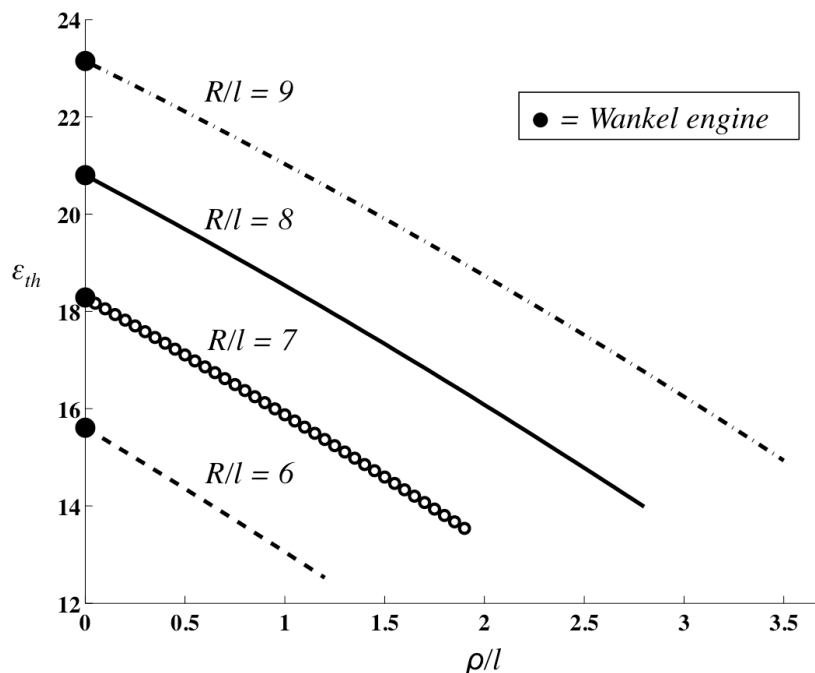
Figure 4.5: Maximum compression ratio for arc-based DF engines.

Figure 4.6 indicates that the DF-designed rotary engines of a certain R/l value have nearly the same specific swept areas as the equivalent Wankel engine. This is because of the conjugate relationship between the apex seal and the housing bore. As the apex seal changes in shape and size, the housing bore also changes proportionately, preventing significant changes to the swept area. If the desired swept area is known, then it can be achieved using the DF method with a range of arc-based apex seals, which can be selected based on other design criteria.

4.3.2 Nonarc-based deviation function

A nonarc-based deviation function was introduced previously for finding engine profiles from an apex seal that does not have a circular arc profile. This was a third order sinusoidal function:

$$e_1(\theta_1) = r_1(a_3 \cos^3 \theta_1 + a_2 \cos^2 \theta_1 + a_1 \cos \theta_1 + a_0), \quad 0 \le \theta_1 \le \theta_{1s} \tag{4.7}$$
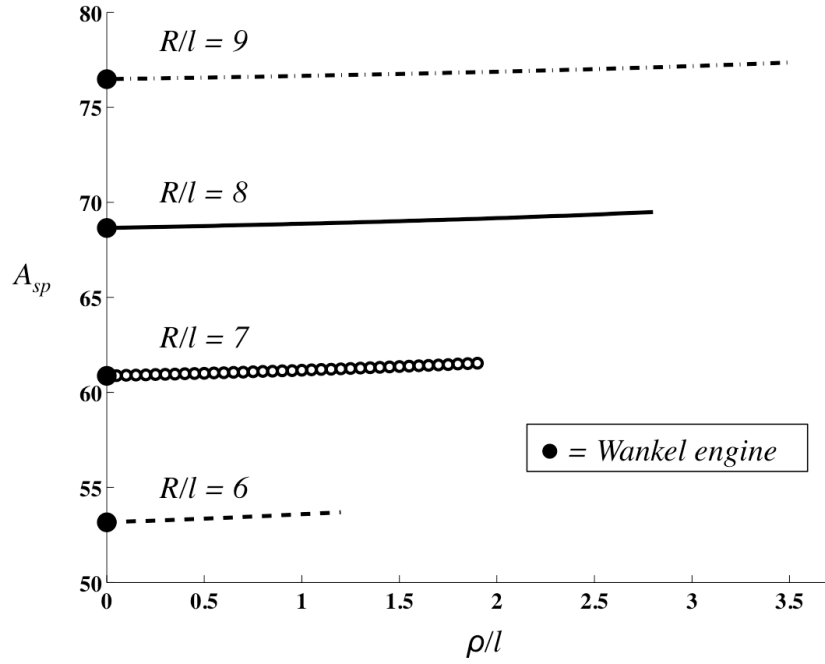
Figure 4.6: Specific swept area for arc-based DF engines.

After applying the boundary conditions summarized in Table 3.1, the coefficients were found:

$$
a_3 = \frac{\cos^2 \theta_{1s}}{2 \sin^5 \theta_{1s}}
$$

$$
a_2 = \frac{\cos \theta_{1s}}{2 \sin^3 \theta_{1s}} - 3a_3 \cos \theta_{1s}
$$

$$
a_1 = \frac{1}{\sin \theta_{1s}} - 3a_3 \cos^2 \theta_{1s} - 2a_2 \cos \theta_{1s}
$$

Inserting equation (4.2) into equation (4.7), the adjustable parameter a_0 becomes

$$
a_0 = 1 - \frac{R}{r_1} - a_3 - a_2 - a_1
$$

Now the rotor radius, R, and switch angle, θ_{1s}, can be used directly to design the rotary engine profile. The rotor radius will determine the size of the profile while the switch angle is the conjugating range of the apex seal. One of the geometric parameters determined by the switch angle is the width of the apex seal.
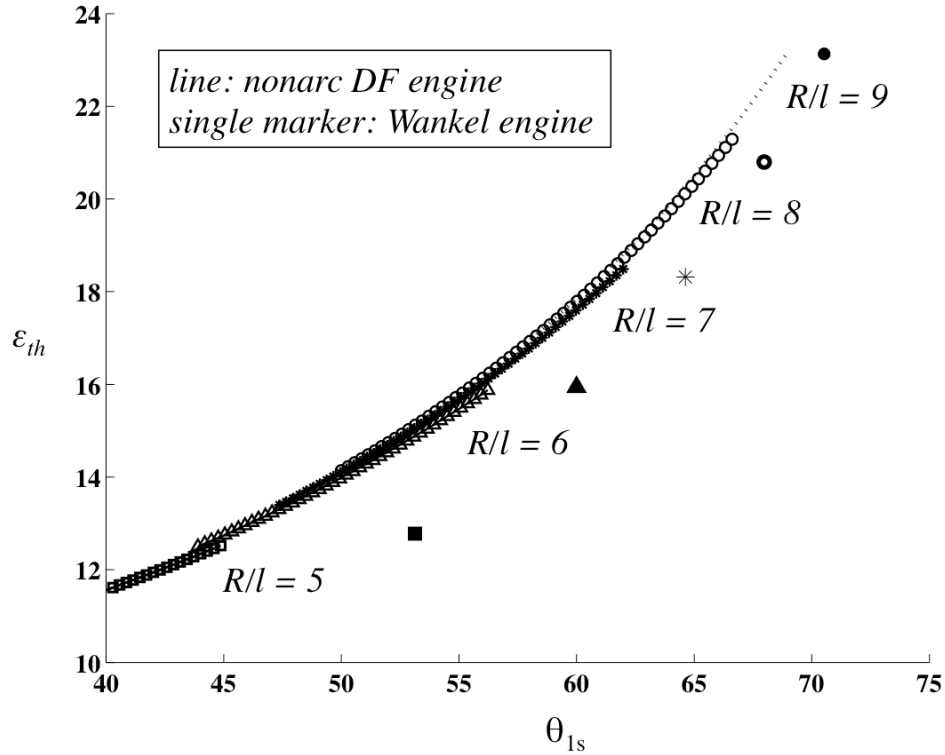
Figure 4.7: The theoretical compression ratio for nonarc-based DF engines.

Figure 4.7 shows the relationship between the switch angle and the maximum theoretical compression ratio for DF-designed rotary engines of five different R/l ratios. The lines representing the ratios each have different markers, and the conventional rotary engines of corresponding K value is represented by the same marker, indicating one profile. All the Wankel engine profiles fall on one curve in Figure 4.7, whereas the nonarc-based DF-designed rotary engines fall inside a band. There is some overlap among different R/l ratios, so if the desired compression ratio is known, there are more than one possible DF profile that can meet that criterion.

Similarly to the arc-based apex seal result, Figure 4.8 shows that the DF-designed nonarc-based profiles have nearly the same swept area as the equivalent conventional profile. For each specific swept area, there is one conventional rotary engine profile, and the relationship is indicated by the single point markers in Figure 4.8. The nonarc-based DF-designed profiles have a range of possibilities for each specific swept area, with different switch angles.
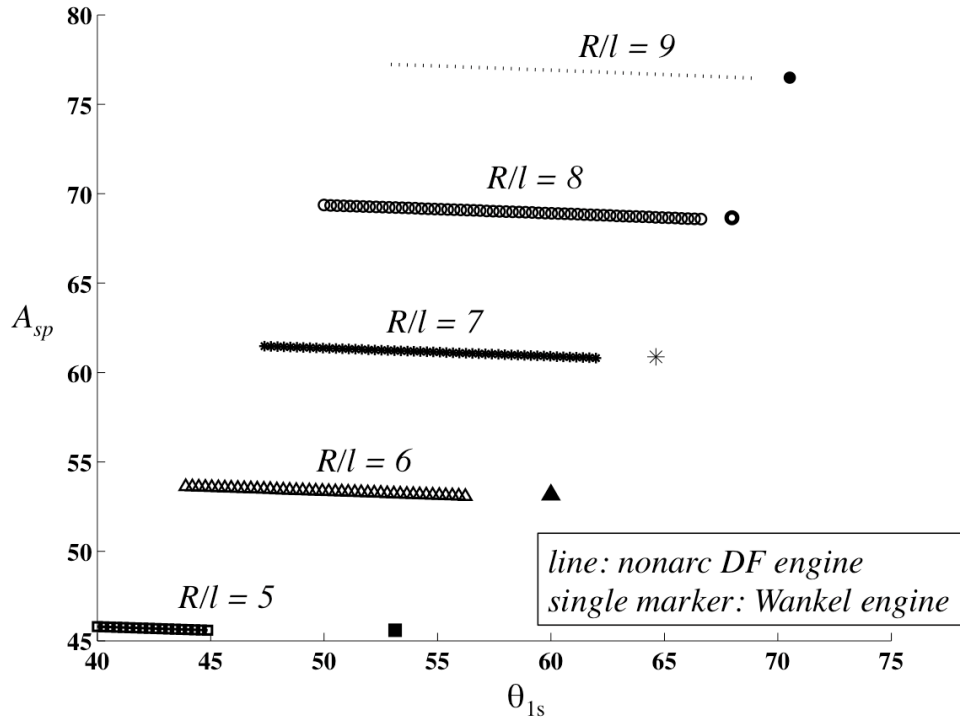
Figure 4.8: The specific swept area of nonarc-based DF engines.

By using the deviation function method for rotary engine design by geometric parameters, more profiles are available for meeting the design criteria. There is only one conventional profile that corresponds with each maximum theoretical compression ratio or specific swept area. If one of these design criterion is rigidly determined then there is no flexibility at the planar profile design stage. The DF method of rotary engine design addresses this limitation and provides a range of profiles for each compression ratio and specific swept area that are accessible by the geometric parameters incorporated into the deviation function, without the conventional limitation on apex sealing.

4.4 Conclusions

The DF design method can incorporate the conventional design parameters, rotor radius, R, and eccentricity, l, into the deviation function equations. This is shown using the arc-based and nonarc-based deviation function examples. The ratio R/l and one other adjustable

parameter, can be used to determine the range of maximum theoretical compression ratios and specific swept areas. For apex seals that have a circular arc profile, the DF parameters are the R/l ratio and the dimensionless radius of curvature of the apex seal, ρ/l. For nonarc apex seal profiles, the DF parameters are the R/l ratio and the switch angle, θ_{1s}. Using the same pitch circle and eccentricity geometry as the conventional rotary engine, the DF-designed engine profiles can be directly compared to the Wankel engine and implemented with conventional engine gearing.

To find engine profiles by using maximum compression ratio or specific swept area, the entire range of conventional engine possibilities can be represented by a single line. In comparison, the DF profiles are represented by a band, i.e., a wider range of possible solutions. For particular specific swept area and maximum compression ratio values, there may not be a conventional rotary engine profile that meets both criteria. By using the deviation function method, there are a range of solutions that can meet both criteria simultaneously, and this flexibility is not at the expense of apex sealing. This is another one of the advantages of the DF method over conventional rotary engine designs.

Chapter 5

Apex Sealing Analysis

One of the most fundamental requirements of rotary engine operation is sealing the chambers between the rotor and the housing. Throughout the development of the rotary engine, the apex seals have proven to be the most challenging aspect of design; and their effectiveness and longevity continue to lag behind the reciprocating engine counterpart, piston rings. The conventional apex seal assemblies include the metal seal, which has a cylindrical surface making contact with the housing bore, and one or two leaf springs to push the seal against the housing. The seal and springs are held in the rotor apex by a rectangular slot. A few inherent advantages that piston rings have over the apex seals are that each ring makes better contact with the cylinder than an apex seal does with the housing bore, and the apex seal must be able to move radially in and out, as well as side-to-side in the slot that holds it [31]. This section examines the differences between apex sealing in the conventional engine and the DF-designed engine by defining and developing a sealing index. This index can be used to quantify, compare, and improve rotary engine apex sealing. For the purposes of comparison, numbers approximating the technical specifications of Mazda's rotary engine are examined here and used to generate hypothetical design results.

5.1 Introduction

The difficulty of effectively sealing the conventional rotary engine is partly due to the discrepancy between theoretical design and implementation. In theory, the rotor apex has a single point of contact with the conjugate epitrochoidal housing; in other words the true apex is in contact for all rotor positions. In actuality apex seals are necessary for engine operation and the seals have a region of contact; in other words the point of contact changes depending on the rotor position. To compensate for this discrepancy, the housing bore and rotor profiles are actually the parallel trochoids of their theoretical conjugate pair design. Mazda's rotary engine profiles are offset by 2 or 3 mm; the housing bore is made slightly larger and the rotor is made slightly smaller. This creates a gap between the rotor and housing which is closed by the apex seals. This design requires some radial and side-to-side movement of the apex seals in the rotor's apex slot, and this movement allows the possible separation of the apex seal from the housing bore [16, 22, 21]. If apex seals were used without any gap between the profiles, then there would be interference. Figures 5.1 and 5.2 show what the interference would be for a rotary engine with a similar rotor radius to that of Mazda's rotary engine, 105 mm [32]. The figures show K values between 6 and 10, the practical range for conventional engines. Mazda's rotary engine has K value of about 7, and the seals used are either 2 mm or 3 mm wide.

Area of interference is determined by calculating the swept area of the rotor with seals, and comparing this to the area of the housing bore. Figure 5.1 shows the area of interference by how much larger (a percentage) the apex seal's swept area is than the designed conjugate housing profile. For Mazda's rotary engine with 2 mm apex seals, the swept area of the seals is about 0.2% larger than the area of the corresponding housing. This area is not evenly distributed around the housing profile, as indicated in Figure 5.2. If the rotor apex is considered to travel 360° during a rotation, then the interference of the apex seal can be calculated for each position. Figure 5.2 shows the radial interference when the rotor apex moves from the minor axis of the housing (0°) to the major axis (90°). For an engine with K
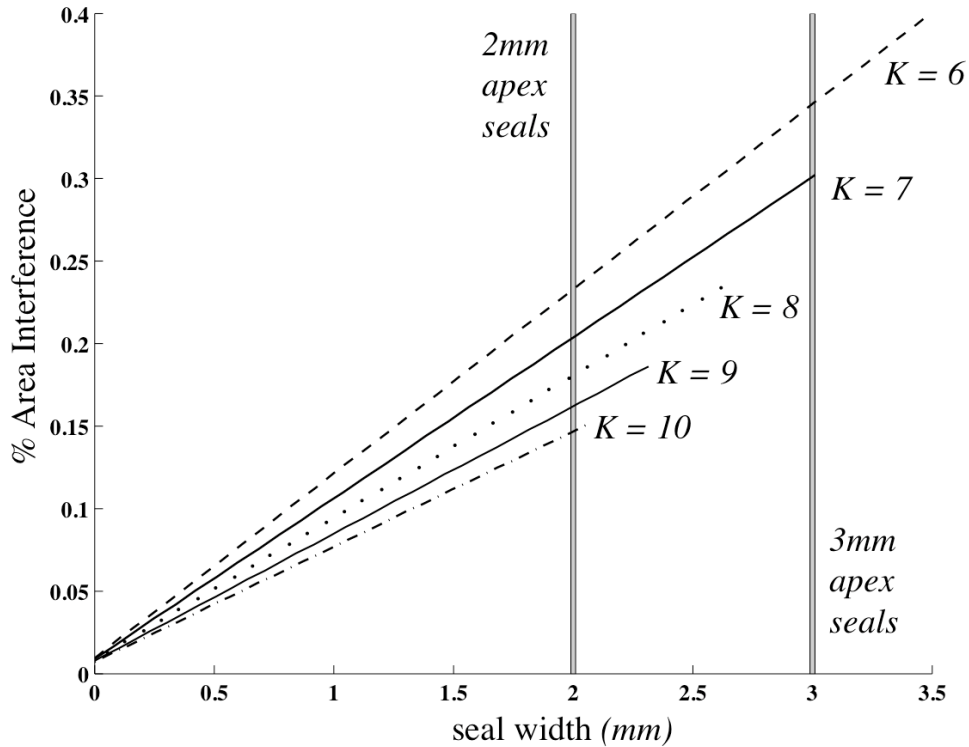
Figure 5.1: Area interference of apex seals in a Wankel engine, $R = 105\,\mathrm{mm}$.

value 7 and radius 105 mm, using 2 mm apex seals, the farthest reach of the seal is about 0.25 mm beyond the conjugate housing profile. To give an idea of the radial tolerances allowed for parts inside a rotary engine, Mazda's specification limit for the apex seal warpage is shown in Figure 5.2. An apex seal is beyond technical specification if it has warped radially outward more than 0.03 mm.

The amount of interference corresponds to the size gap between the rotor and the housing, the length of seal that must extend beyond the rotor profile in order to close the gap, and the spring force needed to push the seal out. This movement by the seal has been related to excess wear and damage to the seal and housing [27, 28]. This is detrimental to the lifespan of the seal, engine, and the sealing effectiveness. The seal movement can also initiate separation from the housing bore, which allows gas leakage [16, 22, 21]. Designing the engine by deviation function and apex seal profile results in a housing profile that conforms to the apex seal and its swept area, eliminating interference between the seal and the housing, so
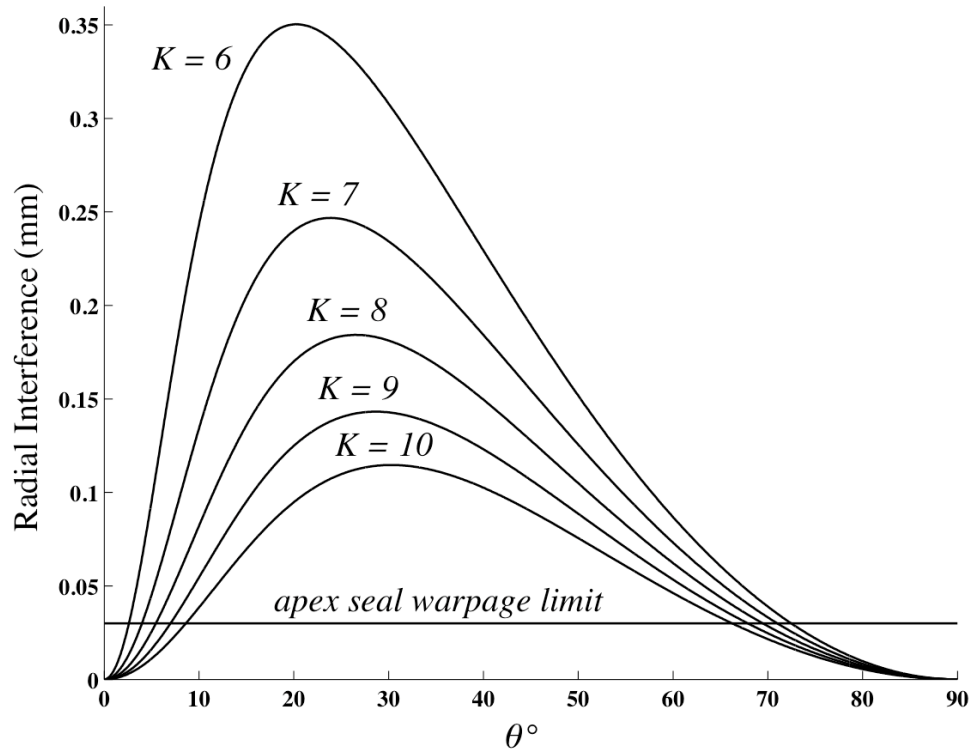
Figure 5.2: Radial interference of $2\,\text{mm}$ apex seals in a Wankel engine, $R = 105\,\text{mm}$.

that the clearance gap closed by the seals can be minimized.

5.2 Sealing Index

5.2.1 Apex Seal Radius of Curvature

The radius of curvature of the apex seal profile can be derived by considering an infinitesimal segment of the g_1 curve. Referring to Figure 5.3, the lower half of an apex seal profile is represented by generated curve g_1 with one quarter of the corresponding pitch p_1. A point on the g_1 curve is labeled G and has pitch point P and angular position θ_1. The normal at G has angle ψ_1 with respect to the X_1 axis. The center of curvature of G is labeled A_1 and the radius of curvature is denoted ρ_{g1}. Now considering an infinitesimal segment GG' on the g_1 curve, the pitch point of G' is P'. The pitch curve segment PP' subtends angle $d\theta_1$ and GG' subtends angle $-d\psi_1$.
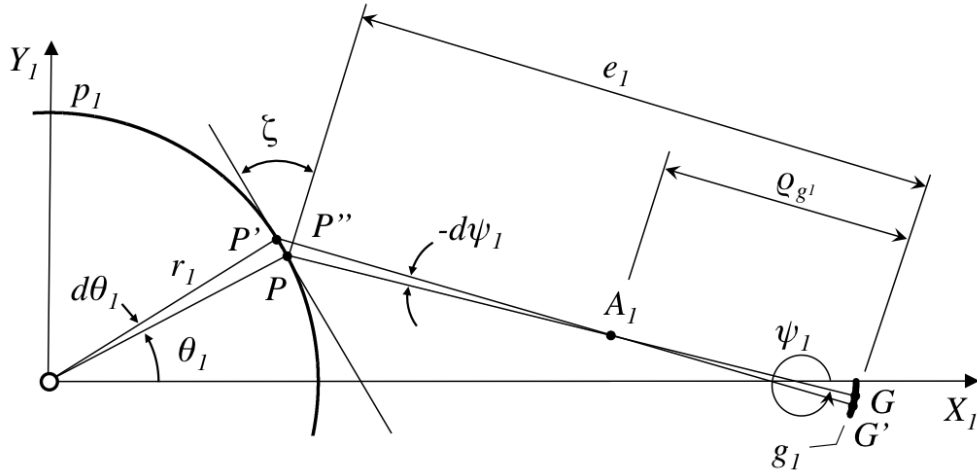
Figure 5.3: Radius of curvature of an apex seal profile.

Now consider a point P'' on $A_1 P'$ such that PP'' is perpendicular to $A_1 P$. The angle between PP'' and the tangent at P is denoted ζ. The circular arc segment PP'' can be expressed in two ways:

$$\overline{PP''} = (e_1 - \rho_{g1})(-d\psi_1) = (\rho_{g1} - e_1)d\psi_1 \tag{5.1}$$

61

$$\overline{PP''} = \overline{PP'} \cos \zeta = r_1 d\theta_1 \cos \zeta \qquad (5.2)$$

By comparing equations (5.1) and (5.2), the radius of curvature can be written:

$$\rho_{g1} = \frac{r_1 \cos \zeta}{d\psi_1/d\theta_1} + e_1$$

The angle ζ can be written in terms of θ_1 and ψ_1, so the equation for the apex seal radius of curvature becomes:

$$\rho_{g1} = \frac{r_1 \cos(\theta_1 - \psi_1)}{d\psi_1/d\theta_1} + e_1 \qquad (5.3)$$

From the g_1 and q_1 envelope equations,

$$\theta_1 - \psi_1 = \arcsin \frac{e_1'}{r_1} \qquad (5.4a)$$

$$\theta_1 - \psi_1 = -\pi - \arcsin \frac{e_1'}{r_1} \qquad (5.4b)$$

Then it follows,

$$\cos(\theta_1 - \psi_1) = \frac{\sqrt{r_1^2 - e_1'^2}}{r_1}$$

$$\rho_{g1} = \frac{\sqrt{r_1^2 - e_1'^2}}{\psi_1'} + e_1$$

where

$$\psi_1' = \frac{d\psi_1}{d\theta_1} = 1 \mp \frac{e_1''}{\sqrt{r_1^2 - e_1'^2}}$$

and $-$ corresponds to the g_1 envelope while $+$ corresponds to the q_1 envelope of the deviation

circles. Therefore, the radius of curvature of the apex seal profile is:

$$\rho_{g1} = e_1 + \frac{r_1^2 - e_1'^2}{\sqrt{r_1^2 - e_1'^2} \mp e_1''} \tag{5.5}$$

where $-$ and $+$ correspond to g_1 and q_1 respectively.

5.2.2 Housing Radius of Curvature

To find the radius of curvature of the conjugate housing profile, the two segments resulting from the forward and reverse contact with the apex seal must be considered separately. The two segments are denoted $g_{2forward}$ and $g_{2reverse}$. The Euler-Savary equations for the forward and reverse contact sections of the housing profile is derived in Appendix A.

Forward:

$$\left(\frac{1}{e_1 - \rho_{g1}} - \frac{1}{e_1 - \rho_{g2forward}}\right)\cos(\theta_1 - \psi_1) = \frac{1}{r_1} - \frac{1}{r_1 - l} \tag{5.6a}$$

Reverse:

$$\left(\frac{1}{e_1 + IJ - \rho_{g1}} - \frac{1}{e_1 + IJ - \rho_{g2reverse}}\right)\cos(\theta_1 - \psi_1) = \frac{1}{r_1} - \frac{1}{r_1 - l} \tag{5.6b}$$

Rearranging (5.6a) and (5.6b) gives the forward and reverse radii of curvature for g_2:

$$\rho_{g2forward} = e_1 - \frac{\sqrt{r_1^2 - e_1'^2}}{\psi_1' + \frac{l}{r_1 - l}} \tag{5.7a}$$

$$\rho_{g2reverse} = e_1 + IJ - \frac{\sqrt{r_1^2 - e_1'^2}}{\psi_1' + \frac{l}{r_1 - l}} \tag{5.7b}$$

where

$$\psi_1' = \frac{d\psi_1}{d\theta_1} = 1 \mp \frac{e_1''}{\sqrt{r_1^2 - e_1'^2}}$$

63

and $-$ corresponds to the g_1 envelope while $+$ corresponds to the q_1 envelope of the deviation circles.

5.2.3 Apex Sealing Index

Sealing capability and effectiveness are quantified here as a sealing index that indicates the conformity of an apex seal profile with the housing profile. The DF-designed rotary engine sealing index is defined here to be the arc length within which the apex seal profile is within a specified clearance of the housing bore profile. This is illustrated in Figure 5.4. The arc length, ΔS, and the clearance, Δt, are very small compared to the radii of curvature of the housing profile and seal profile at the contact point. The apex seal is always a convex curve and therefore ρ_{g1} is always positive. The housing profile changes from convex to concave between $0°$ and $90°$, therefore ρ_{g2} goes from a positive to a negative value. Figure 5.4 shows the top of the housing profile and the rotor apex aligned with $90°$. In this position, the housing profile is concave and ρ_{g2} is negative.
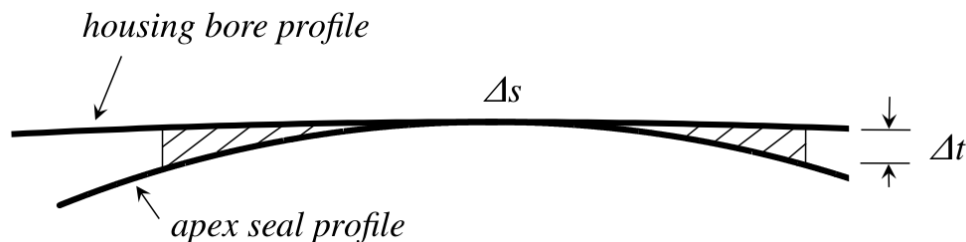
Figure 5.4: Clearance Δt between apex seal and housing.

The formula for the sealing index in terms of the radii of curvature and the clearance is:

$$\Delta S = \sqrt{\frac{8\rho_{g1}\rho_{g2}\Delta t}{\rho_{g1} + \rho_{g2}}} \tag{5.8}$$

where a positive radius corresponds to a convex curve and negative radius is a concave curve. The derivation is provided in Appendix B.

64
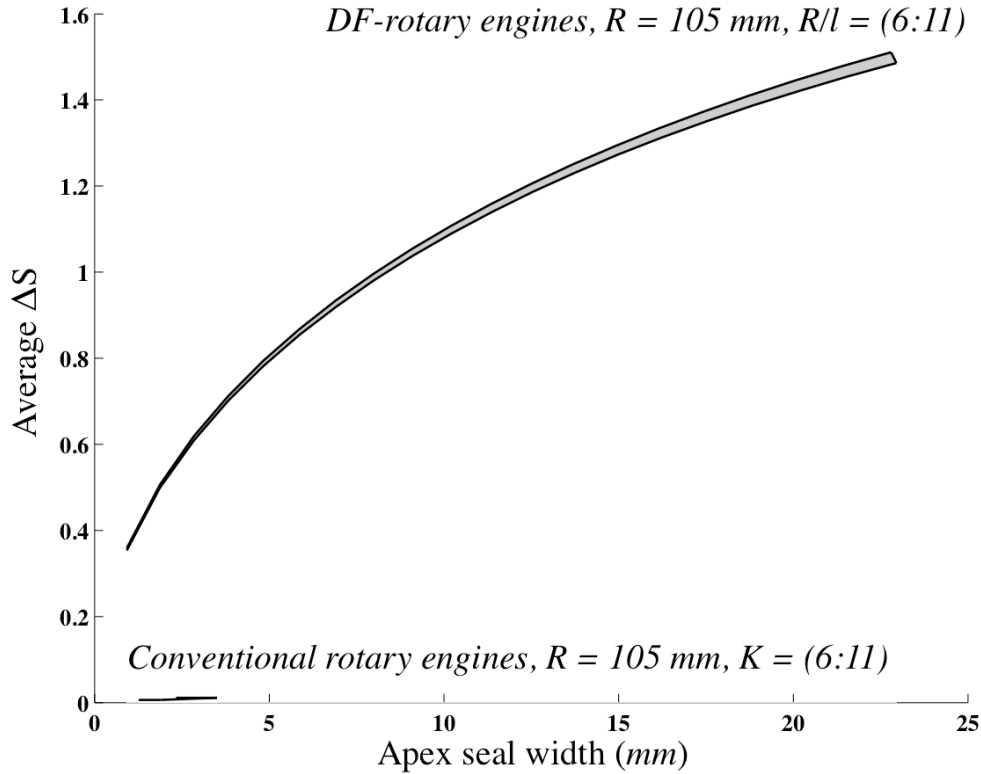
Figure 5.5: Average sealing index over arc-based DF housing profiles.

Figure 5.5 shows the average sealing index, ΔS, calculated over an entire housing profile for a range of arc-based DF-designed engines, and plotted against the apex seal width. In order to make a comparison with the conventional engine used by Mazda, the same rotor radius, $R = 105$, is used and the conventional rotary engine with this radius is shown on the same plot. Conventional engines have very little housing conformity to the apex seal, so the average sealing index is very small compared to the DF-designed engines of the same rotor radius. The sealing index for the conventional engines is calculated for seals between 2 mm and 3 mm wide, since apex seals of those two widths are available for Mazda's engine. The DF method has a higher average sealing index for the same size seals, by about 0.4 to 0.6. All the arc-based DF-designed engine profiles have similar sealing capability and fall inside the indicated band. The highest average sealing index achieved for arc-based seals and 105 mm rotor radius is about 1.5, with seals 22 mm wide. Wider apex seals result in a higher average sealing index. Tables C.1 to C.4 provide the deviation function parameters for the

seal widths and sealing indices shown in Figure 5.5.
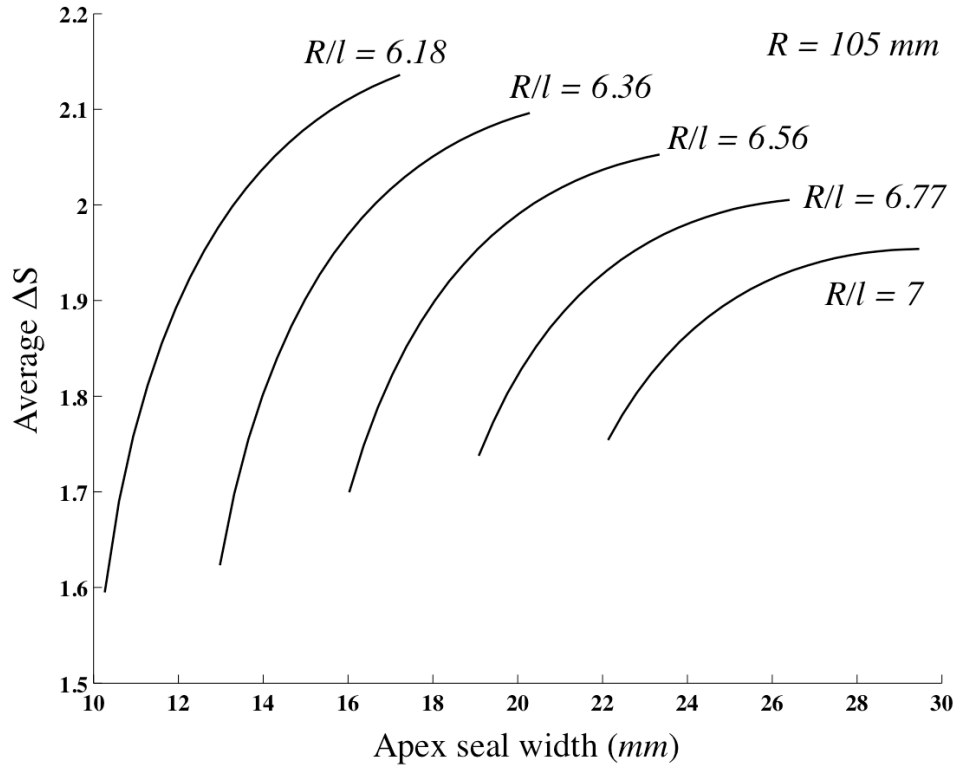
Figure 5.6: Average sealing index over nonarc-based DF housing profiles.

Figure 5.6 shows the average sealing index for a nonarc-based DF engine profile. The nonarc-based apex seals can achieve higher sealing indices than the arc-based seals, but only within a certain range of R/l ratios and seal widths larger than about 10 mm. Narrower seals can be used for smaller engines, in which $R < 105$ mm. Table C.5 provides the deviation function parameters used to obtain these results.

5.3   Conclusions

In comparing conventional rotary engines to DF-designed engines, the most important distinction is the sealing capability. A DF-designed housing bore profile is conjugate to the apex seal profile and conforms to it. Conventional engines do not have housing conformity, nor does the conventional design method incorporate the apex seal profile. Therefore apex

66

seals cannot make good contact inside a conventional rotary engine. In addition, the swept area of the seals interferes with the area enclosed by the housing. Conventional engines require extra clearance to allow the seals radial and side-to-side movement within the rotor slot that holds them. This movement can cause excess friction force on the seals, shorten their lifespan, damage the housing bore, inhibit effective sealing, and lead to seal separation. Since DF engines are designed to have no interference between the seals and the housing, a sealing index can be defined and used to analyze differently shaped seals. The DF method enables the design of different apex seal profiles, various in shape and width. It was found that the sealing index is higher for wider apex seals, indicating that better sealing can be achieved if wider apex seals were used. Mazda's rotary engines currently use 2 mm or 3 mm wide apex seals. The DF engine profiles can be designed by using seals from 1 mm up to 30 mm wide, with any profile that can be defined by a deviation function. Conventional rotary engine designs require minimization of the size and weight of the apex seals in order to minimize the spring force and interference. Therefore wider apex seals are not practical for the conventional engine. The nonconforming housing bore of conventional engine design prevents effective apex sealing, and the minimization of the seal size does not allow optimization. These limitations can be addressed by using the deviation function method of design by apex seal profile.

Chapter 6

Multi-Apex-Sealing Grid

By using the deviation function (DF) method of rotary engine design, the apex seal and engine housing bore are conjugate kinematic pairs, which enables the application of many different apex seal profiles, including much wider apex seals than those currently in use. The wide apex seal is designed from the wide generating curve that is conjugate to the DF-designed housing profile. Instead of using the one wide apex seal profile, multiple, narrower, apex seals can be used to represent the generating curve instead. Each seal is conjugate to the housing at different times during the rotation, and when one seal is not in a conjugate position, it can serve as a backup seal, preventing gas leakage. In the multi-apex-seal configuration, all the seals are in contact with the housing bore at all times, providing multiple barriers to pressure losses and blow by. In addition, the multi-apex-seal system prevents seal chatter and seal separation because each seal only experiences chamber pressure from one side. Seal wear and gas leaks have been attributed to apex seal separation from the bore, initiated by movement within the slot [27, 28]. Seal movement is caused by a reversal of net force direction [16, 22, 21], which occurs naturally in rotating combustion because each chamber cycles through internal combustion stages at different times. In this section, the forces on the apex seals are described and the multi-apex-sealing grid is introduced to mitigate seal movement, seal wear, and therefore improve sealing. Some possibilities for

68

multi-apex-sealing configurations are provided and the interference of this type of sealing is compared to that of a conventional rotary engine.

6.1   Introduction

The conventional apex seal has a cylindrical surface in contact with the housing bore, which was designed to spread the contact region around the rotor's true apex and avoid a concentrated area of contact. But the conventional housing bore is designed for the same point of contact at each of the three apexes, not a range of contact points. In order to reconcile the discrepancy between the apex profile and nonconforming housing profile, some clearance is needed between the rotor and housing. This gap is closed by the apex seal, which now must be able to move radially in and out, as well as side-to-side in the slot that holds it. This movement leads to separation between the seal and the bore under certain conditions identified by Knoll et al. and Matsuura et al. [16, 22, 21]. The three possible circumstances under which the seal can lose contact are: sliding down inside the rotor slot, moving completely from one side of the slot to the other side, and tilting from one side of the slot to the other side. These movements by the seal are caused by the pressure changes inside the chambers on either side of the seal, specifically the reversal of the direction of the resultant pressure force.

Gas pressure forces from the adjacent engine chambers are believed to account for about 80% of the total force on an apex seal [1]. Figure 6.1 shows a free body diagram of a conventional apex seal. The rotation is counterclockwise and the chamber in front of the apex seal (leading) has pressure P_1 while the chamber behind the apex seal (trailing) has pressure P_2. Under these circumstances, the apex seal has full contact along the trailing side of the rotor slot, and is pushed against the housing bore by P_1. The seal has flat sides of height h, width is B, length w (width of the rotor, not shown), and radius a in the cylindrical head. The angle subtended by the cylindrical head is 2β, equal to arcsin $B/2a$. The lean

angle, ϕ, or angle of obliquity, is the angle between the radial line through the rotor's center and apex, along the η axis, and the normal line at the point of contact, indicated by F_C. For conventional rotary engines the lean angle is limited to about 30°; beyond this point the seal is unreliable [24]. All apex seals have a spring underneath, F_S, necessary for starting the engine, when the surrounding pressures aren't enough to hold the seal against the bore. The figure illustrates the position of the apex seal in the slot when $P_1 > P_2$.

Figure 6.1: Body force diagram for an apex seal when $P_1 > P_2$.

The $\epsilon - \eta$ reference frame is attached to the seal. Summing the forces in the ϵ and η directions [16]:

$$F_\epsilon = F_N + F_C \sin\phi - \mu_C F_C \cos\phi + P_1 w(a\cos\beta - a\cos\phi - h) + P_2 w(a\cos\phi - a\cos\beta) \quad (6.1)$$

$$F_\eta = F_S - F_C \cos\phi - \mu_C F_C \sin\phi + \mu_N F_N + P_1 w(\frac{B}{2} - a\sin\phi) + P_2 w(a\sin\phi - \frac{B}{2}) \quad (6.2)$$
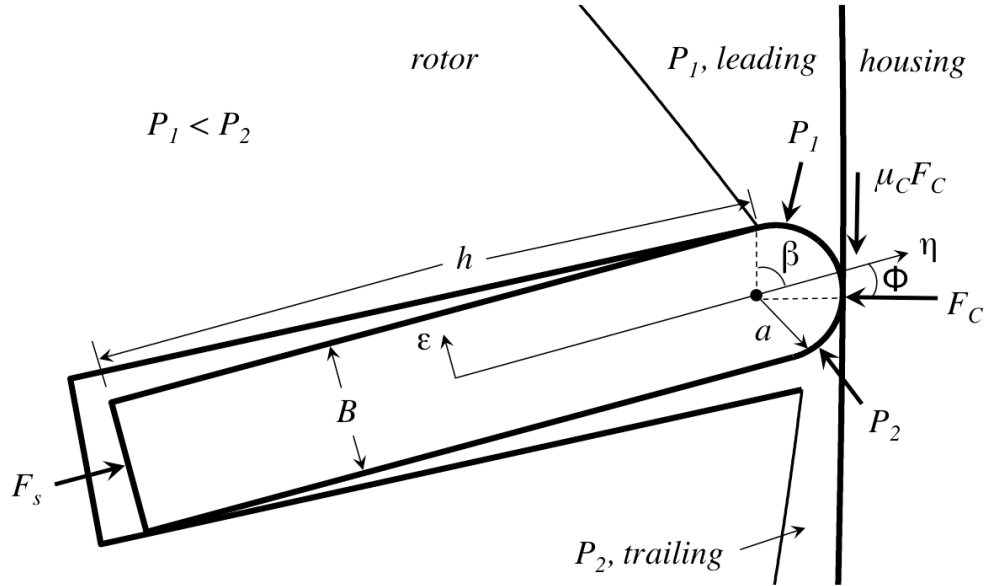
Figure 6.2: Body force diagram for an apex seal when $P_1 < P_2$.

Figure 6.2 illustrates the seal position in the slot when $P_2 > P_1$. The trailing pressure overcomes the leading pressure and tilts the seal inside the slot.

6.2 Multi-Apex-Sealing Grid

6.2.1 Wide Apex Seal Design

A wide apex seal is designed by using the deviation function method and manipulating the generating curve g_1. The g_1 is one-half of the apex seal profile, so the farther g_1 extends, the wider the seal. This is the conjugating range between the rotor and the housing, so the point of contact begins at the true apex and moves to the edge of the seal, then the contact point reverses direction and moves back to the apex of g_1. Figure 6.3 shows the g_1 curve relative to the rotor and the wide apex seal.
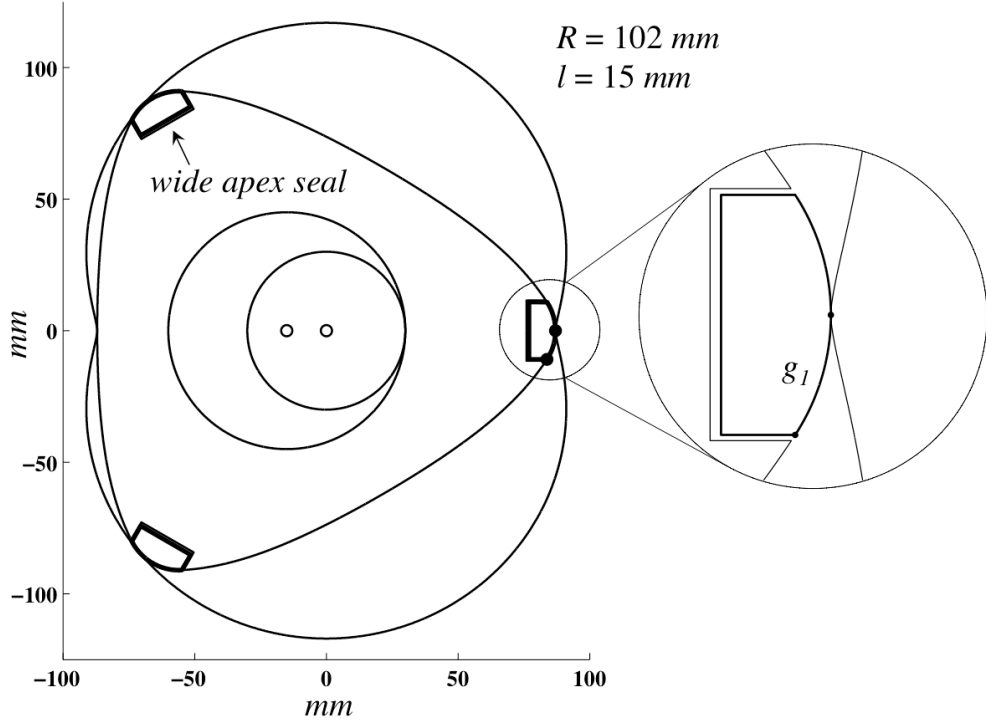
Figure 6.3: DF-designed rotary engine with wide apex seals.

To demonstrate the design of wide apex seals for the rotary engine, two deviation functions are examined here: the arc-based and nonarc-based deviation functions. A range of the widest apex seals that can be achieved with these functions is shown in Figures 6.4 and 6.5 and the corresponding parameters are given in Tables D.1 and D.2. First, the arc-based deviation function in terms of the rotor radius, $R = a + \rho$, is:

$$e_1(\theta_1) = \sqrt{(R - \rho)^2 + r_1^2 - 2(R - \rho)r_1 \cos(\theta_1)} - \rho \qquad 0 \leq \theta_1 \leq \theta_{1s} \qquad (6.3)$$

where ρ is the radius of the arc of the generating curve, i.e., the radius of the apex seal. Choosing a longer radius results in a wider seal.

Secondly, the nonarc-based deviation function is a third-order sinusoidal function, introduced previously:

$$e_1(\theta_1) = r_1(a_3 \cos^3 \theta_1 + a_2 \cos^2 \theta_1 + a_1 \cos \theta_1 + a_0), \quad 0 \leq \theta_1 \leq \theta_{1s} \qquad (6.4)$$

72

After applying the boundary conditions specified by the DF method algorithm, the coefficients were found:

$$a_3 = \frac{\cos^2 \theta_{1s}}{2 \sin^5 \theta_{1s}}$$

$$a_2 = \frac{\cos \theta_{1s}}{2 \sin^3 \theta_{1s}} - 3a_3 \cos \theta_{1s}$$

$$a_1 = \frac{1}{\sin \theta_{1s}} - 3a_3 \cos^2 \theta_{1s} - 2a_2 \cos \theta_{1s}$$

And the adjustable parameter a_0 becomes

$$a_0 = 1 - \frac{R}{r_1} - a_3 - a_2 - a_1$$

Now the rotor radius, R, and switch angle, θ_{1s}, can be used directly to design the rotary engine profile. The rotor radius can be used to size the profile while the switch angle is the conjugating range of the apex seal. One DF-design physical characteristic affected by switch angle is the width of the apex seal.

For the examples shown, the parameters for rotor radius, R, and eccentricity, l, are kept at those of Mazda's 13B rotary engine, which uses 2 mm seals. The DF-designed equivalent of this engine profile is shown in Figure 6.4a. As shown in Figure 6.4, widest apex seals are about 15 times larger than conventional apex seals. The width represents the range of contact the rotor has with the housing bore; for the conventional design method of a Wankel engine, the contact is a single point at the apex. In the DF-design method, the wider seal profile is the generating curve for the housing; the whole seal is conjugate from leading edge to trailing edge. The conventional apex seal profile is not conjugate to the Wankel engine housing profile, limiting the possible width of the apex seals. Figure 6.4b shows nearly the widest arc-based apex seal that can be achieved with the Mazda engine parameters, 29 mm. Wider seals are possible if eccentricity or rotor radius is adjusted. Figure 6.5a shows

(a) 1.99 mm   (b) 29.14 mm   (c) 21.87 mm   (d) 15.43 mm
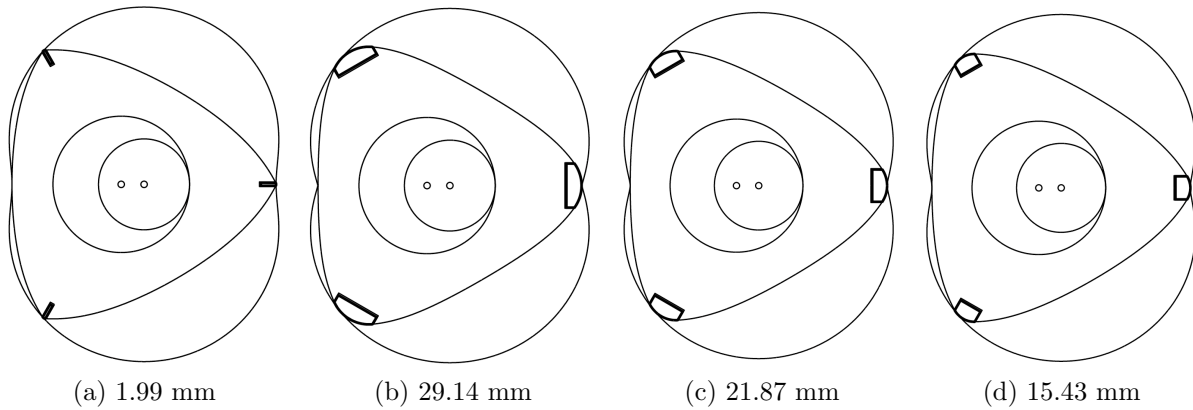
Figure 6.4: DF-designed engines of varying arc-based apex seal widths.

(a) 41.90 mm   (b) 34.47 mm   (c) 26.72 mm   (d) 18.64 mm
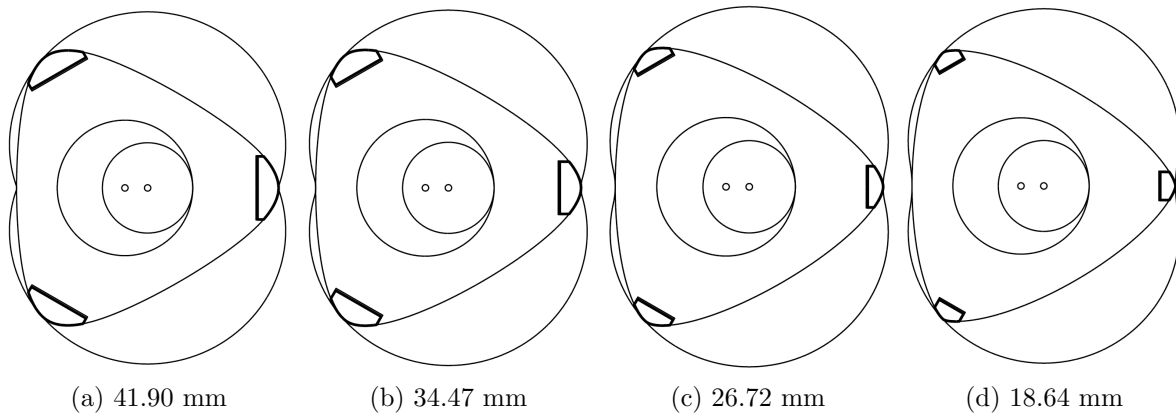
Figure 6.5: DF-designed engines of varying nonarc apex seal widths.

what is nearly the widest nonarc-based apex seal that can be achieved with Mazda engine parameters, about 42 mm. These widths are significantly larger than the maximum width apex seal used in any Mazda rotary engine, which is 3 mm.

6.2.2   Multi-Apex-Seal Design

The standard apex seal used in Mazda's rotary engines is 2 mm wide. Using this standard as an example, two possible multi-apex-seal configurations are shown in Figures 6.6b and 6.8b. In Figures 6.6a and 6.8a the wide apex seal as designed by the DF method is shown with the equivalent DF parameters for Mazda's 13B rotary engine. Figure 6.6a is a 9.7 mm wide apex seal, and the generating curve g_1 is shown as half of an apex seal profile. Figure 6.6b

(a) DF-designed wide apex seal   (b) Three 2 mm apex seals
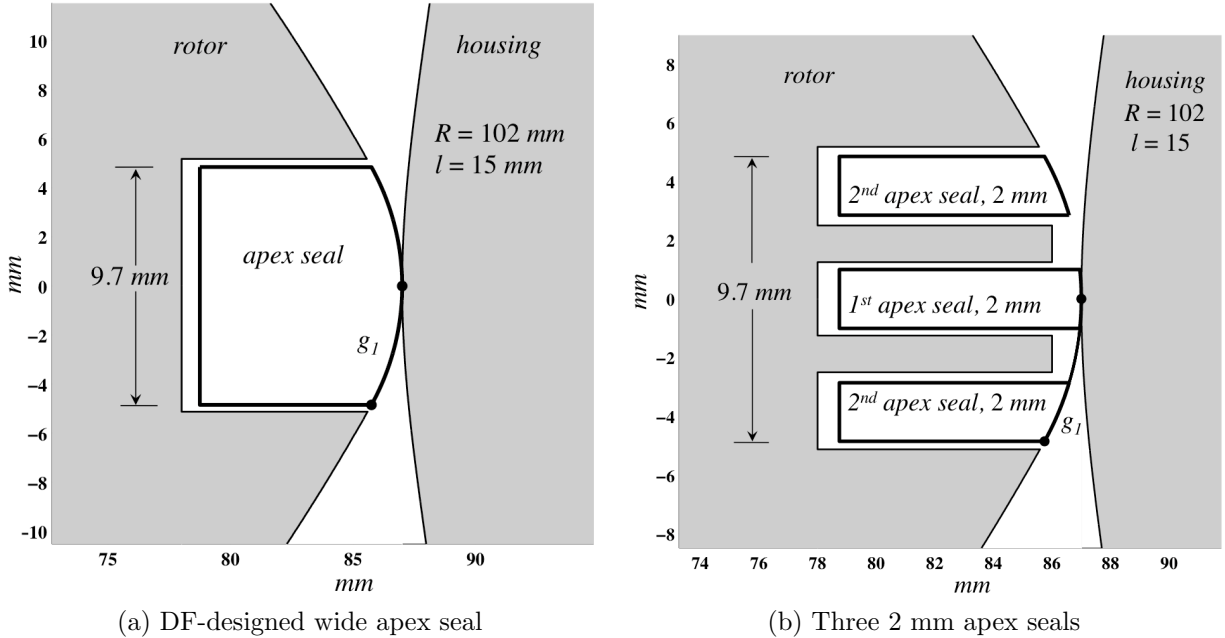
Figure 6.6: Hypothetical 3-seal apex sealing grid designed from a wide apex seal.

shows the same g_1 curve now represented by the profile of two 2 mm apex seals. A gap between them is needed in order for the rotor to have a slot for each individual seal. The ramification of this gap is that when the contact point between the rotor and housing is within this range, there is no conjugate contact, but the seals on either side are in contact due to external forces. All the seals in the multi-apex-seal system are always in contact with the housing bore due to the forces acting on the apex seals, whether conjugate at that position or not. The conventional rotary engine apex seals are not conjugate to the housing bore in any position, but are normally in contact due to external forces.

Figure 6.7 shows the three-seal configuration during operational conditions; all three seals are in contact with the housing. Springs are shown behind each of the seals, but the pressure forces from the adjacent chambers are mainly responsible for the seal maintaining contact during rotation.

Figure 6.8 shows a possible 5-apex-seal configuration for a 22 mm generating curve. As shown in Figure 6.8b, the g_1 curve is represented by the profiles of three 2 mm apex seals. Figure 6.9 shows the same seals in positions of operation; each seal is in contact with the
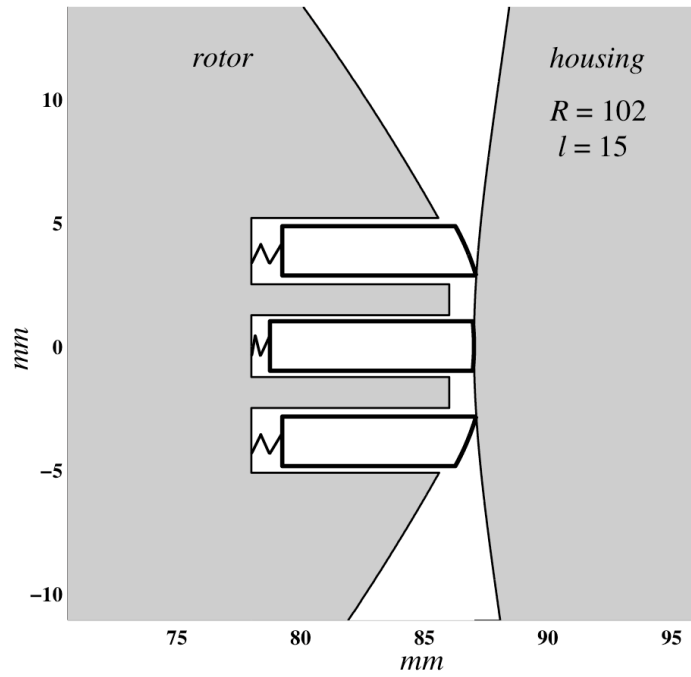
Figure 6.7: Hypothetical 3-seal apex sealing grid with spring-loaded contact.

(a) DF-designed wide apex seal

(b) Five 2 mm apex seals
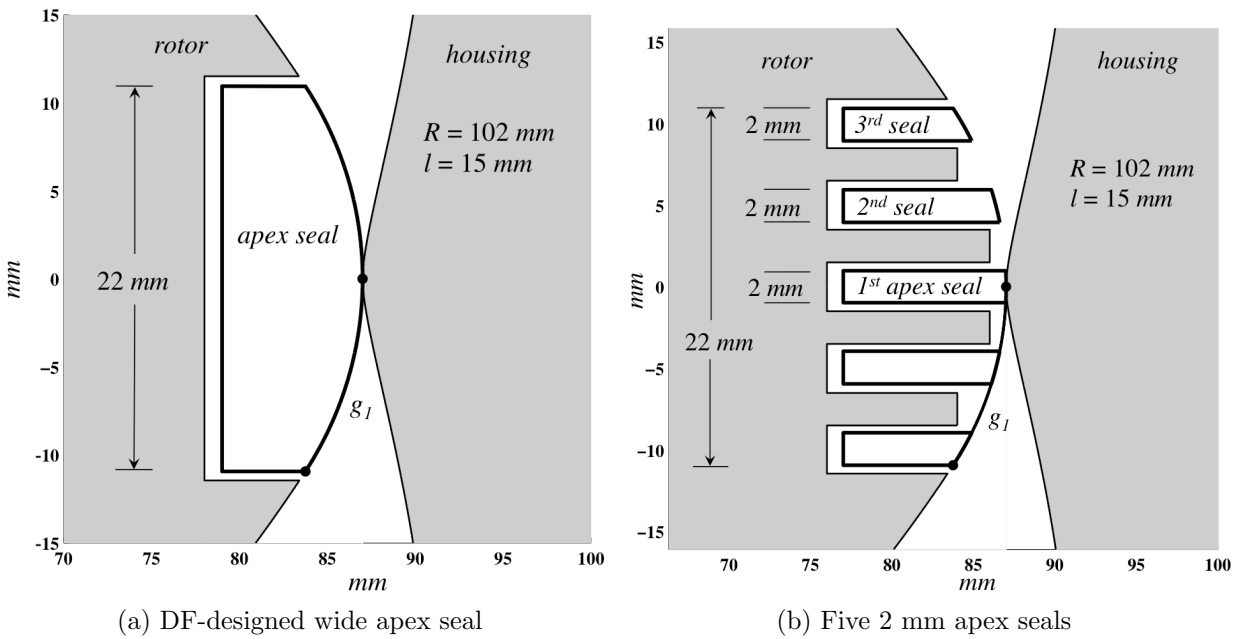
Figure 6.8: Hypothetical 5-seal apex sealing grid designed from wide apex seal.
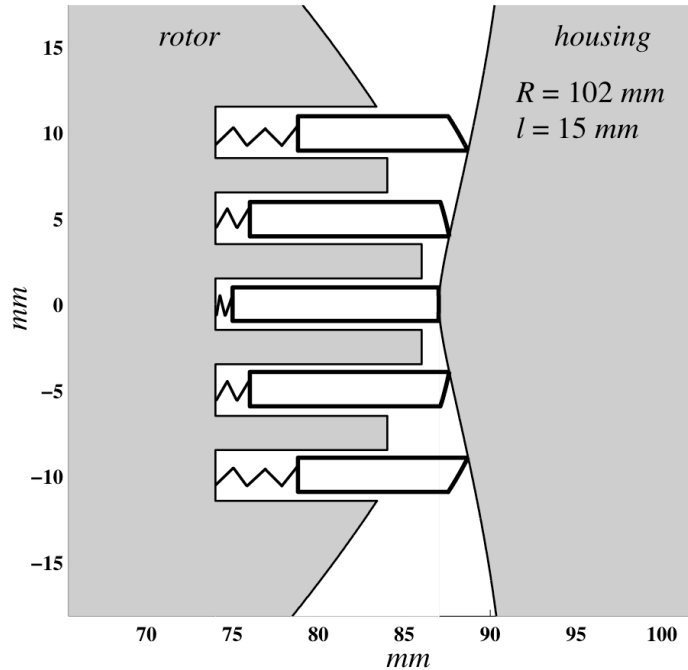
Figure 6.9: Hypothetical 5-seal apex sealing grid with spring-loaded contact.

housing bore. In the rotor position shown, the middle seal is in conjugate contact, the secondary pair of seals, immediately above and below the middle seal, are extended partially beyond the g_1 curve, and the tertiary pair of seals, at the outer edge of g_1, are extended the farthest. As the number of apex seals increases in the sealing grid, the deeper the slots in the rotor and the taller the seals should be in order to prevent the edge seals from falling out. The necessary height of the seal can be determined by the switch angle position. This is the rotor position at which the contact point is at the extreme of the g_1 curve. When the seal farthest from the middle seal, at the edge of the sealing grid, is in conjugate contact with the housing bore, the opposite seal, which is farthest away, is at maximum extension. The examples shown are symmetrical; the same number of apex seals are above and below the middle seal, which is at the true apex of the rotor. Asymmetrical multi-apex-seal configurations are possible that would create different sealing for different rotor positions. Also possible are different numbers of seals and different seal widths. The 2 mm industry standard for apex seals was used to illustrate some possibilities, but wider or narrower seals for the multi-

77

apex-seal grid may be more suitable depending on the application. Considering this and the variety of generating curve lengths, symmetric versus asymmetric configurations, the number of the seals at the apex could vary from 2 seals to more than 10.
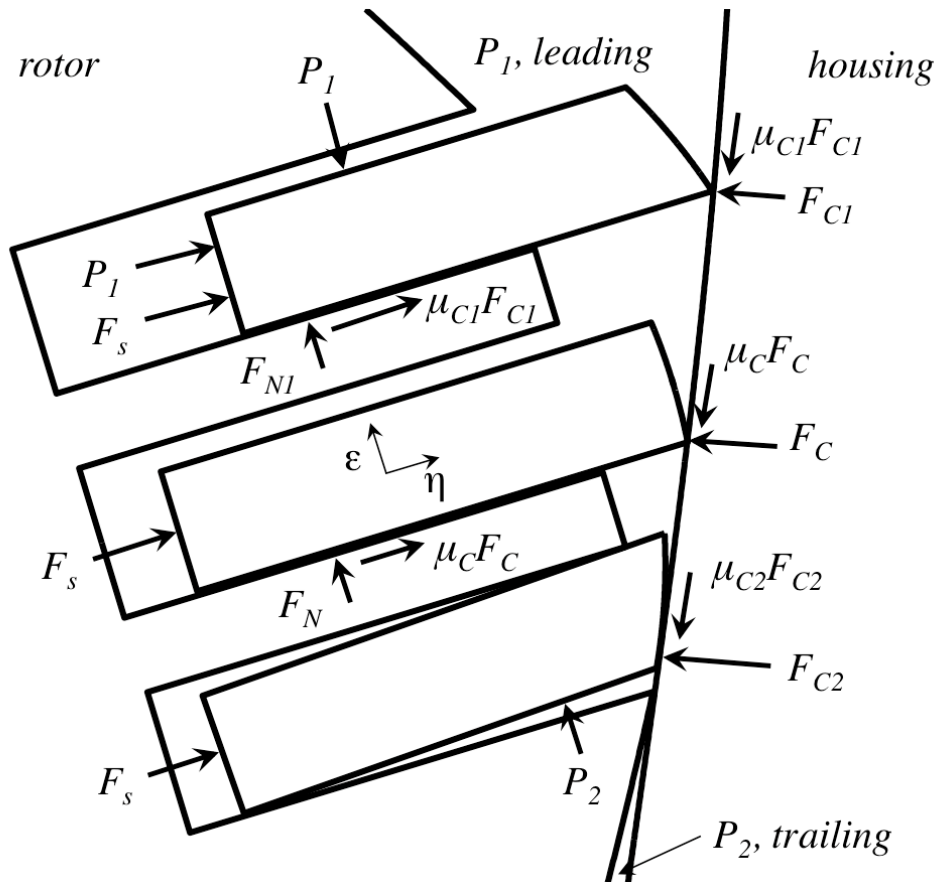
Figure 6.10: Hypothetical 3-seal apex sealing grid with body forces.

6.3 Interference

The multi-apex-sealing grid has significantly more interference than a single apex seal, but using multiple seals can accommodate larger discrepancies between the swept area of the seals and the area of the housing bore. Figure 6.11 shows the theoretical maximum area interference of the multi-apex-sealing system for a DF-designed engine and a conventional rotary engine of the same size. The sealing region width is the width of the apex seal profile

that the DF-engine is based on. The maximum interference was calculated by finding the swept area of the seal farthest from the rotor's true apex. The seal on the edge of the grid reaches the farthest beyond the rotor profile to make contact with the housing bore, and therefore creates the most interference. Figure 6.11 shows that the DF-designed engine has less interference than the conventional rotary engine for all widths of a multi-apex-sealing grid.
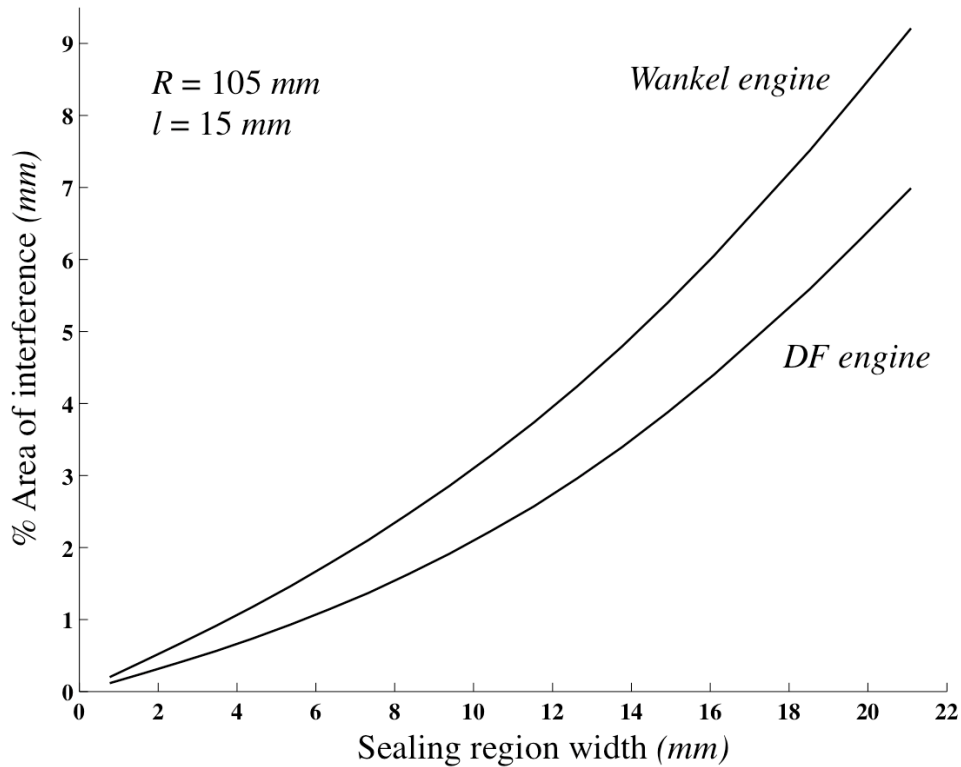
Figure 6.11: Maximum interference for multi-apex-seal grid.

6.4 Conclusions

The rotary engine has an inherent sealing disadvantage when compared with the reciprocating piston engine, and the challenge of effective apex sealing has prevented the rotary engine from achieving the same fuel efficiency and reduced exhaust emissions as piston engines [13]. The apex seals used in rotary engines are prone to damage and failure more frequently than

piston rings, which are used in triplicate for better sealing. One fundamental disadvantage of apex seals compared to piston rings is that there are normally three piston rings in each cylinder, whereas there is only one apex seal at each rotor apex. Secondly, piston rings have better contact with cylinder walls than an apex seal has with the housing bore. Thirdly, conventional apex seals experience high pressures from both the leading and trailing chambers, but at different times. This characteristic of rotating combustion causes regular direction reversals of resultant pressure forces on the apex seals, which can initiate separation. The separation of the seal during normal operation has been related to excess seal and bore damage, besides gas leakage [27, 28].

By designing the housing for a wider apex seal, multiple seals can be used at each apex, similar to the multiple piston rings used in reciprocating engines. All of the apex seals are simultaneously in contact with the housing, providing multiple barriers against gas leakage. In addition to increasing the number of barriers, the multi-apex-seal system also inhibits the rocking phenomenon found in apex seals during normal operation. This and other seal movements caused by pressure changes are prevented because each apex seal will only experience high pressure force from one side. The high pressures from the adjacent chamber tend to hold an apex seal in place, but separation can occur between the seal and the housing bore when the direction of the resultant pressure force reverses; in other words, the lower pressure side becomes the high pressure side. During normal rotary engine operation, this reversal occurs twice on every rotation due to the simultaneous stages of internal combustion occurring on each of the rotor flanks. The multi-apex-seal system isolates all the seals from the pressure changes of at least one of the chambers, and only the seals on the edge of the assembly experience high pressure from one side. This is a more stable configuration for all the apex seals, which can now be held in the same position throughout the rotation. This can improve the fuel and combustion efficiency and seal longevity, the performance discrepancies that have persisted between the rotary and reciprocating engines.

Chapter 7

Rotary Engine Profiles from Noncircular Pitch Curves

One important advantage of using the deviation function method for rotary engine design is the option of choosing noncircular pitch curves. The possibility of noncircular pitch curves for a rotary engine was introduced recently by Yan et al. in the context of gerotor pump design by DF method [38, 34]. They proposed that rotary engines could be designed with noncircular pitch curves using the same generating curves as those used to design gerotor pumps. This section instead applies the noncircular pitch DF method to rotary engine design by apex seal profile. Examples of engine profiles from noncircular pitch curves with arc-based apex seal profiles are provided.

7.1   Introduction

Two bodies engaged in rolling contact have conjugate centrodes which are the loci of poles, or instant centers. The most familiar pitch curves are the pitch circles of a gear pair like the one shown in Figure 7.1. The conjugate pitch circles represent the kinematic relationship between the engaged gears. The instant center of an external gear pair belongs to both corresponding pitch circles and lies on the centerline between the fixed rotation centers. The

circles have pure rolling contact and therefore also represent the angular speed ratio of the gear pair. The ratio of the pitch curve radii determines the speed ratio. If the pitch curves are a pair of circles, the angular speed ratio is constant. If the pitch curves are noncircular, the angular speed ratio is variable.
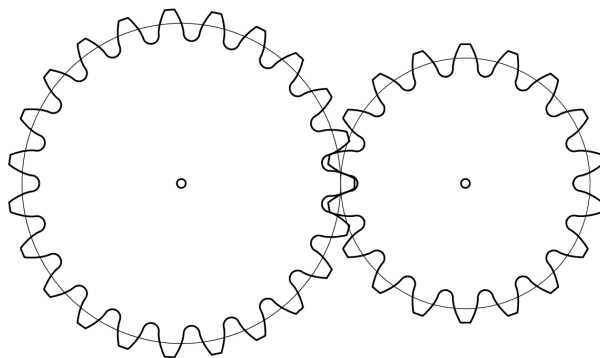
Figure 7.1: Gear pair shown with corresponding pitch circles.

Noncircular pitch curves have been used for noncircular gears, which have applications in mechanisms that require a change in angular velocity, such as quick-return, speed matching, or intermittent mechanisms [29, 19]. Noncircular gears have also been used for precise function generation [29, 19]. Compared to cams and linkages, noncircular gears offer some advantages in functionality and simplicity; they can provide unidirectional motion, are relatively compact, and are well-balanced for high speed operation [29]. The most common application of noncircular gears is a pair of external elliptical gears [12]. For conjugate meshing and complete rotatability, which means having closed centrodes, the elliptical gears are an identical pair [29].

Due to the complexity of the numerical computation involved in noncircular gear design, most of the relevant research addresses elliptical gears and their noncircular pitch curves [43, 33, 38]. Dooner presented a method for applying a pair of elliptical gears to the mitigation of torque and speed fluctuations in an output shaft [11]. Litvin describes a method for obtaining noncircular external pitch curves from predefined functions, but the distance between centers can not be manipulated as a design parameter [18].

Tong and Yang developed an analytical method for generating identical, external noncircular pitch pairs from an original pitch pair. This method is called the Direct-Profile-Design (DPD) method, and it enables the systematic generation of identical, noncircular, external pitch pairs, like the ones shown in Figure 7.2. Tong et al. developed criteria for designing pitch curves with C^1 continuity and a dimensionless parameter to generate families of curves. This parameter was geometrically interpreted as the pitch curve noncircularity. With the DPD method, many different lobes and profiles can be found for identical, external kinematic pairs. This method is applicable to noncircular gears and lobe pumps [42, 33, 34].
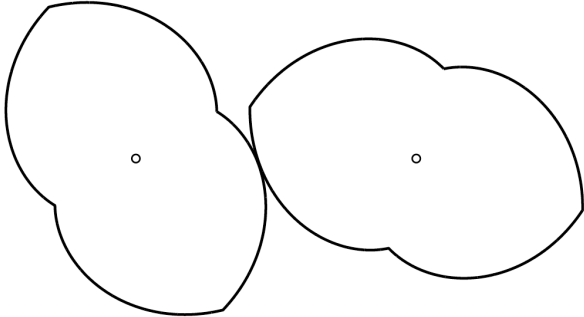
Figure 7.2: External, identical noncircular pitch curves.

Then Yan et al. developed a similar method of reshaping for the generation of noncircular internal pitch curves, like those in Figure 7.3b [38, 40]. The instant center of an internal pitch pair lies on a line extending beyond the two centers instead of between them on the centerline

(a) Circular pitch curves   (b) Noncircular pitch curves
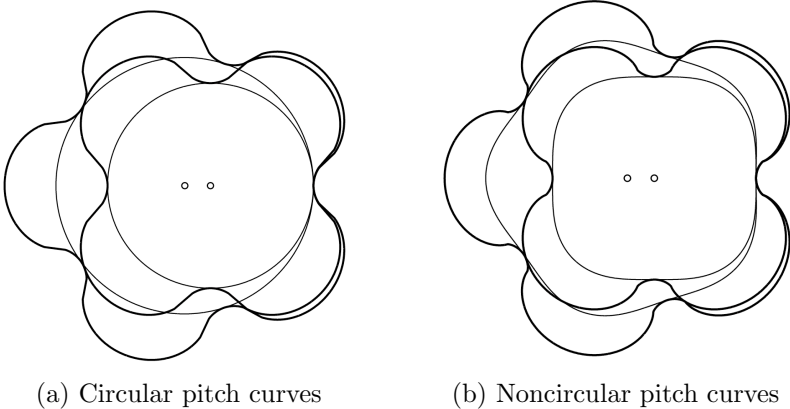
Figure 7.3: Gerotor pump profiles and their corresponding pitch curves.

itself, as for an external pitch pair. Internal pitch curves apply to internal noncircular gears, gerotors, and rotary mechanisms .

7.2   Noncircular Pitch Curve Generation
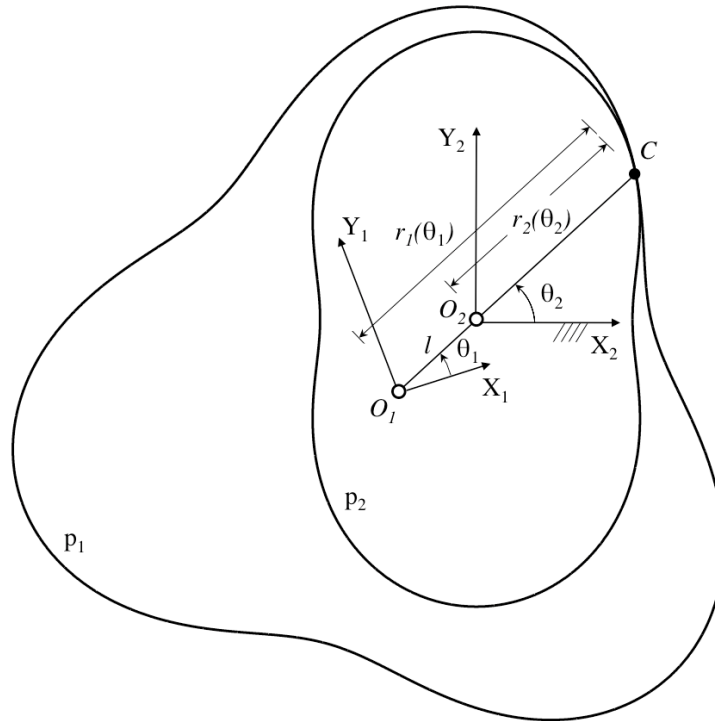
Figure 7.4: Internal noncircular pitch curves.

In Figure 7.4 there are two internal pitch curves, p_1 and p_2, engaged in pure rolling at point C, their instant center and point of contact. The frame $X_1 O_1 Y_1$ is attached to p_1 and the radius function $r_1(\theta_1)$ belongs to this frame, as well as the angle θ_1. Similarly, the pitch curve p_2 is attached to Frame 2, and the radius r_2 is a function of angle θ_2. Angles θ_1 and θ_2 describe the angle between their respective X axes and the centerline connecting the centers O_1 and O_2. According to the Arhnold-Kennedy theorem, the instant center C is also on the centerline, as depicted. At this position of pure rolling, the radii are related by the distance between centers, l:

$$r_1(\theta_1) - r_2(\theta_2) = l \tag{7.1}$$

84

Yan et al. established criteria for the $r_1(\theta_1)$ equation that defines the profile of a half-lobe of p_1. For a smooth profile over the whole pitch curve, there should be radial symmetry, a whole number of lobes, and C^1 continuity at the tips and roots where the r_1 segments join. As a design example, Yan et al. introduced a sinusoidal r_{1o} with three variables in order to satisfy all constraints [38, 40]:

$$r_{1o} = l[\sin(b\theta_1 + \phi) + a]$$

where

$$\alpha = \frac{N_2}{(N_1 - N_2)a}\sqrt{\frac{a}{a - 2}}$$

and

$$(a - 1)^2 < 1$$

The $r_1(\theta_1)$ equation becomes:

$$r_1(\theta_1) = \alpha l[\cos(N_1\theta_1) + a] + (1 - \alpha)l, \qquad 0 \le \theta_1 \le \frac{\pi}{N_1}$$

To incorporate a geometric family parameter for systematic design modification, the pitch curve noncircularity, k, was defined:

$$k = \frac{r_{1max}}{r_{1min}} \tag{7.2}$$

Where the maximum and minimum of r_1 occur at the pitch curve tip and root, respectively. Equation (7.2) can be used to incorporate k into an analytical r_1 equation. For the sinusoidal example:

$$k = \frac{\alpha(a - 2) + 1}{\alpha a + 1}$$

and then the free parameter a becomes:

$$a = -\frac{2}{k - 1} - \frac{1}{\alpha}$$
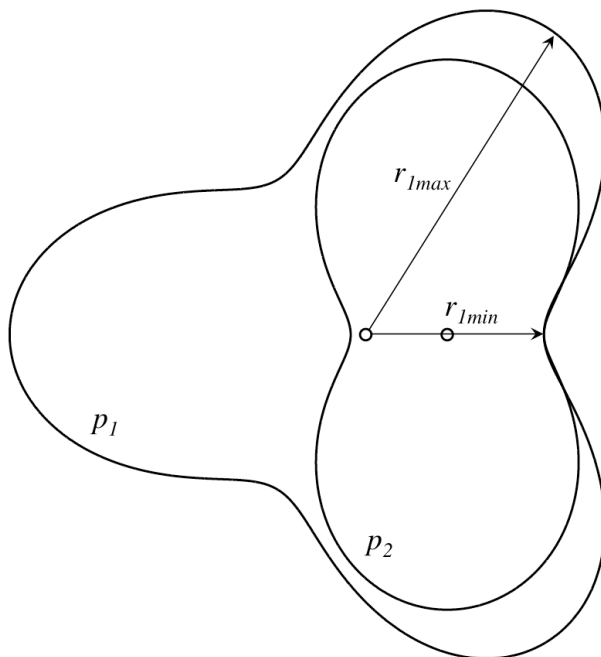
Figure 7.5: Noncircularity is defined by r_{1max}/r_{1min}.

α can be written in terms of the pitch noncircularity and plugged into the $r_1(\theta_1)$:

$$r_1(\theta_1) = \frac{1 - k^2 - (k-1)\sqrt{(k+1)^2 - 4k\left(1 - \frac{N_2^2}{(N_1 - N_2)^2}\right)}}{4k} \times$$

$$\left[\left[\cos(N_1\theta_1) - \frac{2}{k-1} - \frac{4k}{1 - k^2 - (k-1)\sqrt{(k+1)^2 - 4k\left(1 - \frac{N_2^2}{(N_1 - N_2)^2}\right)}} - l\right] + l\right]$$

(7.3)

Figure 7.6 shows a family of internal, noncircular pitch curves generated by equation (7.3), with varying pitch noncircularity. A pair of circular pitch curves have $k = 1$; the larger k value results in more distinct lobes on the profiles, assuming all other parameters are unchanging.

The use of noncircular pitch curves in a rotary engine design would require an unconventional positioning mechanism because the circular pitch position gears in the Wankel would no longer apply. The internal gear pair that position the rotor inside the housing have a 3:2

86

(a) $k = 1.1$ (b) $k = 1.5$ (c) $k = 2.0$
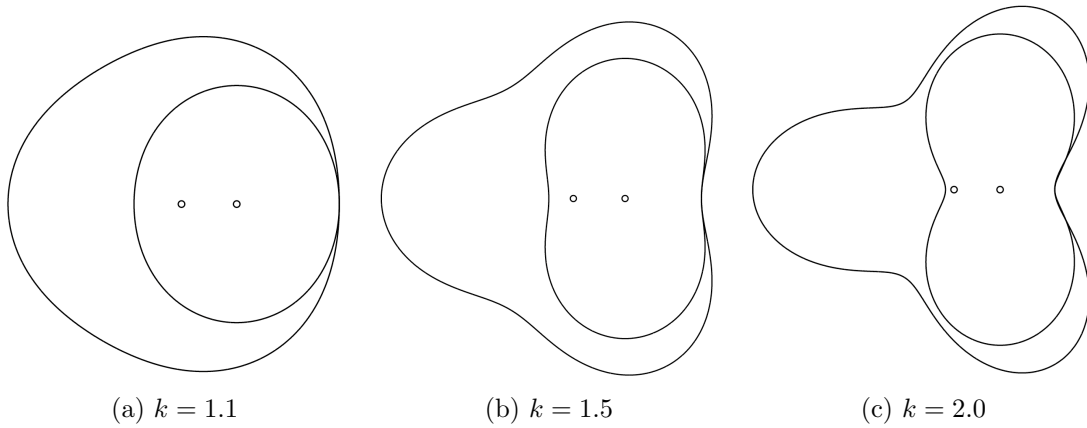
Figure 7.6: Noncircular pitch curves of varying noncircularity, k.

gear ratio and do not transmit torque. Noncircular internal gears could be used instead, and they would have the same noncircular pitch curves that belong to the DF-designed housing and rotor. Alternatively, another mechanism of positioning can be used to accommodate the variable speed ratio, such as magnetic gears [2, 3].

The variable speed ratio of the noncircular pitch curves can be a design advantage for rotary engine development because it also provides a variable speed ratio between the engine's main shaft and the rotor. In a conventional rotary engine, and the circular pitch DF rotary engines, this ratio is constant at 3:1. The main shaft rotates three times for each rotation of the rotor. With noncircular pitch curves, this ratio fluctuates depending on the rotor position. Figure 7.7 shows the fluctuations for different pitch noncircularities during a rotor revolution. For circular pitch curves, $k = 0$, and this is represented by a straight line. The fluctuations in the ratio increase as the noncircularity increases. This means that the rotor apex will travel slightly faster in some places and slightly slower in others.
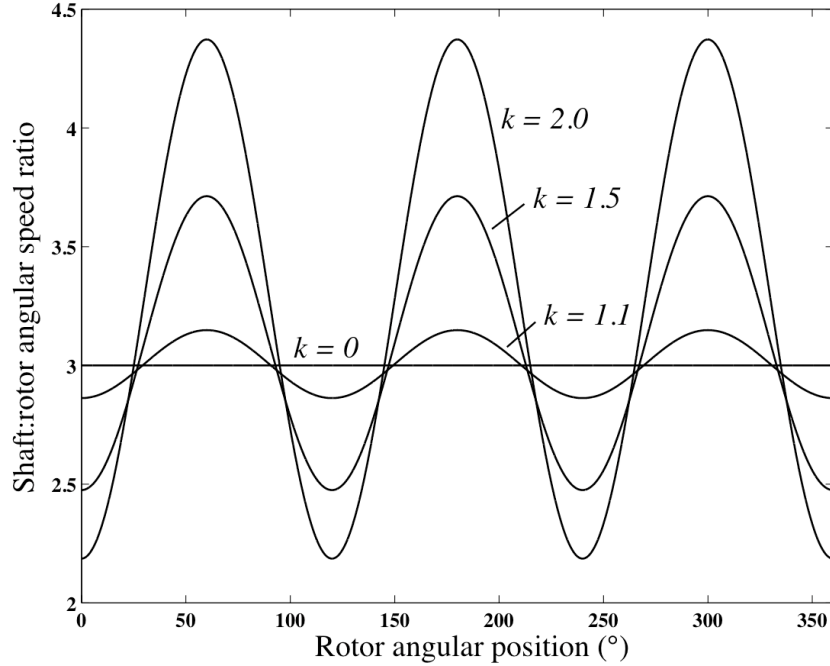
Figure 7.7: Variable speed ratios from noncircular pitch curves.

7.3 DF method for noncircular pitch rotary engine design

Tong et al. developed the deviation function method for gerotor design using noncircular pitch curves [34]. The same steps of the deviation function algorithm also apply to rotary engine design for using noncircular pitch curves. As described previously for the circular pitch rotary engine design, the deviation function method begins by modifying the pitch curves to obtain the rotor profiles, illustrated in Figure 7.8. The figure shows the coordinate system $X_1 O_1 Y_1$ attached to the center of the noncircular pitch curve $p_1(\theta_1)$, which is defined by the radius function $r_1(\theta_1)$. Angle θ_1 is measured from X_1, and each position on p_1 locates the center of a deviation circle, whose radius is defined by the deviation function $e_1(\theta_1)$. The deviation circles are shown in thin lines and their envelopes, $g_1(\theta_1)$ and $q_1(\theta_1)$, are shown in a solid bold line and dashed bold line respectively. The envelopes are found by the common
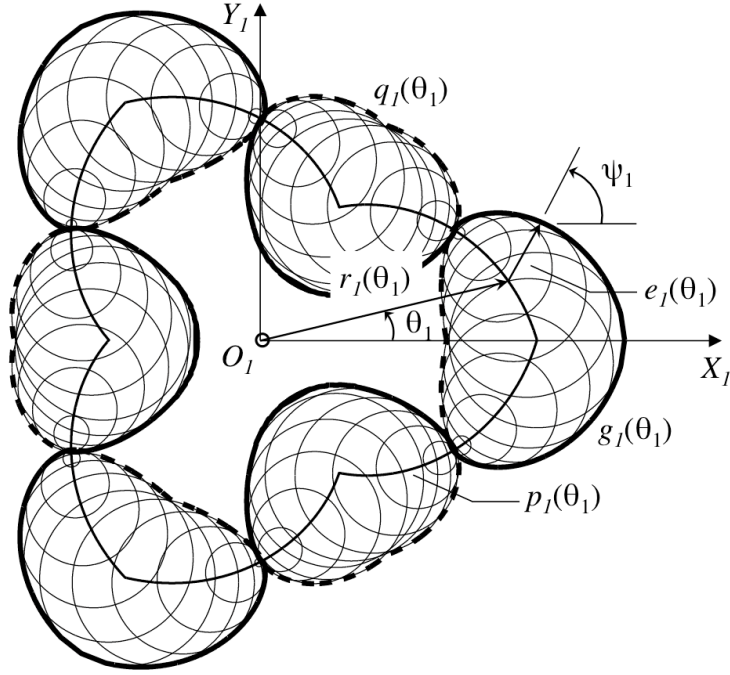
Figure 7.8: DF method using a noncircular pitch curve.

normal angle ψ_1. The envelope equations are:

$$g_{1x} = r_1(\theta_1)\cos\theta_1 + e_1(\theta_1)\cos\psi_1 \tag{7.4}$$

$$g_{1y} = r_1(\theta_1)\sin\theta_1 + e_1(\theta_1)\sin\psi_1$$

where ψ_1 is found by solving:

$$r_1'\cos(\psi_1 - \theta_1) + r_1\sin(\psi_1 - \theta_1) + e_1' = 0 \tag{7.5}$$

where $()'$ is $\dfrac{d}{d\theta_1}()$. The two solutions for ψ_1 are:

$$\psi_1 = \theta_1 - \tan^{-1}\frac{r_1'}{r_1} - \tan^{-1}\frac{e_1'}{\sqrt{r_1^2 + r_1'^2 - e_1'^2}} \tag{7.6a}$$

$$\psi_1 = \theta_1 - \tan^{-1}\frac{r_1'}{r_1} + \tan^{-1}\frac{e_1'}{\sqrt{r_1^2 + r_1'^2 - e_1'^2}} + \pi \tag{7.6b}$$

89

The g_1 and q_1 envelopes correspond to equations (7.6a) and (7.6b) respectively.

7.3.1 Design the apex seal profile, g_1

The DF method used with noncircular pitch curves allows for two possible configurations for p_1 with respect to generating curve g_1. Figure 7.9 shows the tip-to-root orientation, referring to the root of p_1 facing the g_1 curve. Figure 7.10 shows the tip-to-tip orientation in which the tip of p_1 faces the g_1 curve. These are the only two possible orientations because p_1 should be symmetrical with respect to the X_1 axis, and each generates different profiles and results in different kinematic relationships [38, 34].
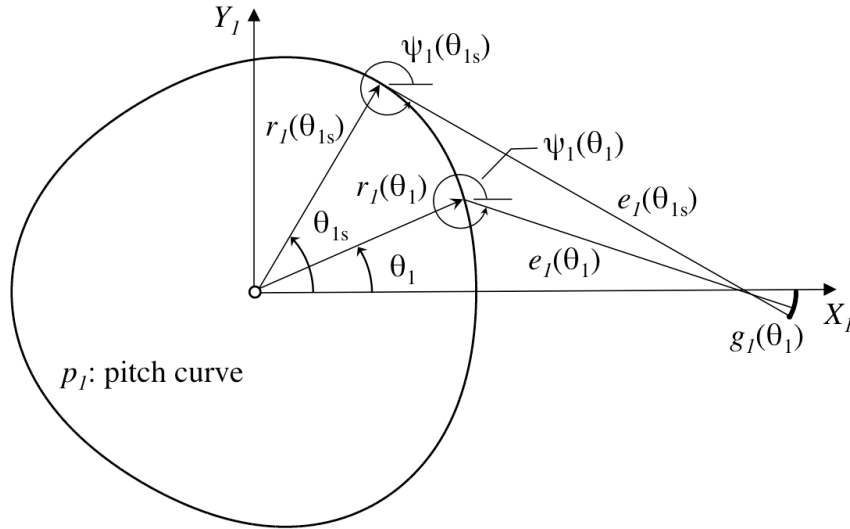
Figure 7.9: Tip-to-root orientation for g_1 and noncircular p_1.

As shown in Figures 7.9 and 7.10, the generated curve g_1 is defined by radius $e_1(\theta_1)$ from the θ_1 position on p_1. The lower limit of g_1 is found by the switch angle θ_{1s}, at which the line normal to $g_1(\theta_1 s)$ is tangent to $p_1(\theta_1 s)$, and has angle $\psi_{\theta_{1s}}$. For smooth rotors, g_1 should have C^1 continuity, so

$$e_1'(0) = \frac{de_1}{d\theta_1}(0) = 0$$

Referring to Figure 7.9, because the line normal to $g_1(\theta_{1s})$ is also tangent to $p_1(\theta_{1s})$, the angle of the normal line can be found using equation (2.3a) and setting the deviation function to
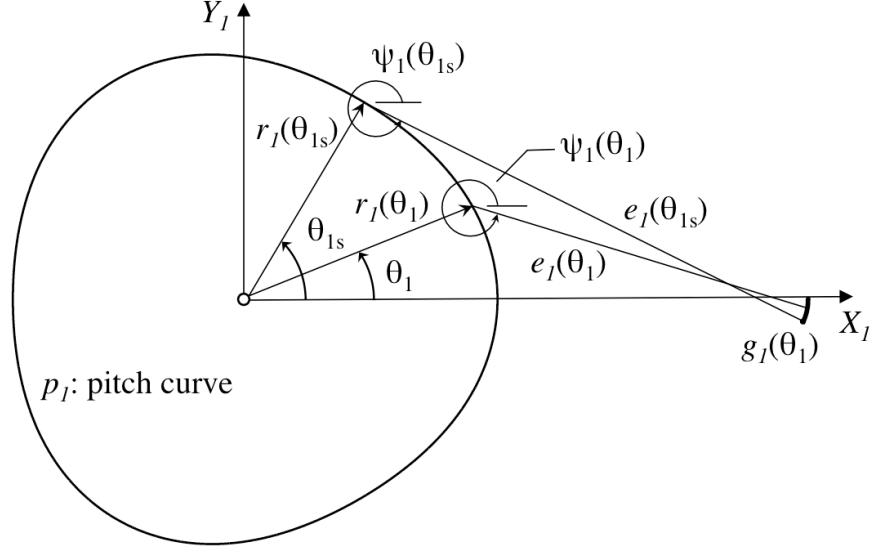
Figure 7.10: Tip-to-tip orientation for g_1 and noncircular p_1.

zero:

$$\psi_1(\theta_{1s}) = \theta_{1s} - \tan^{-1}(\frac{r_1'}{r_1}) \tag{7.7}$$

Since the normal to the curve and the tangent to the curve are separated by angle $\pi/2$, equation (7.7) also gives the tangent angle:

$$\psi_1(\theta_{1s}) - \frac{\pi}{2} = \theta_{1s} - \tan^{-1}(\frac{r_1'}{r_1}) - \frac{\pi}{2} \tag{7.8}$$

At $\theta_1 = \theta_{1s}$, the tangent angle at θ_{1s} is the same for the normal angle at $g_1(\theta_{1s})$, so comparing equations (2.3a) and (7.8):

$$\tan^{-1} \frac{e_1'(\theta_{1s})}{\sqrt{r_1^2(\theta_{1s}) + r_1'^2(\theta_{1s}) + e_1'^2(\theta_{1s})}} = \frac{\pi}{2} \tag{7.9}$$

A new kinematic constraint on e_1 is found:

$$e_1'(\theta_{1s}) = \sqrt{r_1^2(\theta_{1s}) + r_1'^2(\theta_{1s})} \tag{7.10}$$

91

7.3.2 Design the engine housing bore, g_2
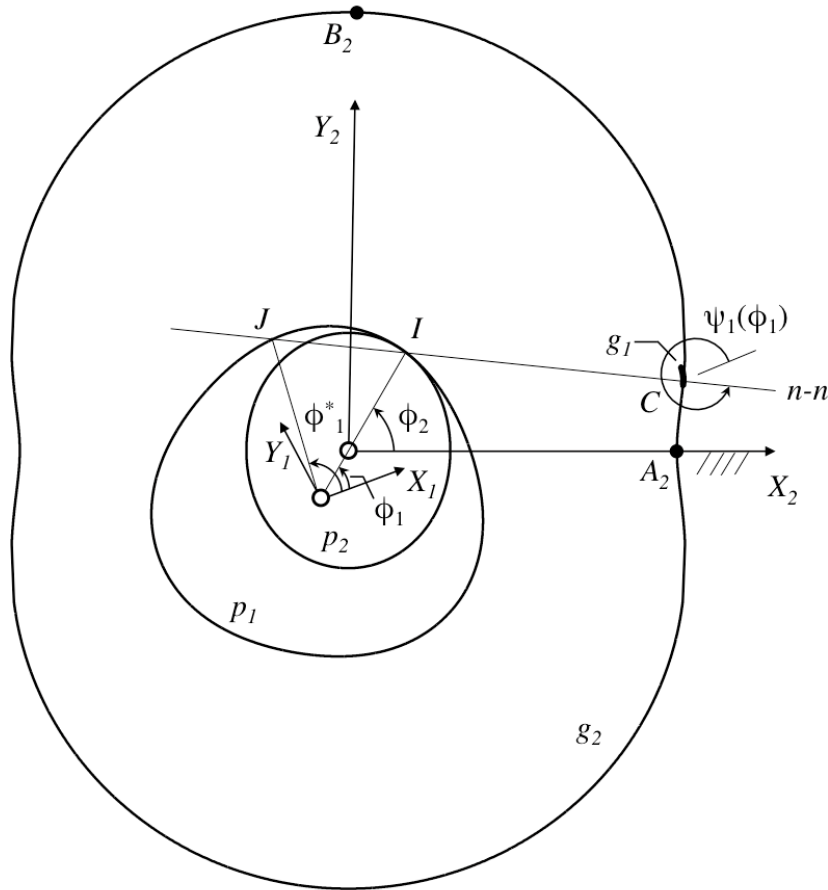
Figure 7.11: Generation of g_2.

The generation of the housing bore g_2 from the generating curve g_1 is shown in Figure 7.11. The pitch curve p_2 has a fixed coordinate system $X_2 O_2 Y_2$ while p_1 with its coordinate system $X_1 O_1 Y_1$ is moving. The distance between the pitch curve centers O_1 and O_2 is eccentricity l, and the instant center lies on an extension of the centerline. The g_1 curve is in conjugate motion with g_2 between points A_2 and B_2, which constitutes a half-lobe. A contact point, C, is indicated with the common normal line at this point drawn and labeled $n - n$. The normal line has angle ψ_1 with respect to the $X_1 O_1 Y_1$ coordinate system, and according to the kinematics of direct contact, the instant center, I, lies on $n - n$. The instant centers are identified by the intersection with p_1; in Figure 7.11 I is the current instant center and

J is a future instant center. The future instant center is associated with the latter section of g_2 when the contact point on g_1 is moving from the bottom to the top. As with circular pitch generation, g_2 is defined by both forward and reverse contact with g_1. During forward contact, the contact point on g_1 moves from top to bottom and at the switch angle, θ_{1s}, the contact point reaches the edge of g_1, and switches direction. As the contact point moves from the bottom of g_1 to the top, it is considered the reverse contact, and the deviation from the pitch curve is $e_1 + \overline{IJ}$, as seen in Figure 7.11. This periodic contact is also true of an apex seal inside a rotary engine.

Forward contact:

$$x_2 = r_2(\theta_1)\cos\phi_2 + e_2\cos\psi_2 \tag{7.11}$$

$$y_2 = r_2(\theta_1)\sin\phi_2 + e_2\sin\psi_2$$

where

$$\phi_1 = \theta_1, \quad 0 \le \theta_1 \le \theta_{1s}$$

$$r_2 = r_1 - l$$

$$\phi_2 = \int_0^{\phi_1} \frac{r_1}{r_2}\, d\phi_1$$

$$\psi_2 = \phi_2 - \phi_1 + \psi_1(\theta_1)$$

$$e_2 = e_1(\theta_1)$$

Reverse contact:

$$x_2 = r_2(\theta_1)\cos\phi_2^* + e_2^*\cos\psi_2^* \tag{7.12}$$

$$y_2 = r_2(\theta_1)\sin\phi_2^* + e_2^*\sin\psi_2^*$$

where

$$\phi_2^* = \int_0^{\phi_1^*} \frac{r_1}{r_2} \, d\phi_1^*$$

$$\psi_2^* = \phi_2^* - \phi_1^* + \psi_1(\theta_1)$$

$$e_2^*(\phi_2^*) = e_1(\theta_1) + IJ, \quad 0 \le \theta_1 \le \theta_{1s}$$

$$IJ = \sqrt{r_1^2(\theta_1) + r_1^2(\phi_1^*) - 2r_1(\theta_1)r_1(\phi_1^*)\cos(\phi_1^* - \theta_1)}$$

and ϕ_1^* is found by solving:

$$r_1(\theta_1)\sin(\psi_1 - \theta_1) = r_1(\phi_1^*)\sin(\psi_1 - \phi_1^*)$$

In order to design a smooth housing bore profile, the forward and reverse contact of g_2 must be continuous at the switch point, θ_{1s}. This means the normal angle of g_2, $\psi_2(\phi_2)$, should be a smooth function, and from the above equations, $\psi_1(\theta_1)$ should also be smooth. The function $\psi_1(\theta_1)$ decreases as θ_1 increases, reaching its minimum at the switch point, $\theta_1 = \theta_{1s}$. Therefore,

$$\psi_1'(\theta_{1s}) = \frac{d\psi_1}{d\theta_1}(\theta_{1s}) = 0$$

Differentiating equation (2.2) with respect to θ_1 and solving for ψ_1:

$$\psi_1' = 1 + \frac{e_1'' + r_1''\cos(\psi_1 - \theta_1) + r_1\sin(\psi_1 + \theta_1)}{r_1'\sin(\psi_1 - \theta_1) - r_1\cos(\psi_1 - \theta_1)} \tag{7.13}$$

The denominator in equation (7.13) approaches zero as θ_1 approaches θ_{1s}, so the numerator must also be zero at the switch point. Setting $\theta_1 = \theta_{1s}$ and solving for e_1'':

$$e_1''(\theta_{1s}) = \frac{r_1'(\theta_{1s})[r_1''(\theta_{1s}) + r_1(\theta_{1s})]}{\sqrt{r_1'(\theta_{1s}) + r_1^2(\theta_{1s})}} \tag{7.14}$$

94

Applying L'Hopital's Rule to equation (7.13):

$$\lim_{\theta_1 \to \theta_{1s}} \frac{e_1'' + r_1'' \cos(\psi_1 - \theta_1) + r_1' \sin(\psi_1 - \theta_1)}{r_1' \sin(\psi_1 - \theta_1) - r_1 \cos(\psi_1 - \theta_1)} = -1$$

$$\lim_{\theta_1 \to \theta_{1s}} \frac{e_1''' + r_1''' \cos(\psi_1 - \theta_1) + 2r_1'' \sin(\psi_1 - \theta_1) - r_1' \cos(\psi_1 - \theta_1)}{r_1'' \sin(\psi_1 - \theta_1) - 2r_1' \cos(\psi_1 - \theta_1) - r_1 \sin(\psi_1 - \theta_1)} = -1$$

Evaluating the limit at θ_{1s} and solving for $e_1'''(\theta_{1s})$ gives a constraint on the deviation function for a smooth housing profile:

$$e_1'''(\theta_{1s}) = \frac{r_1'''(\theta_{1s})r_1'(\theta_{1s}) + 3r_1''(\theta_{1s})r_1(\theta_{1s}) - 3r_1'^2(\theta_{1s}) - r_1^2(\theta_{1s})}{\sqrt{r_1^2(\theta_{1s}) + r_1'^2(\theta_{1s})}} \tag{7.15}$$

In order to check the g_2 curve for cusps, the radius of curvature can be found by:

$$\rho_{g_2} = \frac{1}{\left(\dfrac{1}{r_1 - l} - \dfrac{1}{r_1}\right)\dfrac{\cos \gamma}{\cos \zeta} - \dfrac{1}{e_1 + d_{IJ} + \rho_{g_1}}} + e_1 + d_{IJ} \tag{7.16}$$

where

$$\gamma = \tan^{-1}\left(\frac{r_1'}{r_1}\right)$$

$$\rho_{g_1} = \frac{\sqrt{r_1^2 + r_1'^2}\cos\zeta}{\psi_1'} - e_1$$

$$\zeta = -\tan^{-1}\left(\frac{e_1'}{\sqrt{r_1^2 + r_1'^2 - e_1'^2}}\right)$$

and $d_{IJ} = 0$ for forward contact, $d_{IJ} = IJ$ for reverse contact.

7.3.3   Design of rotor flank, g_3

The rotor flanks that connect the apex seals are found by the inside envelope of the rolled housing profile. Figure 7.12 illustrates the generation of the rotor flank g_3 by generating curve g_2. Now coordinate system $X_1 O_1 Y_1$ is fixed while $X_2 O_2 Y_2$ is moving. The forward contact section of the housing profile is $g_{2forward}$, and it has conjugate motion with the apex

seal g_1 and the rotor flank g_3. The forward contact on $g_{2forward}$ has the same instant centers, I, as when g_1 generated $g_{2forward}$, and the same g_1 curve is found by the forward contact equations. The reverse contact of $g_{2forward}$ has instant centers I_3 and deviation $e_2 + \overline{I_3 I}$. The contact point between $g_{2forward}$ and g_3 is indicated as C_3. The common normal line, $n - n$, has angle ψ_2 with respect to the X_2 axis. Instant center I_3 is identified by the intersection of $n - n$ and pitch curve p_1. The centerline also passes through I_3 and is measured by angle δ_1^* with respect to the X_1 axis.
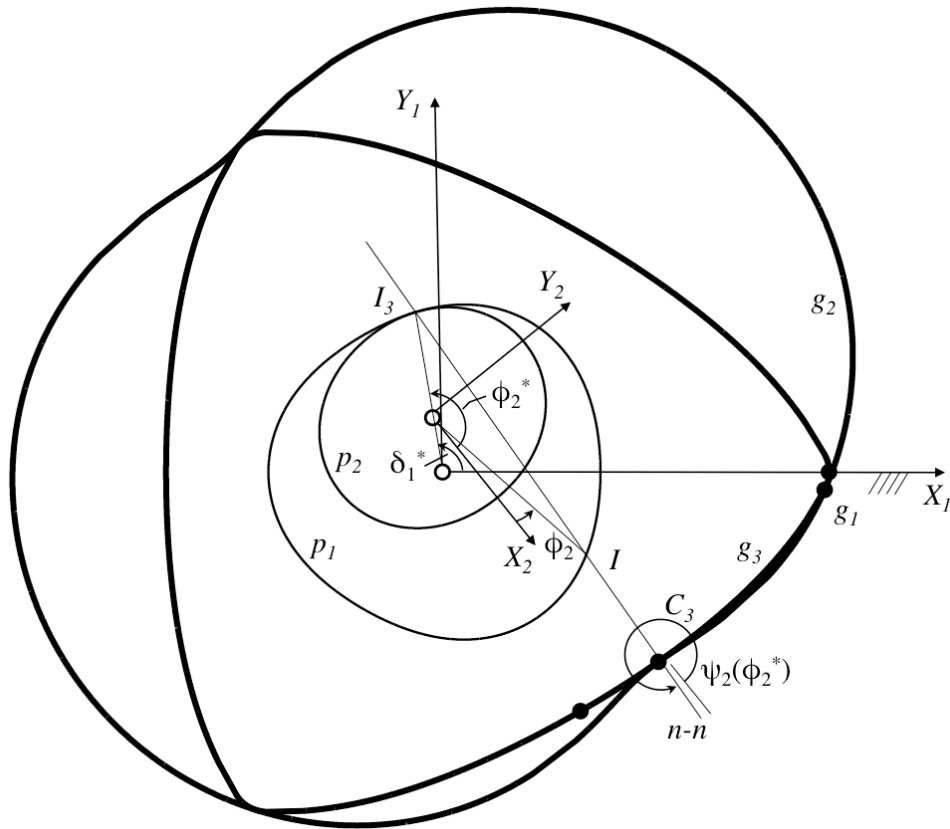
Figure 7.12: Generation of g_3.

Reverse contact:

$$x_3 = r_1(\delta_1) \cos \delta_1 + e_3 \cos \psi_3 \tag{7.17}$$

$$y_3 = r_1(\delta_1) \sin \delta_1 + e_3 \sin \psi_3$$

96

Table 7.1: Deviation function algorithm for rotary engine design

Step 1: select number of lobes	$n = 3$ for rotary engine
Step 2: select e_1 satisfying	$e_1'(0) = 0$
	$e_1'(\theta_{1s}) = \sqrt{r_1^2 + r_1'^2}$
	$e_1''(\theta_{1s}) = \dfrac{r_1'(r_1'' + r_1)}{\sqrt{r_1^2 + r_1'^2}}$
	$e_1'''(\theta_{1s}) = \dfrac{r_1'''r_1' + 3r_1'^2 - r_1^2}{\sqrt{r_1^2 + r_1'^2}}$
Step 3: obtain g_1	Generating curve: g_1 or q_1
Step 4: check for crossovers	g_1 lies outside p_2
Step 5: obtain g_2	Generated housing: g_2
Step 6: check for cusps on g_2	$\rho_{g_2} \neq 0$
Step 7: obtain g_3	Inside envelope of g_2

where

$$\delta_1 = \int_0^{\phi_2^*} \frac{r_2(\phi_2^*)}{r_1(\phi_2^*)} \, d\phi_2^*$$

$$\psi_3 = \delta_1 - \phi_2^* + \psi_2(\phi_2)$$

$$e_3 = e_2(\phi_2^*) + II_3$$

$$II_3 = \sqrt{r_2^2(\phi_2) + r_2^2(\phi_2^*) - 2r_2(\phi_2)r_2(\phi_2^*)\cos(\phi_2^* - \phi_2)}$$

and ϕ_2^* is found by solving:

$$r_2(\phi_2)\sin(\psi_2 - \phi_2) = r_2(\phi_2^*)\sin(\psi_2 - \phi_2^*) \tag{7.18}$$

Table 7.1 summarizes the DF algorithm for noncircular pitch rotary engine design in seven steps.

Table 7.2: Figure 7.13, DF-parameters for tip-to-root orientation

Figure No.	R	l	ρ	θ_{1s}	k	seal width (mm)
7.13a	105	15	-10	1.047	1.1	9.85
7.13b	105	15	-10	0.897	1.75	12.36
7.13c	105	15	-10	0.85	2.0	13.07
7.13d	105	15	-10	0.775	2.5	14.15

7.4 Arc-based Apex Seals with Noncircular Pitch Curves

As an example, the arc-based apex seal profile deviation function is introduced for noncircular pitch curves and some example profiles are found using the noncircular pitch profiles developed previously. All the examples provided have the same size geometry as the Mazda rotary engine; eccentricity is 15 mm and rotor radius is 105 mm. For an arc generating curve, the deviation function can be found by law of cosines:

$$e_1(\theta_1) = \sqrt{(R+\rho)^2 + r_1^2(\theta_1) - 2(R+\rho)r_1(\theta_1)\cos(\theta_1)} - \rho, \qquad 0 \le \theta_1 \le \theta_{1s} \qquad (7.19)$$

where R is the rotor radius and ρ is the radius of the apex seal profile. Once the orientation of the pitch curves is chosen (tip-to-root or tip-to-tip), the free parameters from the noncircular pitch curves are the number of lobes, n, the eccentricity, l, and noncircularity k. For a rotary engine of a specific size, the remaining free parameters are the switch angle, θ_{1s}, and apex seal radius ρ. Figure 7.13 and 7.14 show some examples of noncircular pitch rotary engine profiles created by using the tip-to-root orientation of the pitch curves. Tables 7.2 and 7.3 have the corresponding deviation function parameters as well as the apex seal widths. In Figure 7.13, the apex seal radius is kept constant and the pitch curve noncircularity is changed. The switch angle is limited to a narrow range by all the other parameters, for a smooth profile. Figures 7.13 to 7.15 indicate the width of the apex seal by the endpoints. Figure 7.13 shows wide apex seals and Figure 7.14 has the conventional size of 2 mm.

Figure 7.15 shows some examples of profiles created using the tip-to-tip orientation, and
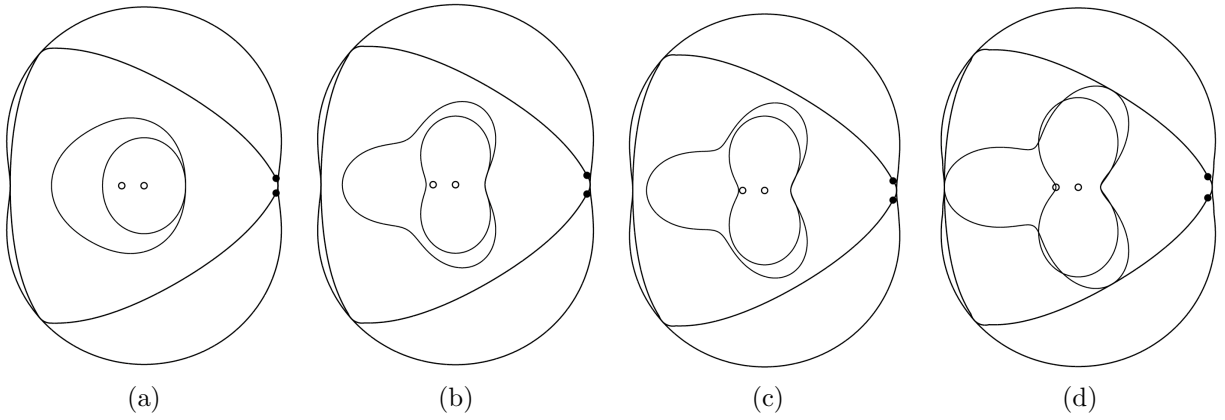
Figure 7.13: Noncircular pitch curves with tip-to-root orientation, $\rho = -10$.
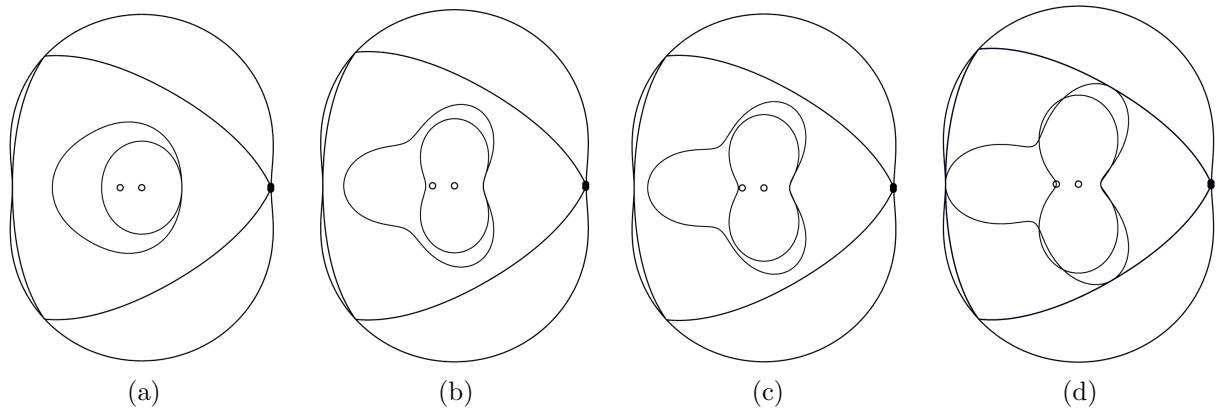
Figure 7.14: Noncircular pitch curves with tip-to-root orientation, seal width 2 mm.

Table 7.3: Figure 7.14, DF-parameters for tip-to-root orientation

Figure No.	R	l	ρ	θ_{1s}	k	seal width (mm)
7.14a	105	15	-2.27	1.047	1.1	2.00
7.14b	105	15	-1.85	0.95	1.75	2.00
7.14c	105	15	-1.73	0.9	2.0	2.00
7.14d	105	15	-1.59	0.82	2.5	2.00
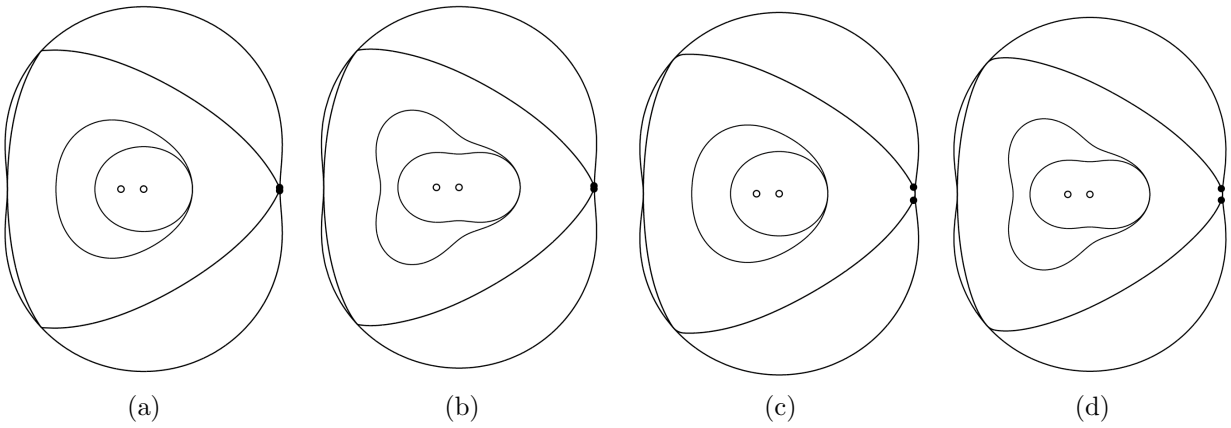
Figure 7.15: Noncircular pitch curves with tip-to-tip orientation.

Table 7.4: Figure 7.15, DF-parameters for tip-to-tip orientation

Figure No.	R	l	ρ	θ_{1s}	k	seal width (mm)
7.15a	105	15	-2.3	1.03	1.1	2.00
7.15b	105	15	-2.23	0.6	1.5	2.00
7.15c	105	15	-10	0.8	1.1	8.64
7.15d	105	15	-10	0.5	1.5	7.85

Table 7.4 provides the corresponding deviation function parameters along with seal width. This orientation for this deviation function limited the noncircularity of the pitch curves more than the tip-to-root orientation. Higher noncircularity values resulted in significantly wider apex seals that also had some dwell on the lower edge of the seal as it moved around the housing profile. For this example, the noncircularity values are limited to $k = 1.5$, and both wide apex seals and conventional apex seal sizes are provided.

7.5 Conclusions

The deviation function method for rotary engine design can generate profiles from noncircular pitch curves, which makes many more profiles possible and accessible in a systematic way, without the use of higher order nonlinear equations. Noncircular pitch designs may enhance certain characteristics such as the shape of the chambers, the apex sealing, or the timing

of the thermodynamic stages by a variable speed ratio. Variable speed ratios between the main shaft and the rotor can be used to modify the velocity of the apex seals or the Otto cycle phase durations, by manipulating the pitch curves. In the examples given, all the profile sizes have the same size geometry as Mazda's rotary engine, but the eccentricity and rotor radius can be changed for even more profile variety or for different applications. Other deviation functions can also be used, such as a nonarc-based deviation function, or a different noncircular pitch curves by changing the radius function.

Chapter 8

Conclusions and Future Work

8.1 Conclusions

In Chapters 2 through 7 the design and analysis of rotary engines by the deviation function method was presented. The most significant contributions are summarized as follows:

1. The deviation function method for rotary engine design by apex seal profile.

By using this method of rotary engine design, the apex seal profile can be designed and incorporated into a highly conforming housing bore profile. The apex seal and housing bore are a conjugate pair that has better apex sealing than conventional rotary engines. Also, by using the apex seal profile as the generating curve, many more engine profiles are possible than with the conventional design method. With a larger variety of profiles now available, the rotary engine design can be optimized for apex sealing as well as other performance characteristics simultaneously.

2. The deviation function selection for rotary engine design by geometric parameters.

For the first time, the selection of rotary engine geometry can be independent of apex sealing capability, and the geometric parameters of the profile do not correspond to limitations on maximum compression ratio and volumetric displacement. This DF method can be used to select the rotor and housing profile geometry for compression ratio and swept area

without the conventional limitation on sealing index. For either criterion, there are a range of DF-designed profiles available, allowing for more design flexibility.

3. Multi-apex-sealing grid design.

This unique sealing configuration addresses the apex sealing challenges of the conventional rotary engine by having multiple barriers against leaks and preventing a single apex seal from experiencing resultant force direction reversal. This configuration begins by using the DF method of rotary engine design by apex seal profile to generate a housing profile from a wide apex seal. The wide apex seal can then be replaced by multiple conventionally narrow seals, creating a sealing system akin to the multiple piston rings on each piston.

4. The deviation function method for noncircular pitch curve rotary engine design.

Many more engine profiles are available by the DF method of noncircular pitch rotary engine design, and the noncircular pitch curves enable variable speed ratios. Controlling the speed ratio between the rotor and the main shaft would allow for some timing and phase development manipulation during the stages of combustion.

8.2 Future Work

Further research topics are listed below:

1. Circular pitch curve rotary engine designs can be further developed with more deviation functions and different apex seal profiles. Alternate selection methods may be developed for other geometric properties and performance criteria.

2. Noncircular pitch curve rotary engines can be further studied for alternate apex seal profiles and more profile variety. The possibilities of a four-chambered rotary engine design should be investigated. The applications and advantages of a variable speed ratio in an engine or other rotary device can be developed. The DF methodology for systematic design using noncircular pitch curves can be extended for certain characteristics or performance criteria.

3. The apex sealing configurations proposed here can be fabricated and experimentally tested for further development and various applications.

4. Some current rotary engine research is focussed on portable rotary engine power systems such as the MEMS and small-scale rotary engines. The DF method of rotary engine design can be applied to these specific applications in order to address the unique design challenges - such as integrated apex sealing without assembly and profiles to optimize waste heat management.

Appendix A

Rotary Engine Design Parameters

Table A.1: Figure 4.5, Compression ratio for arc-based DF with $l = 1$.

R/l	ρ							
	0	0.5	1	1.5	2	2.5	3	3.5
6	15.6081	14.3552	13.0552					
7	18.2857	17.1035	15.8726	14.5935				
8	20.7992	19.6899	18.5347	17.3318	16.0801	14.7820		
9	23.1481	22.1106	21.0305	19.9058	18.7345	17.5151	16.2473	14.9350

Table A.2: Figure 4.6, Specific Displacement for arc-based DF with $l = 1$.

R/l	ρ							
	0	0.5	1	1.5	2	2.5	3	3.5
6	53.1680	53.3581	53.5885					
7	60.8723	61.0083	61.1680	61.3581				
8	68.6524	68.7548	68.8722	69.0083	69.1680	69.3581		
9	76.4825	76.5624	76.6524	76.7548	76.8722	77.0083	77.1680	77.3580

Table A.3: Figure 4.7, Theoretical Maximum Compression Ratio

R/l	θ_{1s}										
	40°	42.5°	45°	47.5°	50°	52.5°	55°	57.5°	60°	62.5°	65°
5	11.5637	12.0392	12.5477								
6			12.7458	13.3427	13.9904	14.6971	15.4690				
7				13.3461	14.0209	14.7594	15.5779	16.4804	17.4810		
8					14.1373	14.9078	15.7577	16.7108	17.7782	18.9800	20.3293
9							15.7693	16.7496	17.8470	19.0872	20.5041

Table A.4: Figure 4.8, Specific Displacement

R/l	θ_{1s}										
	40°	42.5°	45°	47.5°	50°	52.5°	55°	57.5°	60°	62.5°	65°
5	45.7912	45.6861	45.5799								
6			53.5799	53.4725	53.3635	53.2528	53.1400				
7				61.4854	61.3766	61.2661	61.1536	61.0387	60.9212		
8					69.3634	69.2527	69.1399	69.0248	68.9069	68.7858	68.6612
9							77.1399	77.0247	76.9068	76.7858	76.6612

Appendix B

Sealing Index

The Euler-Savary equation is used here to relate the radii of curvature of the apex seal and the conjugate housing profile, first for the forward segment of the housing profile, then for the reverse contact segment. In Figure B.1, the apex seal profile is labeled g_1, and is rolling with its pitch circle p_1. The stationary housing profile is $g_{2forward}$, the forward contact portion, and its fixed centrode is p_2. At the position shown, the pitch point is P and the contact point is labeled C_1. The tangent line and inflection circle are drawn at P, and the diameter of the inflection circle is δ. The curve normal at C_1 passes through P and the two centers of curvature, A_1 and A_2, which correspond to g_1 and $g_{2forward}$ respectively. The angle between the curve normal at C_1 and the tangent at P is denoted ζ.

The Euler-Savary equation can be written:

$$\left(\frac{1}{\overline{PA_1}} - \frac{1}{\overline{PA_2}} \right) \sin \zeta = \frac{1}{\delta} \tag{B.1}$$

$\overline{A_1 C_1}$ and $\overline{A_0 C_1}$ are the radii of curvature for g_1 and g_2, and adhering to the sign convention, that is ρ_{g1} and $-\rho_{g2}$ respectively. Substituting in the previously used notation, $\overline{PC_1}$ is equal to the deviation function, e_1, at the angular position, θ_1, and the curve normal has angle ψ_1
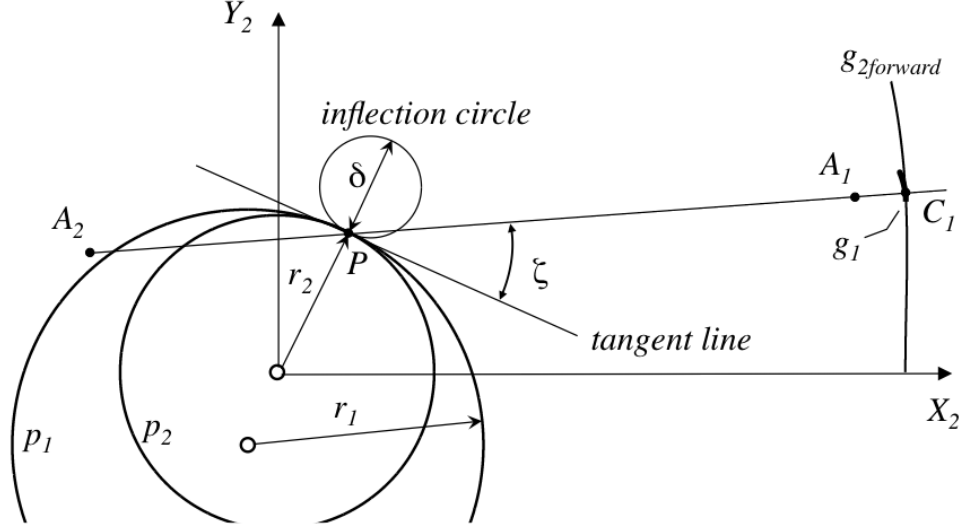
Figure B.1: Euler-Savary equation for DF-designed rotary engine.

with respect to the X_1 axis. So the forward contact Euler-Savary equation becomes:

$$\left(\frac{1}{e_1 - \rho_{g1}} - \frac{1}{e_1 - \rho_{g2}} \right) \cos(\theta_1 - \psi_1) = \frac{1}{\delta} \tag{B.2}$$

The diameter of the inflection circle can be calculated from the radii of the moving and fixed centrodes:

$$\frac{1}{r_1} - \frac{1}{r_2} = \frac{1}{\delta} \tag{B.3}$$

where $r_2 = r_1 - l$ in this case. Therefore the Euler-Savary equation as it applies to the forward contact housing profile can be written:

$$\left(\frac{1}{e_1 - \rho_{g1}} - \frac{1}{e_1 - \rho_{g2}} \right) \cos(\theta_1 - \psi_1) = \frac{1}{r_1} - \frac{1}{r_1 - l} \tag{B.4}$$

Figure B.2 shows the apex seal in a position of reverse contact, along with the whole reverse contact section of g_2. Now the pitch point P is on the opposite side of the pitch curves, and each of these reverse contact instant centers, also labeled J, corresponds to a forward contact instant center I. The quantity IJ must now be considered for lengths $\overline{PA_1}$ and $\overline{PA_2}$. Therefore the Euler-Savary equation as it applies to the reverse contact section of

108
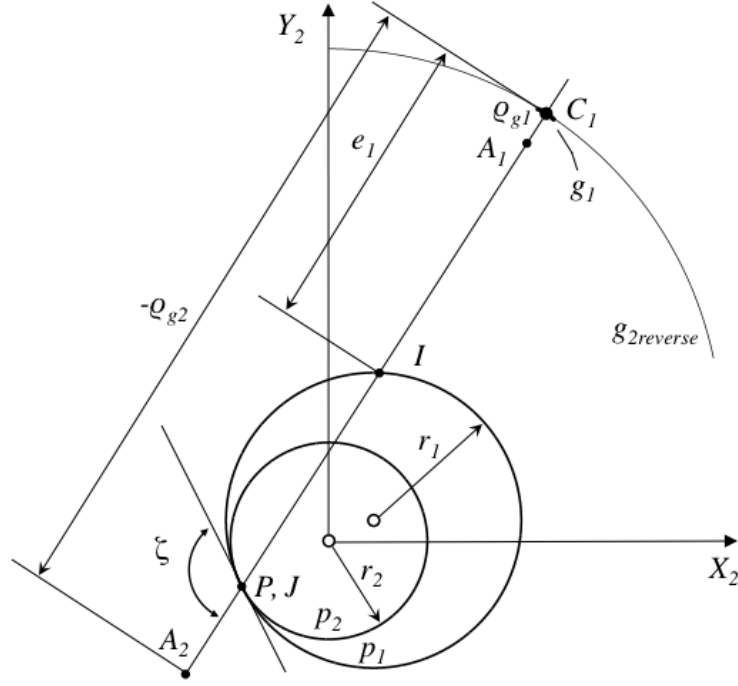
Figure B.2: Euler-Savary equation for DF-designed rotary engine.

the housing profile is:

$$\left(\frac{1}{e_1 + IJ - \rho_{g1}} - \frac{1}{e_1 + IJ - \rho_{g2}} \right) \cos(\theta_1 - \psi_1) = \frac{1}{r_1} - \frac{1}{r_1 - l} \tag{B.5}$$

The sealing index for the DF-designed rotary engine is defined as the arc length of the seal profile, ΔS, within a clearance Δt of the housing profile. Referring to Figure B.3, the apex of the rotor is in the $\theta = 0$ position, which is in the convex region of the housing profile. In this position, both the housing profile and apex seal are convex and therefore both radii of curvature are positive. This derivation assumes that Δt and ΔS are very small compared to ρ_1 and ρ_2.

$$\frac{\Delta S}{2} = \rho_1 \Delta \theta_1$$

$$
\begin{aligned}
\Delta t &= \rho_1(1 - \cos\Delta\theta_1) + \rho_2(1 - \cos\Delta\theta_2) \\
&= \rho_1\left(2\sin^2\frac{\Delta\theta_1}{2}\right) + \rho_2\left(2\sin^2\frac{\Delta\theta_2}{2}\right) \\
&= 2\rho_1\left(\frac{\Delta\theta_1}{2}\right)^2 + 2\rho_2\left(\frac{\Delta\theta_2}{2}\right)^2 \\
&\approx \frac{1}{2\rho_1}(\rho_1\Delta\theta_1)^2 + \frac{1}{2\rho_2}(\rho_2\Delta\theta_2)^2 \\
&= \frac{1}{2\rho_1}\left(\frac{\Delta S}{2}\right)^2 + \frac{1}{2\rho_2}\left(\frac{\Delta S}{2}\right)^2 \\
&= \frac{\Delta S^2}{8}\left(\frac{\rho_1 + \rho_2}{\rho_1\rho_2}\right)
\end{aligned}
$$

$$
\therefore \quad \Delta S = \sqrt{\frac{8\rho_1\rho_2\Delta t}{\rho_1 + \rho_2}}
$$
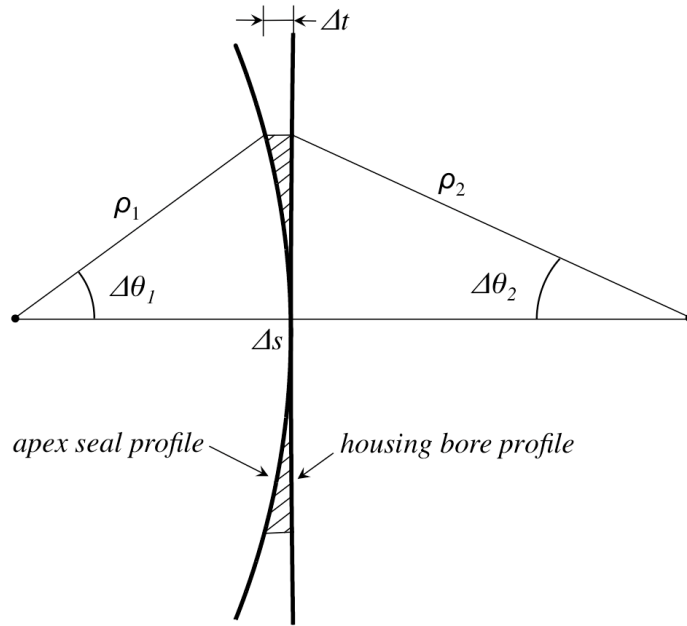
Figure B.3: Rotor apex at $\theta = 0$, two convex curves.

Appendix C

High-Sealing Design Parameters

Table C.1: Arc-based rotor radius 102 mm, $\Delta t = 0.001l$.

R/l	$-\rho$	sealwidth (mm)	mean ΔS
	4	2.1940	0.5464
	8	4.5856	0.7779
11.3333	12	7.1893	0.9516
	16	10.0364	1.0909
	20	13.1609	1.2054
	4	2.6841	0.5932
	8	5.6075	0.8356
9.2727	12	8.7905	1.0163
	16	12.2697	1.1621
	20	16.0878	1.2835
	4	3.1738	0.6413
	8	6.6292	0.8997
7.8462	12	10.3905	1.0909
	16	14.5024	1.2446
	20	19.0156	1.3725
	4	3.6645	0.6868
	8	7.6512	0.9610
6.8	12	11.9918	1.1626
	16	16.7358	1.3239
	20	21.9434	1.4577
	4	4.1553	0.7295
	8	8.6727	1.0185
6	12	13.5923	1.2297
	16	18.9695	1.3977
	20	24.8710	1.5363

Table C.2: Arc-based rotor radius 103 mm, $\Delta t = 0.001l$.

R/l	$-\rho$	sealwidth (mm)	mean ΔS
	4	2.1716	0.5474
	8	4.5367	0.7802
11.4444	12	7.1107	0.9548
	16	9.9208	1.0948
	20	13.0021	1.2099
	4	2.6568	0.5934
	8	5.5479	0.8363
9.3636	12	8.6938	1.0175
	16	12.1282	1.1639
	20	15.8936	1.2859
	4	3.1422	0.6415
	8	6.5592	0.9003
7.9231	12	10.2767	1.0919
	16	14.3358	1.2461
	20	18.7862	1.3746
	4	3.6274	0.6870
	8	7.5700	0.9615
6.8667	12	11.8594	1.1636
	16	16.5435	1.3255
	20	21.6787	1.4599
	4	3.8698	0.7087
	8	8.0754	0.9908
6.4375	12	12.6512	1.1978
	16	17.6473	1.3633
	20	23.1247	1.5003

Table C.3: Arc-based rotor radius 104 mm, $\Delta t = 0.001l$.

R/l	$-\rho$	sealwidth (mm)	mean ΔS
	4	2.1489	0.5486
	8	4.4899	0.7826
11.5556	12	7.0330	0.9582
	16	9.8079	1.0990
	20	12.8470	1.2146
	4	2.6302	0.5937
	8	5.4902	0.8371
9.4545	12	8.5986	1.0188
	16	11.9905	1.1657
	20	15.7047	1.2883
	4	3.1105	0.6417
	8	6.4905	0.9008
8	12	10.1645	1.0929
	16	14.1726	1.2476
	20	18.5625	1.3767
	4	3.5908	0.6872
	8	7.4909	0.9621
6.9333	12	11.7299	1.1646
	16	16.3549	1.3271
	20	21.4202	1.4621
	4	3.8312	0.7089
	8	7.9917	0.9913
6.5	12	12.5130	1.1989
	16	17.4465	1.3649
	20	22.8493	1.5026

Table C.4: Arc-based rotor radius 105 mm, $\Delta t = 0.001l$.

R/l	$-\rho$	sealwidth (mm)	mean ΔS
	4	2.1282	0.5500
	8	4.4428	0.7853
11.6667	12	6.9571	0.9619
	16	9.6976	1.1034
	20	12.6956	1.2196
	4	2.6037	0.5940
	8	5.4333	0.8378
9.5455	12	8.5062	1.0200
	16	11.8552	1.1675
	20	15.5198	1.2907
	4	3.0794	0.6419
	8	6.4232	0.9014
8.0769	12	10.0551	1.0939
	16	14.0134	1.2491
	20	18.3436	1.3787
	4	3.5549	0.6874
	8	7.4138	0.9626
7	12	11.6038	1.1656
	16	16.1713	1.3286
	20	21.1682	1.4642
	4	3.7931	0.7091
	8	7.9088	0.9919
6.5625	12	12.3787	1.1999
	16	17.2502	1.3665
	20	22.5799	1.5048

Table C.5: Nonarc-based rotor radius 105 mm, $\Delta t = 0.001l$.

R/l	θ_{1s}	sealwidth (mm)	mean ΔS
7	0.9550	29.4697	1.9540
	0.9650	27.8240	1.9473
	0.9750	26.1651	1.9260
	0.9850	24.4936	1.8830
	0.9950	22.8086	1.8034
6.7742	0.9550	26.4090	2.0054
	0.9650	24.7658	1.9918
	0.9750	23.1094	1.9614
	0.9850	21.4402	1.9052
	0.9950	19.7571	1.8027
6.5625	0.9550	23.3478	2.0527
	0.9650	21.7077	2.0318
	0.9750	20.0537	1.9915
	0.9850	18.3867	1.9201
	0.9950	16.7061	1.7884
6.3636	0.9550	20.2874	2.0961
	0.9650	18.6491	2.0675
	0.9750	16.9974	2.0163
	0.9850	15.3330	1.9270
	0.9950	13.6551	1.7551
6.1765	0.9550	17.2264	2.1359
	0.9650	15.5906	2.0989
	0.9750	13.9416	2.0353
	0.9850	12.2793	1.9243
	0.9950	10.6036	1.6906

Appendix D

Wide Apex Seal Design Parameters

Table D.1: Figure 6.4, Arc-based wide apex seal DF-parameters

Figure No.	R	l	ρ	seal width (mm)
6.4a	102	15	-2.3	1.99
6.4b	102	15	-25	29.1446
6.4c	102	15	-20	21.8728
6.4d	102	15	-15	15.4315
(not shown)	102	15	-10	9.6985
(not shown)	102	15	-5	4.5512

Table D.2: Figure 6.5, Nonarc-based wide apex seal DF-parameters

Figure No.	R	l	θ_{1s} (rad)	seal width (mm)
6.5a	102	15	0.85	41.9022
(not shown)	102	15	0.88	37.4879
6.5b	102	15	0.90	34.4772
6.5c	102	15	0.95	26.7178
6.5d	102	15	1.00	18.6358
(not shown)	102	15	1.02	15.3157

Bibliography

[1] Richard Ansdale. *The Wankel RC Engine Design and Performance*. Iliffe Books Ltd., London, 1968.

[2] Kais Atallah and David Howe. A novel high-performance magnetic gears. *IEEE Transactions on Magnetics*, 37(4):2844 – 2846, 2001.

[3] Kais Atallah and David Howe. Design, analysis and realisation of a high-performance magnetic gear. *IEE Proceedings Electric Power Applications*, 151(2):135 – 143, 2004.

[4] Automotive News. *Mazda's Unsung Hero of the Now-Gone Rotary Engine*, July 2012.

[5] J.E. Beard and G. R. Pennock. Calculation of the displacement of a wankel rotary compressor. In *Proceedings of the 10th International Compressor Engineering Conference*, pages 11 – 19, 1992.

[6] J.E. Beard and G. R. Pennock. The effects of the design parameters on the displacement and compression ratio of the wankel rotary compressor. In *Proceedings of the 10th International Compressor Engineering Conference*, volume 1, pages 24 – 33, 1992.

[7] J.E. Beard and G. R. Pennock. Acceleration of the apex seals in a wankel rotary compressor including manufacturing process variation in location of the seals. In *Proceedings of the 15th International Compressor Engineering Conference*, pages 735 – 744, 2000.

[8] J. R. Colbourne. The geometry of trochoid envelopes and their application in rotary pumps. *Mechanism and Machine Theory*, 9:421 – 435, 1974.

[9] D. E. Cole. The wankel engine. *Scientific American*, 227:14 – 23, 1972.

[10] Matt Davis. Mazda ceo charts how to reach 2 percent of world market, rotary engine far from dead. Technical report, autoblog.com, 2011.

[11] D. B. Dooner. Use of noncircular gears to reduce torque and speed fluctuations in rotating shafts. *Journal of Mechanical Design*, 119:299 – 306, 1997.

[12] D. B. Dooner and A. A. Seireg. *The Kinematics of Gearing*. John Wiley & Sons, Inc., New York, 1995.

[13] M. K. Eberle and E. D. Klomp. An evaluation of the potential performance gain from leakage reduction in rotary engines. In *SAE Paper No. 730117, presented at the International Automotive Engineering Congress, Detroit, Michigan*, 1973.

[14] Kelvin Fu, Aaron Knobloch, Fabian Martinez, David Walther, Carlos Fernandez-Pello, Al Pisano, and Dorian Liepmann. Design and fabrication of a silicon-based mems rotary engine. In *Proceedings of ASME International Mechanical Engineering Congress and Exposition*, 2001.

[15] Kelvin Fu, Aaron Knobloch, Fabian Martinez, David Walther, Carlos Fernandez-Pello, Al Pisano, Dorian Liepmann, Kenji Miyaska, and Kaoru Maruta. Design and experimental results of small-scale rotary engines. In *Proceedings of ASME International Mechanical Engineering Congress and Exposition*, 2001.

[16] J. Knoll, C. R. Vilmann, H. J. Schock, and R. P. Stumpf. A dynamic analysis of rotary combustion engine seals. *Annual SAE Congress and Exposition*, NASA Technical Memorandum 83536, 1984.

[17] C. H. Lee, K. C. Jiang, P. Jin, and P. D. Prewett. Design and fabrication of a micro wankel engine using mems technology. *Microelectronic Engineering*, 73:529 – 534, 2004.

[18] Faydor Litvin. *Gear Geometry and Applied Theory*. Prentice-Hall, Princeton, NJ, 1994.

[19] Faydor Litvin, Alfonso Fuentes-Aznar, Ignacio Gonzales-Perez, and Kenichi Hayasaka. *Noncircular Gears: Design and Generation.* Cambridge University Press, New York, 2009.

[20] Hung-Cheng Liu, Shih-Hsi Tong, and Daniel C.H. Yang. Trapping-free rotors for high-sealing lobe pumps. *Transactions of the ASME Journal of Mechanical Design*, 122:536 – 542, 2000.

[21] K. Matsuura, K. Terasaki, and I. Watanabe. The relative behavior of a rotary engine apex seal to the walls of a slot. *Bulletin of the Japan Society Mechanical Engineering*, 19:1367 – 1375, 1976.

[22] K. Matsuura, K. Terasaki, and I. Watanabe. The behavior of a rotary engine apex seal against the trochoidal surface. *Bulletin of the Japan Society Mechanical Engineering*, 21:1642 – 1651, 1978.

[23] Anna Mukai, Yuki Hagiwara, and Ma Jie. Mazda ends hummm as rotary gives way to hydrogen cells. Technical report, Bloomberg, 2012.

[24] Jan Norbye. *The Wankel Engine.* Chilton Book Company, Philadelphia, 1971.

[25] G. R. Pennock and J. E. Beard. Force analysis of the apex seals in the wankel rotary compressor including the influence of fluctuations in the crankshaft speed. *Mechanism and Machine Theory*, 32:349 – 361, 1997.

[26] Marton Pettendy. Mazda 'sky rotary' locked in. Technical report, GoAuto.com.au, 2010.

[27] M. F. Prasse, M. E. McCormick, and R. D. Anderson. A critical analysis of the rotary engine sealing problem. In *SAE Paper No. 730118, presented at the National Automobile Engineering Meeting, Detroit, Michigan*, 1972.

[28] T. W. Rodgers, W. Lemke, J. Lefevre, and T. Okzawa. Lubricant studies in rotary combustion engines. In *SAE Paper No. 720467, presented at the National Automobile Engineering Meeting, Detroit, Michigan*, 1972.

[29] Neil Sclater and Nicholas Chironis. *Mechanisms and Mechanical Devices Sourcebook*. McGraw-Hill, New York, 2001.

[30] J. B. Shung and G. R. Pennock. Geometry for trochoidal-type machines with conjugate envelopes. *Mechanism and Machine Theory*, 29:25 – 42, 1994.

[31] Richard Stone. *Introduction to Internal Combustion Engines*. Society of Automotive Engineers, Inc., Warrendale, PA, 1992.

[32] Mike Stubblefield and John Haynes. *Mazda RX-7 Automotive Repair Manual*, 1989.

[33] Shih-Hsi Tong. *New Conjugate Design Pair - Theory and Application*. PhD thesis, University of California - Los Angeles, 1998.

[34] Shih-Hsi Tong, Jia Yan, and Daniel C.H. Yang. Design of deviation-function based gerotors. *Mechanism and Machine Theory*, 44:1595 – 1606, 2009.

[35] Shih-Hsi Tong and Daniel C.H. Yang. On the generation of new lobe pumps for higher pumping flowrate. *Mechanism and Machine Theory*, 35:997 – 1012, 2009.

[36] Kenneth Weston. *Energy Conversion*. West Publishing Company, St. Paul, MN, 1992.

[37] Kenichi Yamamoto. *Rotary Engine*. Toyo Kogyo Co. Ltd., Hiroshima, 1981.

[38] Jia Yan. *On the Design of Deviation-Function Based Gerotors - Theory and Algorithm*. PhD thesis, University of California - Los Angeles, 2007.

[39] Jia Yan, Daniel C.H. Yang, and Shih-Hsi Tong. A new gerotor design method with switch angle assignability. *Journal of Mechanical Design*, 131:011006–1 – 011006–8, 2008.

[40] Jia Yan, Daniel C.H. Yang, and Shih-Hsi Tong. On the generation of analytical non-circular multilobe internal pitch curves. *Journal of Mechanical Design*, 130:092601–1 – 092601–8, 2008.

[41] Daniel C.H. Yang and Shih-Hsi Tong. The specific flowrate of deviation function based lobe pumps - derivation and analysis. *Mechanism and Machine Theory*, 37:1025 – 1042, 2002.

[42] Daniel C.H. Yang, Shih-Hsi Tong, and J. Lin. Deviation-function based pitch curve modification for conjugate pair design. *Transactions of the ASME Journal of Mechanical Design*, 121:579 – 586, 1999.

[43] Todd Zalud. Sometimes it pays to be eccentric. *Machine Design*, 72:75, 2000.